

A Universal Model of Droplet Vaporization Applicable to Supercritical Conditions

A Dissertation
Presented for the
Doctor of Philosophy
Degree
The University of Memphis

Zhou Ji
May, 2000

Acknowledgements

I would like to acknowledge the great help from my major advisor, Dr. Jiada Mo during the years of this research work. It is only under his persistent and inspiring guidance that this work could be possible to be completed and to be successful. I also want to thank all the support from the Department of Mechanical Engineering, Herff Internship of the Engineering College, and the University of Memphis.

Abstract

Ji, Zhou. Ph.D. The University of Memphis. May, 2000. A Universal Model of Droplet Vaporization Applicable to Supercritical Conditions. Major Professor: Jiada Mo, Ph.D.

An evaporation model of a droplet has been constructed with the concern of the droplet under supercritical or near critical condition. The thermodynamic process involving liquid phase and gas phase as well as “blurred” state of the droplet around the critical point is integrated into a general framework. Thermodynamic properties and transport coefficients are modeled as functions of pressure, temperature and composition of the mixture. These functions and the equations of state are formulated over the range covering gas phase, liquid phase, and supercritical state. Numerical implementations of the model were made for an oxygen droplet in a hydrogen gas surrounding. Preliminary numerical results have demonstrated the feasibility of the concept even though further validation of the model is necessary when experimental data are available.

Table of Contents

Abstract	iii
1. Introduction.....	1
1.1 Droplet Vaporization.....	2
1.2 Supercritical Phenomenon.....	16
2. Equations of Modeling.....	22
2.1 Fundamental Equations.....	22
2.2 United Equations.....	28
2.3 Spherically Symmetric Case.....	33
2.4 Initial Condition and Boundary Condition at the Interface of Droplet.....	36
3. Implementation and Numerical Scheme.....	42
3.1 Implementation of Equations of State.....	42
3.2 Physical Properties of Specific Species.....	47
3.3 Numerical Scheme.....	60
4. Results of Numerical Experiments.....	67
4.1 EOS and Properties.....	67
4.2 Diffusion case when only vapor phase exits.....	69
Figures.....	77
5. Discussion.....	99
5.1 Existence of Droplet Surface.....	99
5.2 Evaporatin Rate.....	101
5.3 Surface Tension.....	103
5.4 Future Improvement of the Model.....	105
6. Conclusion.....	107
Reference.....	109
Appendices.....	112
Appendix 1 Properties of H_2 and O_2	112
Appendix 2 Algorithms of Equation Solution.....	113
Appendix 3 Computerized Diagram of Viscosity.....	113
Appendix 4 Linear Fitting of Conductivity.....	115
Appendix 5 Table of Notations.....	116

1. Introduction

Research on the gasification, oxidation, and dynamics of fuel droplets is of both practical and fundamental interest in energy and combustion science. On the practical aspect one recognizes that petroleum oil constitutes a significant share of the world energy supply. Since these fuel oils are usually introduced into the combustors as sprays of droplets, it is reasonable to expect that the collective gasification of individual droplets would intimately influence the bulk spray vaporization and oxidation characteristics, which in turn determines the combustor performance. The droplet behavior is also considered as a major contributor to the spray combustion dynamics in liquid rockets, advanced gas turbines, and diesel engines. From a fundamental aspect, droplet combustion is a problem involving complex chemically reacting multicomponent two-phase flows with phase change, rich in physical and chemical phenomena typically of interest to the study of aerothermochemistry. Furthermore, in spite of the various possible interacting physico-chemical phenomena which may occur during droplet combustion, in certain idealized situations the flow field is sufficiently simple so that the combustion process is amenable to detailed theoretical and experimental study. Therefore, it is sometimes useful to adopt droplet combustion as a model to gain insight into the mechanisms governing complex heterogeneous combustion systems. Besides combustion, the phenomena associated with droplet vaporization and the methods to predict evaporation rate are also important in engineering operations like spray cooling, drying, absorption, deposition, humidification, and even in ink jet printing devices.

Corresponding to the actual phenomena in different ambient environments, there are three levels of the models: 1) droplet staying in a stagnant environment, 2) droplet experiencing a natural convection, and 3) droplet undergoing a forced convection and undergoing chemical reaction. It has been suggested that it is irrelevant to study droplet combustion in that droplet vaporization, instead of combustion, is the dominant process during spray combustion. However, in many applications the vaporization happens at a very high pressure and temperature, which could probably be very close to or above the thermodynamic critical point. At the supercritical condition, the droplet or the environment can be in the state of neither liquid nor gas. The surface between the droplet and the environment does not exist any more. So no well-defined droplet is there. The primary question to be addressed, which is still kept open, is whether the droplets can reach criticality before they have been substantially gasified. This depends on the droplet gasification rate, droplet heating rate and the extent of elevation of the critical pressure due to dissolution of the ambient gas into the liquid. While the physics of criticality is an open question, any modeling taking the supercritical environment into account, or experimental techniques conducted under supercritical conditions will be very helpful for further understanding the phenomenon.

1.1 Droplet Vaporization

1.1.1 Phenomenon of droplet vaporization and combustion

The most important application of droplet vaporization is in fuel evaporation and combustion. If the system pressure is much less than the critical pressure of the liquid such that the critical phenomena are not important, the vaporization of a

motionless, cold, droplet after it is placed in a hot, stagnant, gravity-free environment of infinite extent can be described by Fig. 1a. The lack of forced or natural convection implies that spherical symmetry prevails.

Since the droplet temperature, in particular its surface value, is lower than that of the ambience, heat is transferred towards the droplet through conduction. At the surface, part of this heat is further transferred to the droplet interior causing the droplet to heat up. The rest is used to gasify the liquid such that a high concentration of fuel vapor, generally at its saturation value, exists near the droplet surface. When the fuel vapor concentration in the environment is lower than that at the surface, a concentration gradient exists through which the fuel vapor diffuses outward. The depletion of the fuel vapor at the surface renders further gasification possible. Thus, through the above mechanism, a liquid mass can be continuously converted to vapor and eventually dispersed to the ambience, i.e., vaporization is effected. The rate-controlling processes are heat and mass diffusion.

The initial vaporization rate is slow because the droplet is cold. This rate will increase as the droplet heats up. For a pure liquid, droplet heating up is mostly over in the early part of the droplet lifetime such that the subsequent regression rate of its surface area remains almost constant over a fair period of time.

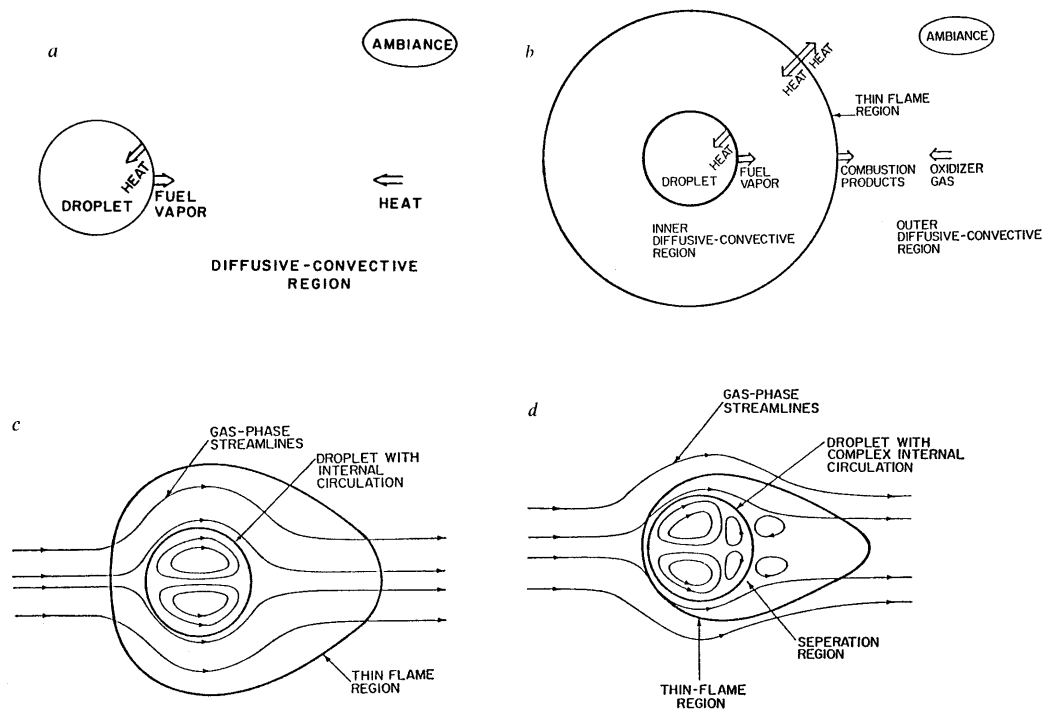


Figure 1 Flow configurations of droplet vaporization

Droplet ignition can be achieved either with an ignition stimulus (e.g. spark discharge) or if the environment is sufficiently hot. The resulting spherically symmetric burning, shown in Fig. 1b, is of the diffusion-flame type in which the outwardly-diffusing fuel vapor and the inwardly diffusing oxidizer gas approach a reaction zone in approximately stoichiometric proportion. In other words, there is no accumulation or depletion for either of the two substances. The ensuing reaction is rapid and intense, implying the reaction zone is thin and very little reactants can leak through the flame. The heat generated is transported both outward to the ambient and inward for droplet heating and gasification. Similar to the vaporization case, for a pure fuel, much of droplet heating is rapidly over and the droplet surface area then regresses at a constant rate.

At this point it is appropriate to recognize the similarity between droplet vaporization and droplet combustion. Apart from the gas-phase reactions, the detailed transport mechanisms within the droplet and gasification process at its surface are qualitatively the same in both cases. Thus during combustion, the droplet simply perceives the flame as a hotter “ambiance” located at a somewhat closer distance. This is an important point mentioned in the beginning section. While much still needs to be done to assess the dominant processes for sprays under different situations, it suffices to note herein that since droplet vaporization and combustion are similar in many aspects, understanding gained from studying droplet combustion frequently can be applied to the modeling of droplet vaporization. Indeed, from an experimental design point of view, droplet vaporization in a high temperature environment can be usefully simulated by studying droplet burning in a cold environment. The flame now conveniently serves as a high-temperature, constant-pressure “chamber” within which vaporization takes place.

For the spherically symmetric configurations shown in Figs. 1a and 1b, only radial transport is possible. In the gas phase this transport consists of both diffusion and convection; the latter, termed Stefan flow, is induced by the net transfer of mass from the droplet surface to the ambiance. In the liquid phase only diffusion exists, although the continuous regression of the droplet surface also constitutes a passive mode of “convection transport” in exposing the droplet interior to the gas.

In the presence of either forced and/or natural convection, a non-radial relative velocity exists between the droplet and the surrounding gas. The shear stress exerted by the gas flow on the surface induces recirculating motion within the droplet. When

the flow Reynolds or Grashof number is not large, a pair of vortices is generated, as shown in Fig. 1c. For higher rates of blowing, flow separation occurs close to the rear stagnation points such that wake regions are created, as shown in Fig. 1d.

The presence of non-radial convection enhances the transport rates and thereby the gasification rate. There also exist two situations for which the intensity of convection can actually result in qualitatively different combustion behavior. First, for sufficiently strong blowing, the envelope diffusion flame can be extinguished. The droplet resumes its pure vaporization mode, with the fuel vapor generated being swept to the wake region where combustion takes place. The resulting wake flame involves both diffusional and premixed burning as a result of oxidizer entrainment. The second situation involves multicomponent droplets. The existence of internal circulation generated by external motion may significantly enhance liquid-phase mass transport which is otherwise extremely slow. When considered together with the volatility-differentials among the fuel components, it has been shown that the intensity of the motion may determine whether combustion occurs quiescently or explosively ^[P-4].

However, the problem becomes significantly different when the pressure and temperature in the real chamber or the “flame chamber” are well above the thermodynamic critical states of the droplet liquid. It is possible that the droplet is heated up with its surface reaching the critical point prior to the end of the droplet lifetime. Then the sharp distinction between gas and the liquid disappears. The enthalpy of the vaporization reduces to zero, and no abrupt phase change is involved in the vaporization process. The density and temperature of the entire field of both

liquid droplet and the ambient gases as well as their gradient vary continuously across the droplet surface. The “droplet” itself does not exist in the usual sense. The different physical states can be depicted in figure 2 ^[P-5]. The word “droplet” can still be used to refer to a “blurred” region with high concentration of the original droplet species. We will come back to the supercritical phenomenon in section 1.2.

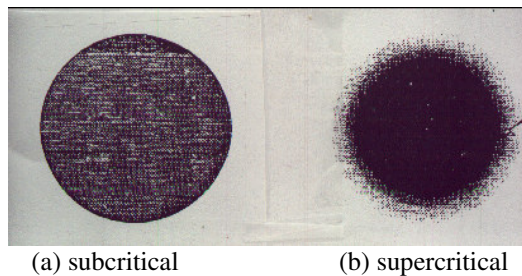


Figure 2 Droplet surface blurred at supercritical condition

1.1.2 d^2 -Law

The basic droplet combustion model was formulated in the 1950’s by Godsave, Spalding, Goldsmith and Penner, and Wise et al. for an isolated, pure-component, droplet burning in a stagnant, oxidizing environment ^[P-4]. This model has since been termed the d^2 -Law because it predicts that the square of the droplet diameter, or equivalently its surface area, decreases linearly with time. In subsequent years research on droplet combustion was mostly concerned with verifying this model and extending it to include other effects. Even for this apparently simple problem, some of the fundamental mechanisms have only recently become understood. In the 1970’s and 1980’s, much interest has focused on multicomponent droplet combustion, which necessitated detailed investigation of the liquid-phase transport processes, and on what can be termed spray effects, which account for the fact that in

realistic situations the droplet is situated in the spray interior and therefore the environment it experiences can be quite different from that of the isolated droplet assumed in the d^2 -Law.

While d^2 -Law is an old and imperfect model, there are two reasons to discuss this theory as an important starting point of research on droplet vaporization. First, it was the first systematic model and still is a framework of new models, and it also provides important guidance to experimental study, although it has many shortcomings, some being concluded as qualitatively incorrect in certain cases. Second, this simplest possible model provides some basic understanding of the general physical phenomena of droplet vaporization and combustion under many situations. It embodies much of the essential physics and yields crude estimates of the droplet gasification rate.

It is instructive to first discuss the major assumptions built into this theory.

(i) Spherical symmetry: Forced and natural convection are neglected. This reduces the analysis to one-dimension.

(ii) No spray effects: The droplet is an *isolated* one immersed in an infinite *oxidizing* environment.

(iii) Diffusion being rate-controlling.

(iv) Isobaric process.

(v) Flame-sheet combustion: Chemical reaction rates are much faster than gas-phase diffusion rates such that the flame is of infinitesimal thickness and can be treated simply as a sink for the reactants and a source of chemical heat release and products.

(vi) Constant gas-phase transport properties: The specific heats and thermal conductivity are constants and the Lewis number $Le_g = \lambda_g / (C_{pg} \rho_g g \delta_g)$ is unity throughout. These cause considerable uncertainty in estimating the gasification rate, which can easily vary by a factor of two or three by using different, but equally reasonable, average property values. The most serious consequence, however, is the failure of the d^2 -Law to predict the flame-front stand-off ratio to any reasonable value.

(vii) Gas-phase quasi-steadiness: Because of the significant density disparity between liquid and gas, the liquid possesses great inertia such that its properties at the droplet surface, for example, the regression rate, species concentration, and temperature, change at rates much slower than those of the gas-phase transport processes. As an example, in the standard environment the gas-phase heat and mass diffusivities, α_g and δ_g , are of the order of $1 \text{ cm}^2\text{s}^{-1}$, whereas the droplet surface regression rate,

$$K = -\frac{d(d_s^2)}{d t}$$

is the order of $10^{-3} \text{ cm}^2\text{s}^{-1}$ for conventional hydrocarbon fuels burning in the standard atmosphere ^[P-4]. Thus their ratio is of the same order as the ratio of the liquid-to gas densities, viz. $\delta_g/K \sim \rho_l/\rho_g$.

If we further assume that properties of the environment also change slowly, then during the characteristic gas-phase diffusion time the boundary locations and conditions can be considered to be constant. Thus the gas-phase processes can be treated as steady, with the boundary variations occurring at longer time scales. Combining with the first assumption, the analysis is now simplified to that of steady,

one-dimensional, flow, being described by ordinary differential equations instead of partial differential equations.

The quasi-steady assumption breaks down in regions far away from the droplet, where the flow velocity is extremely slow, such that the characteristic diffusion is of the same order as the surface regression time. The location d_∞ at which this assumption breaks down can be estimated by equating the diffusing time at d_∞ with the regression time at d_s ,

$$d_\infty^2 / \delta_g \sim d_s^2 / K.$$

But since $(\delta_g / K \sim \rho_l / \rho_g)$, therefore

$$(d_\infty / d_s) \sim \sqrt{(\rho_l / \rho_g)}.$$

In particular, for near- or super-critical combustion, $(\rho_l / \rho_g) = O(1)$. As a result, the assumption is invalid everywhere to some extent.

Although some unsteady theories have attributed certain unique phenomena to be caused by gas-phase unsteady diffusion, it has been shown that these are actually consequences of initial conditions coupled with what we called fuel vapor accumulation effects as appearing in the next assumption. Qualitative trends that are uniquely effects of gas-phase unsteady diffusion have yet to be identified.

(viii) Simultaneous fuel gasification and combustion: This assumes that the amount of fuel gasified at the surface is instantly consumed at the flame, or the instantaneous rate of gasification is equal to that of consumption. This neglects the change of the amount of fuel vapor present between the droplet and flame as a result of the continuous variation of their physical sizes as burning processes.

(ix) Single fuel species: Thus it is unnecessary to analyze liquid-phase mass transport.

(x) Constant and uniform droplet temperature: This implies that there is no droplet heating. Combined with (ix), we see that liquid-phase heat and mass transport processes are completely neglected. Therefore d^2 -Law is essentially a gas-phase model.

(xi) Saturation vapor pressure at droplet surface: This is based on the assumption that the phase-change process between liquid and vapor occurs at a rate much faster than those for gas-phase transport. Therefore gasification at the surface is at equilibrium, producing fuel vapor which is at its saturation vapor pressure corresponding to the droplet surface temperature T_s .

(xii) No Soret, Dufour and radiation effects.

With the above assumptions, the overall continuity for the steady one-dimensional flow is

$$\frac{dm}{dr} = 0,$$

where $m = 4\pi\rho_g v_s r_s^2$ is the mass flow rate. It simply states that $m = \text{constant}$.

With the flame-sheet approximation, the inner and outer regions of the flame are chemically inert. Therefore, conservation equations for energy and mass can be separately written for these two regions.

Inner Region ($r_s \leq r \leq r_f$):

$$\text{Fuel} \quad mY_F - 4\pi\rho_g \delta_g r^2 \frac{dY_F}{dr} = m$$

$$\text{Energy} \quad mC_{pg}(T - T_s) - 4\pi\lambda_g r^2 \frac{dT}{dr} = -mH$$

Outer Region ($r_f \leq r \leq \infty$):

$$\text{Oxidizer} \quad mY_O - 4\pi\rho_g \delta_g r^2 \frac{dY_O}{dr} = -m\sigma$$

$$\text{Energy} \quad mC_{pg}(T - T_s) - 4\pi\lambda_g r^2 \frac{dT}{dr} = -m(H - Q)$$

Boundary Conditions

$$r = r_s: Y_F = Y_{Fs}, \quad T = T_s$$

$$r = r_f: Y_F = Y_{Ff} (= 0), \quad T = T_f, Y_O = 0$$

$$r = \infty: \quad T = T_\infty, Y_O = Y_{O\infty}$$

Y in the equations is mass fraction, with subscripts F and O for fuel and oxidizer. Note that the lower case f subscript denotes flame. δ is mass diffusivity and λ is thermal conductivity coefficient. σ is stoichiometric ratio for oxidizer to fuel. In each of the four equations, the first and second terms respectively represent convective and diffusive transport, while the RHS terms show that their difference is a conserved quantities in a given region. These equations are actually slightly more general than the assumption listed above in that the unity Lewis number condition has not yet been applied, and that the parameter H represents an effective latent heat of gasification which consists of both the specific heat of gasification, L , as well as the amount of heat, H_l , needed to heat the droplet interior per unit mass of liquid gasification. In crossing the flame, the flow gains the additional chemical heat release, mQ , which can be determined by requiring that

$$C_{pg}(4\pi\rho_g \delta_g r^2 \frac{dT}{dr})_{r_f^-} - C_{pg}(4\pi\rho_g \delta_g r^2 \frac{dT}{dr})_{r_f^+} = mQ.$$

Finally an equilibrium gasification relation is needed

$$Y_{Fs} = Y_{Fs}(T_s)$$

to make the equations mathematically closed.

Integrating the differential equations with the boundary condition specified and using Lewis number $Le_g = 1$, the following explicit expressions can be derived for the non-dimensional mass gasification rate $\tilde{m} = m / (4\pi \rho_g \delta_g r_s)$, the flame-front standoff ratio $\tilde{r}_f = r_f / r_s$, the flame temperature T_f , and H .

$$\tilde{m} = \ln(1 + B),$$

$$\tilde{r}_f = \frac{\tilde{m}}{\ln(1 + Y_{O\infty} / \sigma)} = 1 + \frac{\ln\{1 + C_{pg}(T_f - T_s) / H\}}{\ln\{1 + Y_{O\infty} / \sigma\}},$$

$$C_{pg}(T_f - T_s) = \frac{C_{pg}(T_\infty - T_s) + (Y_{O\infty} / \sigma)(Q - H)}{(1 + Y_{O\infty} / \sigma)},$$

$$H = \frac{(1 - Y_{Fs})[C_{pg}(T_\infty - T_s) + (Y_{O\infty} / \sigma)Q]}{Y_{Fs} + (Y_{O\infty} / \sigma) - Y_{Ff}(1 + Y_{O\infty} / \sigma)},$$

where $B = \frac{C_{pg}(T_\infty - T_s) + (Y_{O\infty} / \sigma) / Q}{H}$ is the Spalding transfer number. This solution is applicable to both vaporization and combustion in that it specializes to that of vaporization by setting $Y_{O\infty} = 0$ and $Y_{Ff} = Y_{F\infty}$, and to that of combustion by setting $Y_{Ff} = 0$. For example, with $Y_{O\infty} = 0$, the “flame” is now simply the ambience, with $\tilde{r}_f = \infty$ and $T_f = T_\infty$. For combustion of practical hydrocarbon fuels in air, $L \ll Q$, and $Y_{O\infty} / \sigma \ll 1$, the transfer number for combustion becomes

$$B \approx \frac{C_{pg}(T_f - T_s)}{H},$$

which is just the transfer number for vaporization in an ambience whose temperature is the flame temperature T_f . The finite location of the flame has only a small influence because it is usually situated quite far away from the droplet.

To be more illuminating, the expression of the flame temperature can be rewritten as

$$\left\{ \frac{C_{pg}(T_f - T_\infty)}{Y_{O_\infty} / \sigma} \right\} + \{H + C_{pg}(T_f - T_s)\} = Q,$$

which shows that the total energy needed to heat the oxidizer from T_∞ to T_f , as well as to gasify the fuel and then heat it from T_s to T_f , is the total chemical heat release, Q . Thus T_f is simply the stoichiometric adiabatic flame temperature of the given fuel-oxidizer system.

The above solution is well defined once T_s is known. For the present model there is no droplet heating, implying $H \equiv L$. When Y_{F_s} is given as a function of T_s , T_s then can be determined from the expression of H iteratively. It is significant to note that for this model, T_s , \tilde{m} , \tilde{r}_f , and T_f are constant of a given system. An alternate easier way to get T_s is approximating it by the boiling point T_b .

The Spalding transfer number B represents the ratio of the ‘driving force’ for gasification to the ‘resistance’ to gasification. The driving force consists of a thermal source, $C_{pg}(T_\infty - T_s)$, and a chemical source, $(Y_{O_\infty} / \sigma)Q$. For combustion of practical fuel, the chemical contribution is usually much greater than the thermal contribution, especially when the environment is cold such that T_∞ is close to T_s . Thus an accurate knowledge of T_s is frequently not essential. Further realizing that the droplet is expected to reach its boiling state under the situation of intense heating during steady-

state combustion, it is adequate to assume $T_s = T_b$. In a realistic situation, the state of boiling can never be attained because of the presence of species other than the fuel vapor at the droplet surface. For vaporization, the only source of heat available is from the ambience and B is expected to depend sensitively on T_s . Therefore the boiling point is not generally a good approximation, except when vaporization is in a very hot environment.

Finally, using assumption (vii) we have $m = -\frac{d}{dt}\left(\frac{1}{6}\pi d_s^3 \rho_l\right)$. Considering the above expression for \tilde{m} , the droplet surface regression rate defined previously becomes

$$K = \frac{8\rho_g \delta_g}{\rho_l} \ln(1 + B).$$

The parameter K is also frequently called the evaporation or burning rate constant. Integrating yields $d_s^2 = d_{so}^2 - Kt$, which forms the basis of the d^2 -Law, stating that the square of the droplet diameter decreases linearly with time as gasification proceeds.

The equations of K , \tilde{r}_f , and T_f contain much information on the droplet gasification characteristics. First it is seen that K depends linearly on the transport properties, through $(\rho_g \delta_g)$ or (λ_g/C_{pg}) . Comparing this expression with the square root variation, $\sqrt{\rho_g \delta_g}$, associated with laminar premixed flames, the basic diffusive nature of droplet gasification is evident.

Since K depends linearly on $(\rho_g \delta_g)$ but only logarithmically on B , it is sometimes even more important to strive for an accurate estimate for $(\rho_g \delta_g)$, or (λ_g/C_{pg}) , instead of B . The difficulty here is that $(\rho_g \delta_g)$ is a function of temperature

and composition, both of which vary over wide ranges for hydrocarbon combustion. These variations can cause much uncertainty in estimating K .

The overlooked points in d^2 -Law can be listed as follows in order of their significance: 1) droplet heating; 2) fuel accumulation; 3) variable properties; 4) multicomponent; 5) flame structure; 6) spray effect; 7) supercritical; 8) dissociation, etc. Although the d^2 -Law sometimes seems to be able to predict K and T_f , through judicious selection of the transport parameters, it cannot achieve simultaneous agreement for all the three observables, K , T_f , and the flame-front standoff ratio \tilde{r}_f . Experiments show several important aberrations of d^2 -Law. During a short initial period droplet size hardly changes. This is due to droplet heating. \tilde{r}_f is not a constant due to the vapor accumulation. And the value obtained in experiments is much smaller (<10) than the predicted value (about 35 for n -paraffins burning in air). This is caused by the simplification of constant properties. The actual temperature predicted is so high that dissociation must be important as well.

Many of improvements and modifications have been made to d^2 -Law by improving these simplifications. Some have greatly enhanced the results predicted by the law. Another important factor ignored so far, which is the major concern of this paper, is the supercritical phenomenon. When pressure and temperature are very high and the supercritical phenomena are involved, more difficulties arise and invalidate many of the assumptions in d^2 -Law model.

1.2 Supercritical Phenomenon

Supercritical environment is one of the factors not yet considered in many studies of droplet vaporization. Although it is still a question whether, or how, the

droplet can actually reach critical point before being completely gasified, the pressure and temperature in actual environments like liquid-fueled engines is well above the critical point of the fuel.

From the aspect of thermal equation of state, the critical point is such a special state that the substance behaves quite differently when above or even near it. See Fig. 3 for a p - v diagram. When liquid is heated at constant temperature much lower than critical point it will go through the process of phase change to vapor. During this period, the pressure will not increase and bulk density will decrease dramatically. Continuous change of pressure accompanies an abrupt change of density. If the procedure is isobaric instead of isothermal, the temperature change accompanies abrupt change of density. But when the temperature is above the critical point, there is no sharp difference between two phases. Density always changes continuously with pressure in an isothermal procedure, although the derivative $(\frac{dv}{dp})_T$ is still very large near the critical point.

From p - T diagram of Fig. 4 and 3-dimensional p - v - T diagram of Fig. 5, we can observe the relation in Fig. 3 from different viewpoints and the singularity around the critical point is more manifest. Fig 5, whose projections are actually Figs. 3 and 4, is a very instructive tool.

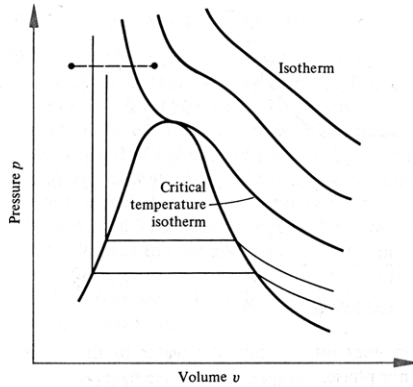


Figure 3 Equation of state (p - v diagram)

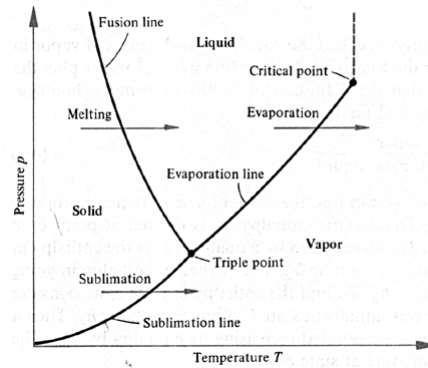


Figure 4 Equation of state (p - T diagram)

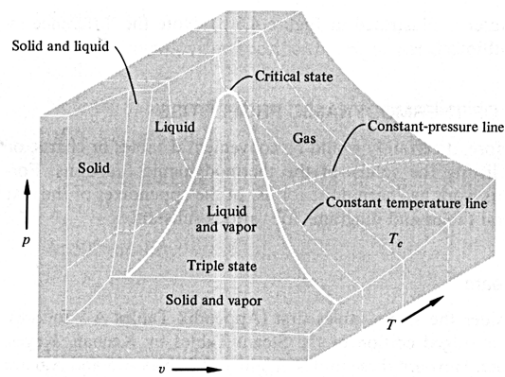


Figure 5(a)

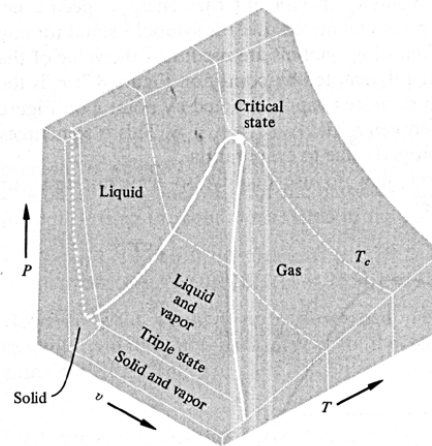


Figure 5(b)

Figure 4 Equation of state (p - v - T diagram)

If the droplet arrives at the critical point, the difference between liquid phase and gas phase does not exist any more. So the interface between the droplet and the surrounding does not exist either. Furthermore, the condition on the interface used for previous modeling is not applicable here. The droplet and environment cannot be processed separately under supercritical conditions. What can be conceived is only the different concentration of different species. The geometry of droplet itself cannot be determined simply by a radius. The value of density, along with pressure and

temperature, may be used to determine if liquid, gas or supercritical state is present at a particular location.

As mentioned in the previous section, without a density difference between two phases, the gas quasi-steady assumption is definitely invalid. While patching two adjacent regions does not work, because the abruptness in the equation of state reduces to very high derivative around the critical point, it is also very difficult to model and solve accurately as a whole.

In one sense, the problem becomes easier because no phase change means we do not need to enforce the relation for phase equilibrium and do not need to describe the procedure of phase change. But we have to renounce all the approximations that are impossible to be valid under this condition, such as constant properties of fuel and oxidizer. We have to describe these properties accurately and we have to have accurate equations of state to describe the relation between these properties, while all these have never been implemented successfully in a general form.

The problem of supercritical condition is one of those aspects that had least development and breakthrough in modeling droplet vaporization in the past years. Even just close to critical point, the vaporization procedure will be quite different and has not been modeled satisfactorily. Actually, the small amount of the existing experimental research doesn't even build a credible standard to judge any theoretical model.

In fact, the difficulty in the critical phenomenon is more pronounced than the singularity of the equation of state. It is imagined as a system in which mutual diffusion of components practically stops, a sound wave is dampened after traveling a

distance of only a few wavelengths, a laser beam is scattered diffusely to prevent its transmission through an optical cell, heat capacity and thermal conductivity diverge, and thermal perturbations do not relax for many hours or even days. The fundamental and most amazing feature of critical phenomenon has been the discovery of critical-point universality: the microscopic structure of fluids becomes unimportant in the vicinity of the critical point. Reliable understanding and description of critical behavior of fluids and fluid mixtures are needed for many innovative applications such as supercritical extraction, enhanced oil recovery, supercritical pollution oxidation, etc.

The idea of universality appears to be also applicable to phase transitions in complex fluids: polymers and polymer solutions, micromulsions and liquid crystals, fluids in porous media, gels, and foams. Large fluctuations, strong susceptibility (response) to external perturbations, and mesoscopic structure are characteristics for all such systems. The research on critical phenomenon could bridge the gap between the modern concept of the fluctuation-caused universality and new challenging application that involve these fascinating materials.

Until a few decades ago, it was thought that the correlation function in fluids of molecules with short-range interactions would always remain short ranged except in the vicinity of a critical point. It now appears that long-range correlation phenomena are ubiquitous in such fluid, and the static- and dynamic-correlation function are always long range in nonequilibrium steady states. This is related with what has become known as self-organized criticality.

In short, the behavior of thermodynamic properties of fluids and fluid mixtures are strongly affected by the presence of critical points. The presence of long-range fluctuations is associated with critical phase-transition phenomena. The presence of long-range fluctuations in fluids and fluid mixtures near-critical-point phase transition also strongly affects the behavior of transport properties. The effects of long range fluctuations on the transport properties can be understood quantitatively with the methods of generalized hydrodynamics. It is a topic in research in physics to obtain an accurate representation of the thermodynamic behavior of fluids and fluid mixtures both close to and not so close to these critical points, and accurate representations of the transport properties over a long range of temperatures and densities, which incorporate the crossover of the thermodynamic behavior from singular critical thermodynamic behavior to regular thermodynamic behavior far away from critical phase transitions. It is still a challenging task to obtain equations of chemical engineering applications that incorporate the universal (affected by fluctuations) critical behavior of fluids and nonuniversal (affected by specific intermolecular interactions) behavior far away from the critical point. In the present model, the accuracy of these representations is not verified with experiments and the equation of states are restricted to specific species like hydrogen and oxygen. But what is of more concern in the proposed model is to integrate these equations into a universal vaporization model.

2. Equations of Modeling

2.1 Fundamental Equations

2.1.1 Conservation Equations

The conservation equations are the fundamental framework of the whole model, although many coefficients which usually are considered as constant will have to be modeled as functions of independent thermodynamic properties like temperature and density. Furthermore, the accuracy of their models becomes a significant factor in the validity of the whole model enclosing the critical point, while the difficulty to achieve it is still not overcome from the aspect of physics.

The following conservation equations of mass, momentum, species and energy are valid even under supercritical conditions, although the problems of how to determine the coefficients of diffusion and what the exact equation of state is still remain.

Mass:

$$\frac{\partial \rho}{\partial t} + \frac{\partial}{\partial x_\beta} (\rho u_\beta) = 0, \quad (1)$$

Momentum in direction α :

$$\frac{\partial}{\partial t} (\rho u_\alpha) + \frac{\partial}{\partial x_\beta} (\rho u_\alpha u_\beta) + \frac{\partial p}{\partial x_\alpha} = \frac{\partial}{\partial x_\beta} \tau_{\alpha\beta}, \quad (2)$$

Species i :

$$\frac{\partial \rho_i}{\partial t} + \frac{\partial}{\partial x_\beta} (\rho_i u_\beta + m_i J_{i\beta}) = 0, \quad (3)$$

Energy:

$$\frac{\partial}{\partial t}(\rho h) + \frac{\partial}{\partial x_\beta}(\rho h u_\beta) = \frac{\partial p}{\partial t} + u_\beta \frac{\partial p}{\partial x_\beta} - \frac{\partial q_\beta}{\partial x_\beta} + \phi_v, \quad (4)$$

where viscous stress tensor $\tau_{\alpha\beta} = \eta\left[\left(\frac{\partial u_\alpha}{\partial x_\beta} + \frac{\partial u_\beta}{\partial x_\alpha}\right) - \frac{2}{3}\delta_{\alpha\beta} \frac{\partial u_\gamma}{\partial x_\gamma}\right]$, viscous dissipation

$\phi_v = \tau_{\alpha\beta} \frac{\partial u_\alpha}{\partial x_\beta}$, and m_i is the molecular weight of species i .

In these equations, the unknowns are density ρ , velocity u_α , species density ρ_i , and enthalpy h , as functions of independent variables time t and spatial coordinates x_α .

2.1.2 Transport Relations

To make the above system of equations complete, the expression of molar flux relative to mass-average velocity, \vec{J}_i , heat flux, \vec{q} , and pressure p must be formulated. Pressure formulation will be discussed in the next section of the equations of state.

1) \vec{J}_i is given by:

$$\vec{J}_i = -\sum_j L_{ij} \nabla(\beta \mu_j) + L_{iq} \nabla \beta, \quad (5)$$

where $\beta = 1/RT$, μ_j is the chemical potential of species j , which is related to temperature T , pressure p and mole fraction X_j , L_{ij} is the matrix of transport coefficients for generalized Fick's diffusion of species i in species j , and L_{iq} are the coefficients for Soret effect (thermal diffusion) of species i . According to the Onsager relation, $L_{ij} = L_{ji}$.

2) \vec{q} is formulated as:

$$\vec{q} = -\sum_j L_{qj} \nabla(\beta\mu_j) + L_{qq} \nabla\beta, \quad (6)$$

where L_{qj} are the coefficients for Dufour diffusion (heat transfer induced by concentration gradients) of species j , and L_{qq} is the coefficient for Fourier diffusion (conductivity). Onsager relation $L_{iq} = L_{qi}$ holds for the interconnection of the Soret and Dufour effects. L_{qq} can be related to thermal conductivity k by $k = \frac{L_{qq}}{RT^2} = \frac{\beta L_{qq}}{T}$.

The formulas (5) and (6) are rigorous descriptions of transport processes using the fluctuation theory based upon molecular distribution functions. Both heat and mass transport are related to a transport matrix and considered to be driven by gradients of chemical potentials. Fick's diffusion for species, thermal mass diffusion (the Soret effect), Fourier diffusion of heat associated with thermal conductivity, and the Dufour effect are all taken into account. To plug these formulas into the conservation equations, the chemical potential μ must be eventually expressed in other variables of the system, ρ , ρ_i and h . The remaining problem is how to represent all these elements in the transport matrix.

2.1.3 Equations of States

Similar to μ , pressure p also has to be related to ρ , ρ_i and h . To put in a common form, p , h and μ can all be expressed as functions of density, temperature, and mixture composition. The first two appear as a thermal equation of state $p=p(\rho, T, X_i)$ and a caloric equation of state $h=h(\rho, T, X_i)$. Composition, represented by the molar fraction of species i , X_i , is related to species density ρ_i . Thus the system of

equations consists of $5+(n-1)$ equations of ρ , u_α , T , and X_i as functions of t and x_α , where $\alpha = 1, 2, 3$, $i = 1, 2, \dots, n$, and n is the number of species.

2.1.4 Chemical Potential

Besides diffusion coefficients L_{ij} , L_{qj} , and the equations of state, the expression of chemical potentials as a function of ρ (or p), T , and X_i need to be developed as well. More precisely, we need the term of $\nabla(\beta\mu_j)$ that appears in the above expressions (5) and (6) of fluxes to be formulated.

For chemical potential of j th component μ_j , we have

$$\beta\mu_j = \beta\mu_j^*(T, p) + \ln X_j \gamma_j, \quad (7)$$

where X_j is the mole fraction of j th component and γ_j is its activity coefficient. $\mu_j^*(T, p)$ is the chemical potential for pure substance j .

The activity coefficient describes the deviation of behavior of species j in a particular mixture from the behavior it would have in an ideal mixture. If we substitute for the mole fraction X_i in the equation derived for an ideal system the activity or the product $\gamma_i X_i$, these equations are valid for real system. All the deviations from ideal behavior are lumped into one factor of activity coefficient.

When the mole fraction X_j approaches 1, γ_j also approaches unity. If X_j approaches 0, the limit of γ_j is infinite dilution activity coefficient $\gamma_j^0(p, T) = \exp(\Delta G^E_0 / RT)$, where ΔG^E_0 is the excess Gibbs free energy of infinite dilution. The excess Gibbs free energy or excess free enthalpy ΔG^E is defined as

$$\Delta G_{mix} - \Delta G_{mix}^* = \sum_i n_i RT \ln \gamma_i = \Delta G^E$$

for real systems, where

$$\Delta G_{mix} = \sum_i n_i RT \ln X_i + \sum_i n_i RT \ln \gamma_i$$

is the change of free enthalpy in mixing the pure liquid constituents, and

$\Delta G_{mix}^* = \sum_i n_i RT \ln X_i$ is for the corresponding ideal solution. If the excess free

enthalpy is known as a function of composition, by the relatively simple operation of partial differentiation with respect to n_i it is possible to obtain a relation giving the dependence of the activity coefficient of this constituent on the composition of the solution, which automatically satisfies the Gibbs-Duhem equation. If the excess free enthalpy is expressed as a function of the effective molar volumetric fraction, the coefficients in the expression have to be determined by experiments.

Then the relations for rewriting equation (5) and (6) in term of thermodynamic properties T , p instead of chemical potential μ need to be established. First, the differential of the first term of the right-hand side in equation (7) is

$$d(\beta \mu_j^*) = \beta d\mu_j^* + \mu_j^* \left(-\frac{dT}{RT^2}\right) = \beta \left(d\mu_j^* - \mu_j^* \frac{dT}{T}\right) \quad (8)$$

For pure substance, $\mu = G/n$ and the total differential of Gibbs free energy can be written as $dG = -SdT + Vdp + \mu dn$, where the capital letters V and S refer to the properties of the whole system. Thus

$$d\mu_j^* = -s_j dT + v_j dp, \quad (9)$$

in which s_j and v_j are the partial molar entropy and volume of species j . Considering $G = H - TS$, it can be rewritten as

$$\mu_j^* = h_j - Ts_j, \quad (10)$$

where h_j is the partial molar enthalpy of species j . Substituting Equations (9) and (10) into (8), it follows that $d(\beta\mu_j^*) = \beta(v_j dp - h_j d \ln T)$ or

$$\nabla(\beta\mu_j^*) = \beta(v_j \nabla p - h_j \nabla \ln T). \quad (11)$$

Then, $d \ln X_j \gamma_j = d \ln X_j + d \ln \gamma_j$

$$\begin{aligned} &= d \ln X_j + \left. \frac{\partial \ln \gamma_j}{\partial X_j} \right|_{T,p} dX_j \\ &= d \ln X_j + X_j \left. \frac{\partial \ln \gamma_j}{\partial X_j} \right|_{T,p} d \ln X_j \\ &= \left(1 + X_j \left. \frac{\partial \ln \gamma_j}{\partial X_j} \right|_{T,p} \right) d \ln X_j. \end{aligned}$$

If we denote $\alpha_{D_j} = 1 + X_j \left. \frac{\partial \ln \gamma_j}{\partial X_j} \right|_{T,p}$, and use equation (11), equation (7) would lead

to

$$\nabla(\beta\mu_j) = \beta(V_j \nabla p - h_j \nabla \ln T) + \alpha_{D_j} \nabla \ln X_j. \quad (12)$$

From Gibbs-Duhem relation $X_1 d\mu_1 + X_2 d\mu_2 + \dots + X_k d\mu_k = 0$, using

$\mu_i - \mu_i^0 = RT \ln a_i$ and $\gamma_i = \frac{a_i}{X_i}$, where a_i is activity of species i and k is the number

of species, we have

$$X_1 \frac{\partial \ln \gamma_1}{\partial X_1} + X_2 \frac{\partial \ln \gamma_2}{\partial X_2} + \dots + X_k \frac{\partial \ln \gamma_k}{\partial X_k} = 0.$$

For the case of two species, $X_1 = 1 - X_2$, so $\alpha_{D_1} = \alpha_{D_2} = \alpha_D$.

2.2 United Equations

To unite all the fundamental equations to a closed system, we will rewrite the fundamental equations only for the case of two species in this section, and by using molar concentration instead of density, molar fraction instead of species density as unknowns in continuity equation, species equation, and the expressions of mass and heat fluxes.

2.2.1 Conservation Equations

First, several new variables must be defined. The molar concentration of the mixture is defined as $n = \rho / m$, where ρ is the mixture density and m is number-mean molecular weight of the mixture.

$$m = X_1 m_1 + X_2 m_2, \quad (13)$$

where m_1 and m_2 are the molecular weights of the two species. The molar concentration of each species $n_j = n X_j = \rho_j / m_j$, where ρ_j is the density concentration of species i appeared in equation (4). Thermal expansion ratio is

defined as $\alpha_V = \frac{1}{V} \frac{\partial V}{\partial T} \Big|_{p, X_j}$. The operator of substantial derivative

$\frac{D}{Dt} = \frac{\partial}{\partial t} + u_\beta \frac{\partial}{\partial x_\beta}$, where subscript β is the index of coordinates, will also be used

in the following presentation.

Equation (1), the equation of mass, can be formulated in terms of n

$$\frac{\partial n}{\partial t} + \frac{\partial}{\partial x_\beta}(nu_\beta) = -\frac{n}{m} \frac{Dm}{Dt} = -\frac{n}{m} \sum_i m_j \frac{DX_j}{Dt}, \quad (14)$$

where the second equal sign is only to show an alternative form.

For two species, only one species equation (3) is needed in addition to the global mass equation. Substituting $\rho_1 = nm_1 X_1$, equation (3) becomes

$$n \frac{\partial(m_1 X_1)}{\partial t} + m_1 X_1 \frac{\partial n}{\partial t} + nu_\beta \frac{\partial(m_1 X_1)}{\partial x_\beta} + m_1 X_1 \frac{\partial(nu_\beta)}{\partial x_\beta} + m_1 \nabla \cdot \vec{J}_1 = 0.$$

Using equation (14), it becomes

$$n \frac{D(m_1 X_1)}{Dt} - m_1 X_1 \frac{n}{m} \sum_j m_j \frac{DX_j}{Dt} + m_1 \nabla \cdot \vec{J}_1 = 0.$$

For two species this simplifies to

$$\frac{DX_1}{Dt} [nm_1 - m_1 X_1 \frac{n}{m} (m_1 - m_2)] = -m_1 \nabla \cdot \vec{J}_1.$$

$$\begin{aligned} \text{Using } n - X_1 \frac{n}{m} (m_1 - m_2) &= \frac{nm - X_1 (nm_1 - nm_2)}{m} \\ &= \frac{n(X_1 m_1 + X_2 m_2) - X_1 (nm_1 - nm_2)}{m} \\ &= \frac{n(1 - X_1)m_2 + X_1 nm_2}{m} \\ &= \frac{nm_2}{m}, \end{aligned}$$

it finally becomes

$$\frac{DX_1}{Dt} = -\frac{m}{nm_2} \nabla \cdot \vec{J}_1 = -\frac{DX_2}{Dt}. \quad (15)$$

The right-hand side of the second equal sign is obviously the same as the left-hand side of the first equal sign considering $X_1 = 1 - X_2$.

Now let us consider the energy equation as the following, which is in a little different form from equation (4).

$$\frac{D(\rho h)}{Dt} + \rho h \frac{\partial u_\beta}{\partial x_\beta} = \frac{Dp}{Dt} - \frac{\partial q_\beta}{\partial x_\beta} + \phi_v, \quad (16)$$

where $h = (X_1 h_1 + X_2 h_2) / m$ is the enthalpy per unit mass of the mixture. By

utilizing the continuity equation $\frac{D\rho}{Dt} + \rho \frac{\partial u_\beta}{\partial x_\beta} = 0$, the left-hand side of the above

equation is reduced to $\rho \frac{Dh}{Dt}$.

According to the fundamental thermodynamics relation, the following equation holds for a multi-component system

$$dH = C_p' dT + [V - T \left(\frac{\partial V}{\partial T} \right)_{p, X_j}] dp + \sum_{j=1}^{k-1} \left. \frac{\partial H}{\partial X_j} \right|_{T, p} dX_j,$$

where C_p' is the specific heat of the system.

For the case in hand, the number of the species, k , is 2. So the summation in the above equation only contains a single term. Therefore, we have

$$\frac{Dh}{Dt} = C_p \frac{DT}{Dt} + \frac{1}{\rho} \frac{Dp}{Dt} - \alpha_v T \frac{Dp}{Dt} + \frac{\partial h}{\partial X_1} \frac{DX_1}{Dt} \quad (17)$$

The definition of α_v has been incorporated in the above equation and C_p is the molar specific heat.

From the definition of h ,

$$\begin{aligned}
\frac{\partial h}{\partial X_1} &= \frac{\partial}{\partial X_1} \left[\frac{X_1 h_1 + (1 - X_1) h_2}{m} \right] \\
&= \frac{1}{m} (h_1 - h_2) - \frac{X_1 h_1 + X_2 h_2}{m^2} \frac{\partial m}{\partial X_1} \\
&= \frac{1}{m^2} [m(h_1 - h_2) - (X_1 h_1 + X_2 h_2) \frac{\partial}{\partial X_1} (X_1 m_1 + X_2 m_2)] \\
&= \frac{1}{m^2} [(X_1 m_1 + X_2 m_2)(h_1 - h_2) - (X_1 h_1 + X_2 h_2)(m_1 - m_2)] \\
&= \frac{1}{m^2} [h_1 m_2 - h_2 m_1],
\end{aligned}$$

and from equation (15) $\frac{DX_1}{Dt} = -\frac{m}{nm_2} \nabla \cdot \vec{J}_1$.

Then by plugging equation (17) into the left-hand side of equation (16), we can get the energy equation as

$$\rho C_p \frac{DT}{Dt} = \alpha_v T \frac{Dp}{Dt} - \nabla \cdot \vec{q} + \phi_v + m_1 \left(\frac{h_1}{m_1} - \frac{h_2}{m_2} \right) \nabla \cdot \vec{J}_1 \quad (18)$$

Keeping the momentum equation in its original form

$$\frac{\partial}{\partial t} (\rho u_\alpha) + \frac{\partial}{\partial x_\beta} (\rho u_\alpha u_\beta) + \frac{\partial p}{\partial x_\alpha} = \frac{\partial}{\partial x_\beta} \tau_{\alpha\beta}, \quad (2)$$

finally, equations (14), (15), (18), and (2) constitute the fundamental equations of a binary mixture fluid which is independent of the thermodynamic phase.

2.2.2 Expressions of Fluxes

The next task is to develop the expressions for \vec{J}_1 and \vec{q} . First, consider the transport matrix. In the two-species case we only need to express the flux for one species. Therefore only one of the two ‘‘main terms (diagonal elements)’’ L_{II} in the

transport matrix needs to be considered. Then the cross terms (off-diagonal terms) in the transport matrix can be determined by using the intrinsic relation.

Since \vec{J}_1 is the molar flux relative to mass-average velocity, we have

$$m_1 \vec{J}_1 + m_2 \vec{J}_2 = 0. \quad (19)$$

In the case of $\nabla(\beta) = 0$, $\nabla(\mu_2) = 0$, equation (5) becomes

$$\vec{J}_1 = -L_{11} \nabla(\mu_1), \quad \vec{J}_2 = -L_{21} \nabla(\mu_1). \quad (20)$$

Substitute (20) into (19), we get $m_1 L_{11} + m_2 L_{12} = 0$.

Similarly, we also need L_{q2} besides L_{q1} in the formulation. In the case of $\nabla(\beta \mu_1) = \nabla(\beta \mu_2) = 0$, equation (5) becomes

$$\vec{J}_1 = L_{1q} \nabla \beta, \quad \vec{J}_2 = L_{2q} \nabla \beta. \quad (21)$$

Substitute (21) into (19), we get $m_1 L_{q1} + m_2 L_{q2} = 0$.

If we define the mutual diffusion coefficient $D_m = L_{11} \frac{V}{X_1 X_2} \left(\frac{m}{m_2}\right)^2$, and ratio

of thermal diffusion to mutual diffusion $k_T = \frac{L_{1q}}{L_{11}} \beta \frac{m_2}{m}$, where partial molar volume

of the mixture $V = \frac{m}{\rho} = \frac{1}{n}$, we have

$$L_{11} = X_1 X_2 n D_m \left(\frac{m_2}{m}\right)^2, \quad (22)$$

$$L_{12} = -X_1 X_2 n D_m \left(\frac{m_2}{m}\right)^2 \frac{m_1}{m_2}, \quad (23)$$

$$L_{1q} = L_{q1} = L_{11} k_T \frac{1}{\beta} \frac{m}{m_2} = X_1 X_2 k_T n D_m \frac{1}{\beta} \frac{m_2}{m}, \quad (24)$$

$$L_{q2} = X_1 X_2 k_T D_m n \frac{1}{\beta} \frac{m_1}{m}. \quad (25)$$

Substituting equations (22) and (23) into equation (5) and using equation (12), it yields that

$$\begin{aligned} \bar{J}_1 &= -[L_{11} \nabla(\beta\mu_1) + L_{12} \nabla(\beta\mu_2)] + L_{1q} \nabla\beta \\ &= -X_1 X_2 n D_m \left(\frac{m_2}{m}\right)^2 \{\beta(V_1 \nabla p - h_1 \nabla \ln T) + \alpha_D \nabla \ln X_1 \\ &\quad - \frac{m_1}{m_2} [\beta(V_2 \nabla p - h_2 \nabla \ln T) + \alpha_D \nabla \ln X_2]\} - X_1 X_2 k_T n D_m \frac{m_2}{m} \nabla \ln T \\ &= -X_1 X_2 n D_m \frac{m_2}{m} \left\{ \alpha_D \nabla X_1 \frac{m_2}{m} \left(\frac{1}{X_1} + \frac{m_1}{m_2} \frac{1}{X_2}\right) + \beta \frac{m_1 m_2}{m} \left[\left(\frac{V_1}{m_1} - \frac{V_2}{m_2}\right) \nabla p + \left(\frac{h_2}{m_2} - \frac{h_1}{m_1}\right) \nabla \ln T\right] \right\} \\ &\quad - X_1 X_2 k_T n D_m \frac{m_2}{m} \nabla \ln T \\ &= -X_1 X_2 n D_m \frac{m_2}{m} \left\{ \frac{\alpha_D \nabla X_1}{X_1 X_2} + \beta \frac{m_1 m_2}{m} \left[\left(\frac{V_1}{m_1} - \frac{V_2}{m_2}\right) \nabla p + \left(\frac{h_2}{m_2} - \frac{h_1}{m_1}\right) \nabla \ln T\right] - k_T \nabla \ln T \right\}. \end{aligned}$$

Denoting

$$\bar{J}_b = n D_m \left\{ \alpha_D \nabla X_1 + \beta \frac{m_1 m_2 X_1 X_2}{m} \left[\left(\frac{V_1}{m_1} - \frac{V_2}{m_2}\right) \nabla p + \left(\frac{h_2}{m_2} - \frac{h_1}{m_1}\right) \nabla \ln T\right] \right\}, \quad (26)$$

finally we have

$$\bar{J}_1 = -\frac{m_2}{m} (\bar{J}_b + X_1 X_2 k_T n D_m \nabla \ln T). \quad (27)$$

Similarly substituting equations (24) and (25) into equation (6) generates

$$\begin{aligned} \bar{q} &= -[L_{q1} \nabla(\beta\mu_1) + L_{q2} \nabla(\beta\mu_2)] + L_{qq} \nabla\beta \\ &= -\frac{k_T}{\beta} \frac{m}{m_2} [L_{11} \nabla(\beta\mu_1) + L_{12} \nabla(\beta\mu_2)] + \frac{kT}{\beta} \nabla\beta. \end{aligned}$$

$$\bar{q} = -(k_T R T) \bar{J}_b - k \nabla T \quad (28)$$

2.3 Spherically Symmetric Case

If we constrain ourselves to the spherically symmetric case and spherical coordinates are used, as illustrated in Fig. 1(a) or (b) of the situations without convection, we can significantly simplify the foregoing fundamental equations further as follows. With spherical symmetry, velocity components $v_\theta = 0$, $v_\phi = 0$, and partial derivatives $\frac{\partial}{\partial \theta} = 0$, $\frac{\partial}{\partial \phi} = 0$. Therefore, the material derivative becomes

$$\frac{D}{Dt} = \frac{\partial}{\partial t} + v_r \frac{\partial}{\partial r}, \quad (29)$$

and

$$\nabla A = \frac{\partial A}{\partial r} \bar{e}_r, \quad (30)$$

where \bar{e}_r is the unit vector in the radial direction, A can be any scalar,

$$\nabla \cdot \bar{B} = \frac{1}{r^2} \frac{\partial}{\partial r} (r^2 B_r), \quad (31)$$

where B_r is the radial component of any vector \bar{B} .

Conservation equations corresponding to Eq. (1) to (3) then become:

$$\text{Mass:} \quad \frac{\partial \rho}{\partial t} + \frac{1}{r^2} \frac{\partial}{\partial r} (\rho r^2 v_r) = 0, \quad (32)$$

$$\text{Species } i: \quad \frac{\partial \rho_i}{\partial t} + \frac{1}{r^2} \frac{\partial}{\partial r} [r^2 (\rho_i v_r + m_i J_{ir})] = 0, \quad (33)$$

$$\text{Momentum:} \quad \rho \left(\frac{\partial v_r}{\partial t} + v_r \frac{\partial v_r}{\partial r} \right) = -\frac{\partial p}{\partial r} - \frac{1}{r^2} \frac{\partial}{\partial r} (r^2 \tau_{rr}), \quad (34)$$

in which $\tau_{rr} = -\frac{4}{3} \eta \left(\frac{\partial v_r}{\partial r} - \frac{v_r}{r} \right)$,

$$\text{Energy: } \rho \left(\frac{\partial h}{\partial t} + v_r \frac{\partial h}{\partial r} \right) = \frac{\partial p}{\partial t} + v_r \frac{\partial p}{\partial r} - \frac{1}{r^2} \frac{\partial}{\partial r} (r^2 q_r) + \phi_v, \quad (35)$$

$$\text{where } \phi_v = -\frac{4}{3} \eta \left(\frac{\partial v_r}{\partial r} - \frac{v_r}{r} \right)^2.$$

Similarly to equation (14), we can also formulate the mass equation as

$$\frac{\partial n}{\partial t} + \frac{1}{r^2} \frac{\partial}{\partial r} (nr^2 v_r) = -\frac{n}{m} \frac{Dm}{Dt}. \quad (36)$$

The formulation of species equation (15), energy equation (18) and the expressions of flux in equation (27) and (28) are still applicable, except that the substantial derivative and nabla operator are calculated by equations (29) through (31) and ϕ_v takes the simplified expression as well. Now the system of equations to be solved consists of the equations (36), (34), (15), (18) with the fluxes expressed in the equations (27) and (28).

With all the fluxes expressed as spherically symmetric, the resulting system of the fundamental equations is summarized as follows, in which n , X_1 , u , T are the unknowns of the system.

$$\frac{\partial n}{\partial t} + \frac{1}{r^2} \frac{\partial}{\partial r} (nr^2 u) = -\frac{n}{m} \left(\frac{\partial m}{\partial t} + u \frac{\partial m}{\partial r} \right), \quad (37)$$

$$\rho \left(\frac{\partial u}{\partial t} + u \frac{\partial u}{\partial r} \right) = -\frac{\partial p}{\partial r} - \frac{1}{r^2} \frac{\partial}{\partial r} (r^2 \tau_{rr}), \quad (38)$$

$$\frac{\partial X_1}{\partial t} + u \frac{\partial X_1}{\partial r} = -\frac{m}{nm_2} \frac{1}{r^2} \frac{\partial}{\partial r} (r^2 J_1), \quad (39)$$

$$\begin{aligned} \rho C_p \left(\frac{\partial T}{\partial t} + u \frac{\partial T}{\partial r} \right) &= \alpha_v T \left(\frac{\partial p}{\partial t} + u \frac{\partial p}{\partial r} \right) - \frac{1}{r^2} \frac{\partial}{\partial r} (r^2 q_r) \\ &+ \phi_v + m_1 \left(\frac{h_1}{m_1} - \frac{h_2}{m_2} \right) \frac{1}{r^2} \frac{\partial}{\partial r} (r^2 J_1), \end{aligned} \quad (40)$$

where

$$\tau_{rr} = -\frac{4}{3}\mu\left(\frac{\partial u}{\partial r} - \frac{u}{r}\right), \quad (41)$$

$$\phi_v = -\frac{4}{3}\mu\left(\frac{\partial u}{\partial r} - \frac{u}{r}\right)^2, \quad (42)$$

$$J_1 = -\frac{m_2}{m}[J_b + X_1(1 - X_1)k_T nD_m \frac{1}{T} \frac{\partial T}{\partial r}], \quad (43)$$

$$q_r = -(k_T RT)J_b - k \frac{\partial T}{\partial r}, \quad (44)$$

$$J_b = nD_m \left\{ \alpha_D \frac{\partial X_1}{\partial r} + \beta \frac{m_1 m_2 X_1 (1 - X_1)}{m} \left[\left(\frac{V_1}{m_1} - \frac{V_2}{m_2} \right) \frac{\partial p}{\partial r} + \left(\frac{h_2}{m_2} - \frac{h_1}{m_1} \right) \frac{1}{T} \frac{\partial T}{\partial r} \right] \right\}. \quad (45)$$

Also needed are the exact caloric equation of state, $h_i = h_i(V, T, X_i)$, and the thermal equation of state, $p = p(V, T, X_i)$ for the mathematical closure of the system, which will be discussed in details in section 3.1.

2.4 Initial Condition and Boundary Condition at the Interface of Droplet

In this section we will discuss the initial condition and boundary condition at the interface of the droplet in general. Suppose we have a liquid spherical droplet with its radius of R_d surrounded by gas at the initial time. We can summarize the initial condition for the substance distribution as:

$r < R_d$, liquid, indicated by an index L in the following discussion;

$r > R_d$, gas, marked by an index G ;

$r = R_d$, interface between droplet and the surrounding, shown by an

index b .

If expressed in the independent variables as mentioned above, the initial physical

condition of the problem can be written as

$$u = 0;$$

$$p = p_0;$$

$$X_l = 1, T = T_1, \quad \text{for } r < R;$$

$$X_l = 0, T = T_2, \quad \text{for } r > R.$$

Although the droplet may be at critical and supercritical conditions, it has an interface at least at the initial time. The condition on the interface at initial time has to be specified. More about the influence of these conditions will be discussed later.

Since only one velocity component, v_r , exists for the radially symmetric case, it is more convenient to use u instead of v_r to denote the radial velocity in the following discussion.

The mass balance can be expressed as $(u_b^L - \frac{dR_d}{dt})\rho_b^L = (u_b^G - \frac{dR_d}{dt})\rho_b^G$. After rearranging, it becomes

$$u_b^G = \frac{\rho_b^L}{\rho_b^G} u_b^L - \frac{dR_d}{dt} \left(\frac{\rho_b^L}{\rho_b^G} - 1 \right), \quad (46)$$

Now let us consider the energy relation on the interface. On the outside interface of the droplet, the partial molar enthalpy of each species j is $h_j^G = h_j(p_b, T_b, X_{lb}^G)$, so the partial molar enthalpy of mixture is

$$h_m^G = X_{1b}^G h_1^G + X_{2b}^G h_2^G = h_2^G + (h_1^G - h_2^G) X_{1b}^G.$$

Similarly, the partial molar enthalpy on the inside interface of the droplet is $h_m^L = h_2^L + (h_1^L - h_2^L) X_{1b}^L$, where $h_j^L = h_j(p_b, T_b, X_{lb}^L)$. $h_1^G - h_1^L$ is called latent heat of evaporation of species 1 (basically the droplet), and $h_2^G - h_2^L$ is the heat of solution of

species 2 (the surrounding). So the difference in enthalpy per unit mass between the surroundings and the droplet is

$$L_b = h^G - h^L = \frac{h_m^G}{m^G} - \frac{h_m^L}{m^L},$$

where h^G and h^L are enthalpy per unit mass of surrounding and droplet, m^G and m^L are number-mean molecular weights of surrounding and droplet. The enthalpy increasing rate on the interface due to the changing droplet radius would be $-L_b \frac{dm_d}{dt}$, where m_d is the mass of the droplet. Thus the energy balance on the interface can be expressed as

$$A_d (q_b^G - q_b^L) = -L_b \frac{dm_d}{dt}, \quad (47)$$

where q_b^G and q_b^L are the heat fluxes at the gas side and the liquid side of the interface, respectively. This flux is supposed to be positive when flowing into the droplet along the radial direction. The surface area of the droplet is $A_d = 4\pi R_d^2$.

Since $\frac{dm_d}{dt}$ is unknown, let us define mass emission flux as

$$F_{ems} = -\frac{1}{A_d} \frac{dm_d}{dt}. \quad (48)$$

It can be calculated at the molecular level as

$$F_{ems} = \sum_{j=1,2} [\alpha_{cj} m_j u_{Tj} (n_{j,equil}^G - n_j^G)], \quad (49)$$

where α_{cj} are the accommodation coefficients, $n_{j,equil}^G$ is the molar concentration of species j at equilibrium, and u_{Tj} is the mean normal velocity of a molecule of species j due to thermal fluctuations.

Accommodation coefficient is defined by $\alpha_c = \frac{T_3 - T_1}{T_2 - T_1}$, where T_1 is the temperature of gas molecules striking a surface which is at a temperature of T_2 , and T_3 is the temperature of the gas molecules as they leave the surface. It is, therefore, a measure of the extent to which the gas molecules leaving the surface are in thermal equilibrium with it.

$$n_{1,equl}^G = X_{1b}^L \gamma_{1b}^L p_{sat,1}(T_b) \frac{W_1}{Z_b^G RT_b}, \quad (50)$$

where $W_1 = \phi_{1,sat} \exp\left(\int_{p_{sat,1}}^{p_b} \frac{V_1^L dp}{RT_b}\right) \frac{1}{\phi_{1,b}^G}$ and factor $Z_G = pV / (RT)$ is the compressibility. $\phi_1 = \frac{f_1}{P}$ is the fugacity coefficient, in which the fugacity f_i is defined by $d\mu_i = RT d \ln f_i$.

$$n_{2,equl}^G = \frac{\rho_b^G}{m^G} X_{2b}^L \left(\frac{\gamma_{2b}^L}{\gamma_{2b}^G}\right) \exp\left(\frac{\mu_2^{*L} - \mu_2^{*G}}{RT_b}\right). \quad (51)$$

For a perfect gas, $u_{Tj} = \left(\frac{RT}{2\pi m_j}\right)^{\frac{1}{2}}$. For a pure liquid, it can be calculated from

Eyring's theory $u_T = \frac{RT}{N_A h_p} \left(\frac{V}{N_A}\right)^{\frac{1}{3}} \exp(-\beta \Delta G_0)$, where $N_A = 6.02 \times 10^{23}$ /mole is the

Avogadro's number, $h_p = 6.62 \times 10^{-34}$ joule·sec is the Planck's constant, and ΔG_0 is the barrier height or activation energy, which can be calculated in either of the following two ways. From experimental data for correlating viscosities, we have

$$\Delta G_0 = 0.408(\Delta h_{vap} - RT)_{T=T_{nb}},$$

where T_{nb} is the temperature of normal boiling point, Δh_{vap} is the enthalpy increase per mole (latent heat) of the vaporization. Or we can get barrier height from diffusion coefficients as

$$\Delta G_0 = -\frac{1}{\beta} \ln \left[\frac{2\pi D}{a} \frac{N_A h_p}{RT} \left(\frac{N_A}{V} \right)^{\frac{1}{3}} \right],$$

where D is the diffusion coefficient and $a = \left(\frac{V}{N_A} \right)^{\frac{1}{3}}$ according to J. Harstad [P2]. It is not clear why both a and $1/a$ are kept in this expression.

As long as the interface exists, there are 9 unknowns to be determined, i.e., u_b^L , u_b^G , R_d , X_{1b}^L , X_{1b}^G , T_b , p_b , ρ_b^L , and ρ_b^G . The extra unknowns besides those not at the interface come from the difference of u , X_1 , ρ across the interface and the position of the interface in term of R_d . Correspondingly, the following relationships are needed to define them:

- 1) equation of state $p = p(\rho, T)$
- 2) conservation of mass (37)
- 3) conservation of species (15) or (39)
- 4) conservation of momentum (38)
- 5) conservation of enthalpy (18) or (40)
- 6) evaporation law (49) and surface heat flux (47), or

$$q_b^G - q_b^L = L_b F_{ems}, \quad (52)$$

where F_{ems} is calculated by equation (37).

- 7) the relation between mass emission flux F_{ems} and radius change rate $\frac{dR_d}{dt}$:

The time derivative of $m_d = \int_0^{R_d} \rho^L 4\pi r^2 dr$ is

$$\frac{dm_d}{dt} = 4\pi \rho_b^L R_d^2 \frac{dR_d}{dt} + 4\pi \int_0^{R_d} \frac{\partial}{\partial t} (\rho^L r^2) dr.$$

Considering mass equation (32), $\frac{\partial}{\partial t} (\rho r^2) = -\frac{\partial}{\partial r} (\rho r^2 u)$, we get

$$\frac{dm_d}{dt} = 4\pi R_d^2 \rho_b^L \frac{dR_d}{dt} - 4\pi \rho^L R_d^2 u_b^L = A_d (\rho^L \frac{dR_d}{dt} - \rho^L u_b^L).$$

The relation should be

$$\frac{dR_d}{dt} = u_b^L - \frac{1}{\rho_b^L} F_{ems}. \quad (53)$$

8) mass balance at the interface:

Using the equation (53), equation (46) becomes

$$u_b^G = u_b^L - \left(\frac{1}{\rho_b^G} - \frac{1}{\rho_b^L} \right) F_{ems}. \quad (54)$$

9) continuity of species flux, $\bar{J}_{lb}^G = \bar{J}_{lb}^L$. (55)

3. Implementation and Numerical Scheme

With the proper initial and boundary conditions, the system of equations (37) through (40) can be solved for unknowns X_I , n , T , and u_r with the expressions of mass and heat fluxes in equations (43) to (45). Also needed are the following properties: mixture viscosity η , heat conductivity of the mixture k , mutual diffusion D_m , the ratio of thermal diffusion to mutual diffusion k_T , and the following information related to the equations of state (EOS): thermal EOS $V_i = V_i(p, T)$, caloric EOS $h_i = h_i(p, T)$, $C_p(p, T) = (\partial h / \partial T)_{p, X}$, and $\alpha_D(p, T) = 1 + X_i(\partial \ln \gamma_i / \partial X_i)_{T, p}$.

3.1 Implementation of Equations of State

Physically, equations of state are the key issue in studying the problem concerning supercritical phenomena. To make the system of fundamental equations complete, h_1 , h_2 , and p in these equations need to be expressed in term of arguments n , u , X_I , T .

The equations of state in the present model are based on the Peng-Robinson equation of state

$$P = \frac{RT}{V-b} - \frac{a}{V(V+b)+b(V-b)}, \quad (56)$$

where $b = \frac{0.07780RT_c}{P_c}$, $a = \frac{0.45724R^2T_c^2}{P_c}[1 + f(1 - T_r^{1/2})]^2$, in which

$f(\omega) = 0.37464 + 1.54226\omega - 0.26992\omega^2$ is a function of acentric factor ω . The subscript c indicates the critical properties. $T_r = T / T_c$ is reduced temperature. This equation was developed in 1976 and has been used widely since then. The major

advantage of this equation over previous ones, like the Van der Waals or the Soave-Redlich-Kwong (SRK) equation of state, is the improvement of accuracy for liquid state. The caloric EOS will be considered first.

3.1.1 Caloric EOS

Basically, the caloric equation of state for enthalpy for species i is expressed as

$$h_i = h_i^0 + \Delta h_i, \quad (57)$$

where h_i^0 is the reference enthalpy and Δh_i is the departure function. It is necessary to note that the enthalpy of a pure component is different from the molar partial enthalpy of a species in the mixture. The enthalpy of the mixture $h_m = \sum X_i h_i + \Delta H$, where h_i is enthalpy of pure component and ΔH is the heat of mixing. In the current model, the heat of mixing is ignored, so that h_i is the same as molar partial enthalpy.

The reference enthalpy used here was proposed by J. Harstad ^[P2], which is developed by subtracting the departure function from the Cryodata exact equation of state, then curve fitting. The departure function used to get that reference enthalpy and used in (57) are derived from the Peng-Robinson equation of state with respect to an ideal gas.

The first term in equation (57), reference enthalpy h_i^0 , does not necessarily assume an ideal gas. It is evaluated by the procedure as: first, obtain the departure function Δh_i^0 using Peng-Robinson equation of state; then, use the exact equation of state from Cryodata Inc. for $h_{i,cryodata}$ to calculate h_i^0 , i.e. $h_i^0 = h_{i,cryodata} - \Delta h_i^0$; finally, curve-fit the result of h_i^0 to be used in equation (57). According to Harstad, the curve

fit agrees extremely well with the EOS from Cryodata for the range “that those EOS exist and that are of interest here”. However, a question arises to this comment that how the curve-fitting can be compared with EOS from Cryodata if the range “that are of interest here” is not in “that those EOS exist”. Harstad also summarized the advantages of this approach over NIST and Peng-Robinson equation of state: 1) Exact EOS from NIST do not cover the high temperature range; 2) No mixing rules have been developed for exact EOS; and 3) Peng-Robinson EOS has been developed for hydrocarbons and does not necessarily agree with the exact EOS for other species like H_2-O_2 . The last point suggests that there is no problem using Peng-Robinson EOS if hydrocarbons instead of oxygen and hydrogen are modeled. The results from this method show: 1) agreement with exact values within the same error range as the NIST correlations and 2) small departures from non-ideality for enthalpy.

Similar to the case of a pure component, the enthalpy for a mixture is also evaluated by departure function and reference h^0 . We can still use the Peng-Robinson EOS to calculate departure function. h^0 can be calculated through the mixing rule $h^0 = \sum X_i h_i^0$, where h_i^0 is the reference enthalpy of a pure component as discussed previously. Similar concepts and relationships can be used to calculate the entropy.

The result of curve fitting of the reference enthalpy for H_2 and O_2 is respectively

$$h_1^0 = RT(3.413 + 0.0193\sqrt{p/p_{c1}}), \quad (58)$$

$$h_2^0 = RT(3.514 + 0.0136\sqrt{p/p_{c2}}). \quad (59)$$

Generally the departure function can be obtained from pressure explicit equation of state using

$$\Delta h = -\int_{\infty}^V \left(p - \frac{RT}{V}\right) dV + T \int_{\infty}^V \left[\left(\frac{\partial p}{\partial T}\right)_V - \frac{R}{V}\right] dV + RT(Z-1), \quad (60)$$

where $Z = pV/RT$. From the Peng-Robinson equation of state (56), we have

$$\left(\frac{\partial p}{\partial T}\right)_V = \frac{R}{V-b} - \frac{1}{V(V+b) - V(V-b)} \frac{\partial a}{\partial T}, \quad (61)$$

where $\frac{\partial a}{\partial T} = -\frac{a}{T} \frac{f(\omega) \sqrt{\frac{T}{T_c}}}{1 + f(\omega) \left(1 - \sqrt{\frac{T}{T_c}}\right)}$.

Substituting equations (59) and (61) into (60),

$$\begin{aligned} \Delta h &= -RT \ln \frac{V-b}{V} + \frac{1}{2\sqrt{2}b} \ln \frac{V+b-\sqrt{2}b}{V+b+\sqrt{2}b} \left(a - T \frac{\partial a}{\partial T}\right) + TR \ln \frac{V-b}{V} + RT \left(\frac{pV}{RT} - 1\right) \\ &= \frac{1}{2\sqrt{2}b} \ln \frac{V+b-\sqrt{2}b}{V+b+\sqrt{2}b} \left(a - T \frac{\partial a}{\partial T}\right) + pV - RT. \end{aligned}$$

For each species, this can be written as

$$\Delta h_i = \frac{1}{2\sqrt{2}b_i} \ln \frac{V_i + b_i - \sqrt{2}b_i}{V_i + b_i + \sqrt{2}b_i} \left(a_i - T \frac{\partial a_i}{\partial T}\right) + p_i V_i - RT. \quad (62)$$

3.1.2 Thermal EOS

The thermal equation of state is at first an expression with the molar partial volume V as function of P , T and X_1 .

$$V = V_{PR} + \Delta V_c + \Delta V_D, \quad (63)$$

where V_{PR} is molar partial volume in the Peng-Robinson equation of state;

$\Delta V_c = \sum_i X_i \Delta V_{ci}$, in which $\Delta V_{ci} = V_{ci} - 0.3074 \frac{RT_{ci}}{P_{ci}}$, is to give the proper

compressibility factor Z_c for the pure limits; $\Delta V_D = \left(\frac{\partial h^0}{\partial p} - \frac{\partial h^p}{\partial p} \right)_{p_c, T_c}$ gives effect of

the calculated reference state, in which superscript p refers to perfect gas while 0

refers to actual reference state. The last modification term ΔV_D corresponds to the

technique when the reference state is not an ideal gas. Note that both modification

terms are only related to the mixture composition instead of functions of pressure and

temperature. But, the hidden problem is the mixing rule of critical properties, which

has not yet been well established yet. The only recourse is an empirical

approximation. We have the general thermodynamic relation $\left(\frac{\partial H}{\partial p} \right)_T = V - T \left(\frac{\partial V}{\partial T} \right)_p$.

The form of ΔV_D comes from assuming that $\left(\frac{\partial V}{\partial T} \right)_p$ is the same. To estimate ΔV_D ,

considering $\frac{\partial h^p}{\partial p} = 0$ for perfect gas and supposing C_p is constant with respect to T ,

substitute (11) into ΔV_D , we get

$$\Delta V_D = \left(\frac{0.0193RT_{c1}}{2\sqrt{P_{c1}}} X_1 + \frac{0.0136RT_{c2}}{2\sqrt{P_{c2}}} X_2 \right) \frac{T_c}{\sqrt{P_c}} \quad (64).$$

Using the Peng-Robinson equation of state (56), equation (63) is rearranged as

pressure-explicit form

$$p = \frac{RT}{V - \Delta V_c - \Delta V_D - b} + \frac{a}{(V - \Delta V_c - \Delta V_D)^2 + 2b(V - \Delta V_c - \Delta V_D) - b^2}. \quad (65)$$

Equation (65) is used for mixture, so the critical properties in coefficients a and b are of the mixture, which will be discussed in next section. The partial pressure in (62) will be $p_i = X_i p$.

The EOS for fugacities ϕ is also based on the Peng-Robinson EOS. It is discussed in detail in the next section where it is used to determine the coefficient α_D .

3.2 Physical Properties of Specific Species

The species studied in this work are H_2 and O_2 , denoted as species 1 and 2 respectively. To actually carry out the computation, it is necessary to evaluate the physical properties of the substances appearing in the fundamental equation. Some basic information for hydrogen and oxygen is listed in appendix 1. The purpose of this section is to describe these properties as functions of pressure and temperature, and of the components, i.e., the mixing rules.

3.2.1 Critical Properties

The critical properties of H_2 and O_2 used in the model are listed here.

Species	Pressure (atm)	Temperature ($^{\circ}$ C)	Density (g/cc)
H_2	12.8	-239.9	0.0310
O_2	49.7	-118.8	0.430

The pseudo-critical temperature T_{Pc} and pressure p_{pc} are applied instead of true critical properties for the mixture, since the representations are much more simple while resulting in a considerable improvement of correlation ^[B16]. Pseudo-critical temperature is give by Kay as

$$T_{Pc} = \sum X_i T_{ci} . \quad (66)$$

Pseudo-critical pressure is calculated in this model with the modified Prausnitz-Gunn relation.

$$p_{pc} = \frac{RT_{pc} \sum X_i Z_{ci}}{\sum X_i V_{ci}}, \quad (67)$$

where the critical compressibility factor may be estimated by using Kay-type relation.

$$Z_{cm} = \sum X_i Z_{ci}. \quad (68)$$

3.2.2 Diffusivity

To use any numerical values for the mutual diffusivity D_m in the model, the following question needs to be answered first, i.e., what is the relation between D_m defined in the previous section as

$$D_m = L_{11} \frac{V}{X_1 X_2} \left(\frac{m}{m_2} \right)^2, \quad (69)$$

and the available tabulated values of diffusion coefficients such as in R. H. Perry's handbook ^[B16]?

Using the general expression of mass flux (5) and the definition of D_m (69), it can be verified first that D_m has dimensions of $[L^2T^{-1}]$, which are the same as those of the ordinary diffusion coefficient, or D_{AB} and D_{ij} in equations (16.2-3) and (18.4-8) in *Transport Phenomena* by R. B. Bird et al. ^[B3]

$$\vec{J}_{Ay} = -D_{AB} \frac{d}{dy}(\rho_A). \quad (70)$$

$$\vec{J}_i^{(x)} = \frac{c^2}{\rho RT} \sum_{j=1}^n M_i M_j D_{ij} [x_j \sum_{\substack{k=1 \\ k \neq j}}^n \left(\frac{\partial \bar{G}_j}{\partial x_k} \right)_{T,p,x_s, s \neq j,k} \nabla x_k]. \quad (71)$$

The lower case \vec{j} indicates mass flux relative to the mass-average velocity. Thus, $\vec{j}_i = m_i \vec{J}_i$, where m_i is the molecular weight of the i th species. The upper case M in equation (71) is the same as the lower case m in the previous sections. Lower case x_j is the same as X_j as well. c is the same as $n = \rho/m$. The superscript (x) describes ordinary diffusion, excluding pressure diffusion, forced diffusion and thermal diffusion (Soret effect) in the total mass flux for a multicomponent system. \bar{G}_j is the partial molar free enthalpy, or the chemical potential μ_j . If only the ordinary diffusion is considered, equation (71) can be written for a binary system as

$$\vec{j}_1 = \frac{c^2}{\rho RT} (M_1 M_1 D_{11} x_1 \nabla \mu_1 + M_1 M_2 D_{12} x_2 \nabla \mu_2). \quad (72)$$

Equations (18.4-12), i.e., $D_{ii} = 0$ and (18.4-13), i.e.

$\sum_{i=1}^n \{M_i M_h D_{ih} - M_i M_k D_{ik}\} = 0$ of Bird's book ^[B3] are equivalent to $D_{11} = 0$ and

$D_{12} = D_{21}$ in the current application. Thus, equation (72) becomes

$$\vec{J}_1 = \frac{c^2}{\rho RT} M_2 D_{12} x_2 \nabla \mu_2 = \frac{\rho}{m^2} \beta m_2 D_{12} X_2 \nabla \mu_2. \quad (73)$$

When the temperature gradient is absent, or $\nabla \beta = 0$, equation (5) can be written as $\vec{J}_1 = -L_{11} \beta \nabla \mu_1 - L_{12} \beta \nabla \mu_2 = -L_{11} \beta (1 + \frac{X_1 m_1}{X_2 m_2}) \nabla \mu_1$, through considering

Gibbs-Duhem relation $X_1 d\mu_1 + X_2 d\mu_2 = 0$, or $\nabla \mu_2 = -\frac{X_1}{X_2} \nabla \mu_1$. Substituting the

definition of D_m (27), we have

$$\begin{aligned}\bar{J}_1 &= -\frac{X_1 X_2}{V} \left(\frac{m_2}{m}\right)^2 D_m \beta \left(1 + \frac{X_1 m_1}{X_2 m_2}\right) \left(-\frac{X_2}{X_1}\right) \nabla \mu_2 \\ &= \frac{\rho}{m^2} \beta m_2 D_m X_2 \nabla \mu_2\end{aligned}\quad (74)$$

Comparing (73) and (74), it can be seen that D_m is identical to diffusivity D_{12} based on free energy force. This diffusivity is the same as the ordinarily used binary diffusivity \mathcal{D}_{12} documented in experiments for ideal solutions (i.e., activity proportional to mole fraction). To get (74), relations $V = \frac{1}{n} = \frac{m}{\rho}$ and $m = X_1 m_1 + X_2 m_2$ are used.

So the ordinary diffusivity of H_2 - O_2 system is D_m in the present model. There are many methods to predict diffusivities in gas or liquid. A generally applicable formula is not available. Furthermore, mutual diffusion of components could actually stop in a system under supercritical condition. At temperature of 0°C and pressure of 1 atm, the diffusivity of the H_2 - O_2 pair (gas) is $D_{12} = 0.697$ cm²/sec. This, in conjunction with a linear relation to temperature, is used in this model to determine diffusivity,

$$\frac{D_m \eta_m}{T} = \text{constant},$$

where η_m is in centipoise, T is absolute temperature in °K, and D_{12} is in cm²/sec. This equation was originally used to adjust data for diffusivity in liquid and η_m is solution viscosity. The value of η_m and its relation with temperature will be discussed in the next section.

3.2.3 Thermal-To-Mutual Diffusion Ratio

Let us consider the term of Soret effect in equation (5), i.e., $\bar{J}_1^{(T)} = L_{1q} \nabla \beta$.

With the definition of thermal-to-mutual diffusion ratio k_T from section 2.2.2

$$k_T = \frac{L_{1q}}{L_{11}} \beta \frac{m_2}{m}, \quad (75)$$

the following equation can be derived

$$\begin{aligned} \bar{J}_1^{(T)} &= -\beta L_{1q} \nabla \ln T \\ &= -\beta k_T \frac{L_{11}}{\beta} \frac{m}{m_2} \nabla \ln T \\ &= -k_T X_1 X_2 n D_m \left(\frac{m_2}{m}\right)^2 \frac{m}{m_2} \nabla \ln T \\ &= -k_T X_1 X_2 n D_m \frac{m_2}{m} \nabla \ln T \end{aligned} \quad (76)$$

From (18.4-11) of [B3], we have $\bar{J}_i^{(T)} = -D_i^T \nabla \ln T$. A “thermal diffusion ratio” k_T is defined as $k_T = (\rho / c^2 M_A M_B) \times (D_A^T / D_{Ab})$ for a binary system. To show the difference of this “thermal diffusion ratio” from the above used k_T in equation (5), it is denoted as $(k_T)_{Bird} = \frac{\rho}{n^2 m_1 m_2} \frac{D_1^T}{D_{12}}$. Then

$$\bar{J}_1 = -\frac{1}{m_1} (k_T)_{Bird} \frac{n^2 m_1 m_2}{\rho} D_{12} \nabla \ln T = -(k_T)_{Bird} n D_{12} \frac{m_2}{m} \nabla \ln T \quad (77)$$

Considering $D_m = D_{12}$ leads to $k_T = \frac{(k_T)_{Bird}}{X_1 X_2}$ by comparing (76) and (77). In

other words, the thermal-to-mutual ratio k_T in this model is actually the “thermal diffusion factor” α defined by Bird et al [B3], instead of the “thermal diffusion ratio”

$(k_T)_{Bird}$. α is almost independent of species concentration for gases. In table 18.4-1 of [B3], experimental thermal diffusion ratios are given for some liquids and gases, among which the most similar components with O_2-H_2 are N_2-H_2 . These values are at the temperature of 264 °K. The corresponding k_T are calculated and presented in the following table.

$X_A (N_2)$	$(k_T)_{Bird}$	K_T
0.294	0.0548	0.264
0.775	0.0663	0.380

According to these results, an approximation of $k_T = 0.3$ is used in the implementation of this model.

However, the partition of diffusion as ordinary and thermal portion is arbitrary to some extent, depending on the choice of the driving force. Different driving forces and reference velocities are also used by some researchers for multi-component flux equation, but most of the answers are of very limited value [B-6].

3.2.4 Viscosity

The viscosity η of the mixture is also needed in this model. Although comprehensive research has been conducted and considerable data and formulas are available for viscosities of liquids and gases, little is known of the viscosity near critical condition. It is even more difficult for a mixture of multiple species. A relatively simple form of correlation is used in this model to calculate the viscosity of mixture, i.e.,

$$\eta_m = \frac{\sum X_i \eta_i (m_i)^{\frac{1}{2}}}{\sum X_i (m_i)^{\frac{1}{2}}} \quad (78)$$

It should be mentioned that this equation was developed for a low-pressure gas mixture, and has a larger deviation for mixture containing much H_2 . In general, it is impossible to relate the viscosity of a liquid mixture to the pure-component viscosities alone. Equation (78) is satisfactory in this preliminary implementation.

Even the viscosities of pure species used in (78) are still strong functions of the species and thermodynamic condition. Although no general formula is available, a computerized diagram based on R. H. Perry's handbook ^[B16] has been developed to calculate the viscosities of various substances at different temperatures and 1 atm pressure, shown in Appendix 3. The effect of pressure on gas viscosity becomes significant only for pressures exceeding 10 atm. For liquid, the effect of pressure is rarely significant for pressures less than about 40 atm. The pressure effect is neglected in the current stage of model development.

3.2.5 Thermal Conductivity

In section 2.2.2, thermal conductivity is defined as:

$$k = \frac{L_{qq}}{RT^2} = \frac{\beta L_{qq}}{T} . \quad (79)$$

Comparing the second term in equation (28) and Fourier's law, $\vec{q} = -k\nabla T$, it can be seen that k in equation (79) is just the conventional coefficient of heat conductivity. R

$= 8.3144 \text{ kg m}^2\text{sec}^{-1}\text{mole}^{-1}\text{K}^{-1}$ is the universal gas constant¹ as used in the equation of state of ideal gas $p = nRT$.

Similar to diffusivity, different formulas to calculate thermal conductivity of liquid and gas are applicable to different situations. Regarding thermal conductivity, especially for gas, considerable knowledge is available in literature. For instance, the effect of pressure is small for liquids, but often significant for gases if the pressure is larger than a few atmospheres. Nevertheless, the theoretical background of actual methods is not convincing for the case in hand. The following equation, which was developed for a gas mixture, is chosen to evaluate thermal conductivity of mixture from individual component conductivity [B-16].

$$k_m = \frac{\sum X_i k_i (m_i)^{\frac{1}{3}}}{\sum X_i (m_i)^{\frac{1}{3}}} \quad (80)$$

Linear function fitting from tabulated experimental data is used to get conductivities for pure components H_2 and O_2 . Considering the initial temperature range of the current practice, we use the data at temperatures of 100, 150, 200, 250, 300 °K.

	100 °K	150 °K	200 °K	250 °K	300 °K
H_2	6.7	10.1	13.1	15.7	18.3
O_2	0.93	1.38	1.83	2.26	2.66

¹ The “mole” in this unit is “g-mole”, not “kg-mole”, which may be used in other references. Reference [B3] denotes the two in explicit different forms. Avogadro’s number is $N = 6.023 \times 10^{23}$ molecules g-mole⁻¹. If the molecular weight of a gas is M , one g-mole of it is M g, while one kg-mole of it is M kg. In other words, one g-mole is 6.023×10^{23} in number, while one kg-mole is 6.023×10^{26} . Or 1kg-mole = 1000 g-mole.

The unit is $\text{W/m}^2\text{K}\times 10^{-4}$ in the above table. Fitting with respect to temperature T with minimum absolute deviation, the results are:

$$k_1 = 2.289 + 0.053T, \quad (81)$$

$$k_2 = 0.043 + 0.009T. \quad (82)$$

The details are given in Appendix 4.

3.2.6 Coefficient α_D

The coefficient α_D defined in section 2.1.4 denotes the effect of non-ideality of the mixture, i.e.,

$$\alpha_D = 1 + X_i \frac{\partial \ln \gamma_i}{\partial X_i} = 1 + \frac{\partial \ln \gamma_i}{\partial \ln X_i} = 1 + \frac{\partial \ln \phi_i}{\partial \ln X_i}, \quad (83)$$

where γ_i is activity coefficient and ϕ_i is fugacity coefficient. Considering the similar correction (63) with molar partial volume, fugacity coefficient of i component in the mixture satisfies

$$\ln \phi_i = (\ln \phi_i)_{P-R} + \frac{p}{RT} \Delta V_{ci} + \frac{1}{R} \left[\left(\frac{h_i^0}{T} - s_i^0 \right) - \left(\frac{h_i^0}{T_{ci}} - s_i^0 \right)_{P_{ci}, T_{ci}} \right], \quad (84)$$

where $(\ln \phi_i)_{P-R}$ can be obtained from the following general formula with the Peng-Robinson equation plugged in it.

$$\ln \phi_i = - \int_{\infty}^V \left(\left[\frac{\partial (nZ)}{\partial n_i} \right]_{T, n_j, j \neq i} - 1 \right) \frac{dV}{V} - \ln Z, \quad (85)$$

where Z is for mixture.

Using the Peng-Robinson equation of state (56),

$$nZ = n \frac{pV}{RT} = \frac{1}{V-b} - \frac{a}{RT} \frac{1}{V^2 + 2bV - b^2}.$$

Considering $V = \frac{1}{n} = \frac{1}{n_1 + n_2}$, $\frac{\partial V}{\partial n_1} = -\frac{1}{n^2} = -V^2$,

$$\frac{\partial(nZ)}{\partial n_1} = -\frac{1}{(V-b)^2}(-V^2 - \frac{\partial b}{\partial n_1}) - \frac{\alpha}{RT} \left[-\frac{1}{(V^2 + 2bV - b^2)^2} \right] [(2V + 2b)(-V^2) + (2V - 2)b \frac{\partial b}{\partial n_1}]$$

$$- \frac{\partial \alpha}{\partial n_1} \frac{1}{RT} \frac{1}{V^2 + 2bV - b^2}$$

where $\frac{\partial b}{\partial n_1} = 0.07780R \frac{\partial}{\partial n_1} \left(\frac{T_c}{p_c} \right)$, $\frac{\partial a}{\partial n_1} = 0.45724R^2 [1 + f_\omega (1 - T_r^{\frac{1}{2}})]^2 \frac{\partial}{\partial n_1} \left(\frac{T_c^2}{p_c} \right)$. In

the derivative of a , reduced temperature T_r is assumed independent to n_1 for simplicity. Using pseudo-critical properties of mixture in section 3.2.1 instead of true critical properties generates

$$\frac{\partial}{\partial n_1} \left(\frac{T_c}{p_c} \right) = \frac{\partial}{\partial n_1} \left(\frac{\sum X_i V_{ci}}{R \sum X_i Z_{ci}} \right) = \frac{\partial}{\partial n_1} \left(\frac{\sum n_i V_{ci}}{R \sum n_i Z_{ci}} \right)$$

$$= \frac{V_{c1}}{R \sum n_i Z_{ci}} - \frac{\sum n_i V_{ci}}{R (\sum n_i Z_{ci})^2} Z_{c1},$$

$$\frac{\partial}{\partial n_1} \left(\frac{T_c^2}{p_c} \right) = \frac{\partial}{\partial n_1} \left(\frac{\sum X_i T_{ci} \sum X_i V_{ci}}{R \sum X_i Z_{ci}} \right)$$

$$= \sum X_i T_{ci} \left[\frac{V_{c1}}{R \sum n_i Z_{ci}} - \frac{\sum n_i V_{ci}}{R (\sum n_i Z_{ci})^2} Z_{c1} \right] + \frac{\sum X_i V_{ci}}{R \sum X_i Z_{ci}} \left(\frac{T_{c1}}{n} - \frac{\sum n_i T_{ci}}{n^2} \right).$$

In the second and third terms on the right-hand side of (84), no X_I is involved, so

$$\frac{\partial \ln \phi_1}{\partial X_1} = - \left\{ \left[\frac{\partial(nZ)}{\partial n_i} \right]_{T, n_j, j \neq i} - 1 \right\} \frac{1}{V} \frac{\partial V}{\partial X_1} - \frac{\partial \ln Z}{\partial X_1}$$

$$= - \left\{ \frac{1}{(V-b)^2} (V^2 + \frac{\partial b}{\partial n_1}) - \frac{\alpha}{RT} \frac{2}{(V^2 + 2bV - b^2)^2} [(V+b)(V^2) + (V-b) \frac{\partial b}{\partial n_1}] \right.$$

$$\left. - \frac{\partial \alpha}{\partial n_1} \frac{1}{RT} \frac{1}{V^2 + 2bV - b^2} - 1 \right\} \frac{1}{V} \frac{\partial V}{\partial X_1} - \frac{1}{Z} \frac{p}{RT} \frac{\partial V}{\partial X_1}$$

Using equations (63) and (64), and taking the coefficients a and b in the Peng-Robinson equation to be constant with respect to X_1 for simplicity, we have

$$\frac{\partial V}{\partial X_1} = \Delta V_{c1} + \frac{0.0193RT_{c1}}{2p_{c1}} = V_{c1} - 0.3074 \frac{RT_{c1}}{p_{c1}} + \frac{0.0193RT_{c1}}{2p_{c1}} = \frac{m_1}{\rho_{c1}} - \frac{0.29775RT_{c1}}{p_{c1}}.$$

Finally,

$$\alpha_D = 1 - \left\{ \frac{1}{(V-b)^2} \left(V^2 + \frac{\partial b}{\partial n_1} \right) - \frac{\alpha}{RT} \frac{2}{(V^2 + 2bV - b^2)^2} [(V+b)(V^2) + (V-b) \frac{\partial b}{\partial n_1}] \right. \\ \left. - \frac{\partial \alpha}{\partial n_1} \frac{1}{RT} \frac{1}{V^2 + 2bV - b^2} \right\} \frac{X_1}{V} \left(\frac{m_1}{\rho_{c1}} - \frac{0.29775RT_{c1}}{p_{c1}} \right), \quad (86)$$

where

$$\frac{\partial b}{\partial n_1} = 0.07780 \frac{1}{n_1 Z_{c1} + n_2 Z_{c2}} \left[V_{c1} - \left(\frac{n_1 V_{c1} + n_2 V_{c2}}{n_1 Z_{c1} + n_2 Z_{c2}} \right) Z_{c1} \right] = 0.07780 \frac{X_2 (V_{c1} Z_{c2} - V_{c2} Z_{c1})}{(X_1 Z_{c1} + X_2 Z_{c2})^2},$$

$$\frac{\partial a}{\partial n_1} = 0.45724R \left[1 + f_\omega (1 - T_r)^{\frac{1}{2}} \right]^2 [(X_1 T_{c1} + X_2 T_{c2}) \frac{X_2 (V_{c1} Z_{c2} - V_{c2} Z_{c1})}{(X_1 Z_{c1} + X_2 Z_{c2})^2} \\ + \frac{X_1 V_{c1} + X_2 V_{c2}}{X_1 Z_{c1} + X_2 Z_{c2}} \frac{X_2}{n} (T_{c1} - T_{c2})].$$

3.2.7 Thermal expansion ratio

Information for the thermal expansion ratio, or coefficient of expansion,

$\alpha_v = \frac{1}{V} \left(\frac{\partial V}{\partial T} \right)_p$ is available ^[B14] for H_2 and O_2 . At an initial pressure of 760 mm Hg,

they are 3660.3×10^{-6} and 3674×10^{-6} respectively. At 1095 mm Hg, it is 3659.0×10^{-6}

for H_2 . At 1000 mm Hg, it is 3676.3×10^{-6} for O_2 . But for a mixture, no experimental

data is available, so it is estimated with the formula of Smith et al. ^[B14] as

$$\alpha_v = \frac{0.04314}{(T_c - T)^{0.641}},$$

where T_c will be replaced by the pseudo-critical temperature T_{Pc} (66) of the mixture in the present model.

3.2.8 Acentric Factor

An acentric factor ω is used in the Peng-Robinson equation of state. It is defined as

$$\omega = -\log_{10}(p_r^{sat})_{T_r=0.7} - 1.000, \quad (87)$$

where $p_r^{sat} = p^{sat} / p_c$ is reduced vapor pressure, $T_r = T / T_c$ is reduced temperature.

At $T_r = 0.7$, actual temperature $T = T_r T_c = 0.7 T_c$.

For H_2 , $T = 0.7 T_c = 0.7(-239.9+273.15) \text{ K} = 23.275 \text{ K} = -249.875 \text{ }^\circ\text{C}$. From reference [B14], $p^{sat} = 2\text{atm}$ at $T = -250.2 \text{ }^\circ\text{C}$, and $p^{sat} = 5\text{atm}$ at $T = -246.0 \text{ }^\circ\text{C}$.

Using linear interpolation, we get $(p^{sat})_{T_r=0.7} = 2.2321 \text{ atm}$,

$$(p_r^{sat})_{T_r=0.7} = 2.2321 \text{ atm} / 12.8 \text{ atm} = 0.1744.$$

Substituting into equation (87), the value of the acentric factor is obtained as

$$\omega_1 = -0.2415.$$

Similarly for O_2 , $T = 0.7 T_c = 0.7(-118.8+273.15) \text{ K} = 108.045 \text{ K} = -165.105 \text{ }^\circ\text{C}$. Interpolating between $p^{sat} = 2\text{atm}$ at $T = -176.0 \text{ }^\circ\text{C}$ and $p^{sat} = 5\text{atm}$ at $T = -164.5 \text{ }^\circ\text{C}$, we get $(p^{sat})_{T_r=0.7} = 4.8422 \text{ atm}$, $(p_r^{sat})_{T_r=0.7} = 4.8422 \text{ atm} / 49.7 \text{ atm} = 0.09743$.

Finally, the acentric factor becomes $\omega_2 = 0.01132$.

For a mixture, the following evaluation of the acentric factor is used in the Peng-Robinson equation of state.

$$\omega = -\log_{10}(X_1 P_{r1}^{sat} + X_2 P_{r2}^{sat})_{T_{Pr}=0.7} - 1.000$$

T_{Pr} is a function of X_1 , so P_{ri}^{sat} must be evaluated by interpolation. Since T_{Pr} must be between T_{r1} and T_{r2} , P_{ri}^{sat} is also between 2 atm and 5 atm as in the previous case of single component.

3.2.9 Heat Capacity

The model of constant-pressure heat capacity $C_p = \left(\frac{\partial H}{\partial T}\right)_p$ is rarely accurate at high pressure. In the present model, it is calculated with the mixing rule of enthalpy h_m as

$$C_p = \left(\frac{\partial h_m}{\partial T}\right)_{p, X_1} = X_1 \frac{\partial h_1}{\partial T} + X_2 \frac{\partial h_2}{\partial T},$$

the heat of mixture being ignored as mentioned in section 3.1.1.

From equation (57), $\frac{\partial h_i}{\partial T} = \frac{\partial h_i^0}{\partial T} + \frac{\partial \Delta h_i}{\partial T}$. It is straightforward to get from

(58) and (59) that

$$\frac{\partial h_1^0}{\partial T} = 3.413R, \quad \frac{\partial h_2^0}{\partial T} = 3.514R. \quad (88)$$

From (62), it can be derived that $\frac{\partial \Delta h_i}{\partial T} = \frac{a_i}{V_i^2 + 2b_i V_i - b_i^2} \frac{\partial V_i}{\partial T} + p \frac{\partial V}{\partial T} - R$.

Considering $V = X_1 V_1 = X_2 V_2$, we have $\frac{\partial V}{\partial T} = X_i \frac{\partial V_i}{\partial T}$. From (63), it is obvious that

$\frac{\partial V_i}{\partial T} = \frac{\partial V_{i,PR}}{\partial T}$. Taking the time derivative of the Peng-Robinson equation of state

(56),

$$0 = \frac{R}{V_i - b_i} - \frac{RT}{(V_i - b_i)^2} \frac{\partial V_i}{\partial T} + \frac{a_i(2V_i + 2b_i)}{(V_i^2 + 2b_iV_i - b_i^2)^2} \frac{\partial V_i}{\partial T}.$$

Thus,

$$\frac{\partial V_i}{\partial T} = \frac{\frac{R}{V_i - b_i}}{\frac{RT}{(V_i - b_i)^2} - \frac{a_i(2V_i + 2b_i)}{(V_i^2 + 2b_iV_i - b_i^2)^2}} = \frac{R(V_i - b_i)(V_i^2 + 2b_iV_i - b_i^2)^2}{RT(V_i^2 + 2b_iV_i - b_i^2)^2 - 2a_i(V_i + b_i)(V_i - b_i)^2}.$$

Finally,

$$\frac{\partial \Delta h_i}{\partial T} = \left[\frac{a_i}{V_i^2 + 2b_iV_i - b_i^2} + X_i p \right] \frac{R(V_i - b_i)(V_i^2 + 2b_iV_i - b_i^2)^2}{RT(V_i^2 + 2b_iV_i - b_i^2)^2 - 2a_i(V_i + b_i)(V_i - b_i)^2} - R. \quad (89)$$

3.3 Numerical Scheme

3.3.1 Computational Grid

For the spherically symmetric problem, only a one-dimensional grid is needed. A uniform interval along the radial direction will be used inside the droplet at the initial instant. Considering the variation of physical variables, a grid stretched as power function is used outside the droplet, which generates a relatively fine grid in the vicinity of the initial interface, but a coarse grid at the far field.

$$(\Delta r)_{in} = R_d / N_{in}$$

$$(\Delta r)_{i,out} = (\Delta r)_{in} (1 + \varepsilon)^{i_{out}}, \quad i_{out} = 1, 2, \dots$$

When ε is 0, it is reduced to uniform grid.

In this practice, 10 nodes are used inside the droplet with 1mm diameter. A finer grid was also tested, but no significant difference was observed in the solution.

The outside grid region has a choice for both the number of points and the size of the

solution domain. The criterion is to ensure that the disturbance from the interface will not arrive at far field during the period of interesting.

3.3.2 Finite Difference Scheme

Since more attention is focused on proving the concept of the model at this stage, the quantitative accuracy of the numerical scheme is not a key point. A simple explicit backward scheme (FTBS, forward-time-backward-space) is appropriate. This classic scheme is numerically stable for the model equation

$$\frac{\partial u}{\partial t} + a \frac{\partial u}{\partial x} = 0 \quad (a > 0), \quad (90)$$

$$\text{when } \lambda = a \frac{\Delta t}{\Delta x} \leq 1. \quad (91)$$

But, in the case of droplet evaporation, the radial velocity would not be necessarily positive everywhere. The discontinuity at the interface is also difficult to catch. To get a more stable result, an explicit Mac-Cormack two-step predictor-corrector method is used. The discretized scheme for equation (39) is:

$$\text{Predictor step: } X_i^* = X_i^j + \Delta X_i^j; \quad (92)$$

$$\text{Corrector step: } X_i^{j+1} = \frac{1}{2}(X_i^* + X_i^j + \Delta X_i^*), \quad (93)$$

$$\text{where } \Delta X_i^j = \left[-\frac{m_i^j}{n_i^j (m_2)_i^j} (\nabla J_1)_i^j - \frac{X_{i+1}^j - X_i^j}{r_{i+1} - r_i} u_i^j \right] \Delta t^j, \quad (94)$$

$$\Delta X_i^* = \left[-\frac{m_i^*}{n_i^* (m_2)_i^*} (\nabla J_1)_i^* - \frac{X_i^* - X_{i-1}^*}{r_i - r_{i-1}} u_i^* \right] \Delta t^j. \quad (95)$$

For clarity, the original subscript “1” for species is dropped. Equations (37), (38) and (40) take similar formats.

The gradients of fluxes J_1 and q_r actually result in terms of second order derivatives of the primitive variables X_1 , p , T in the difference equations. In this implementation J_1 and q are evaluated using forward differences and the gradients calculated using backward difference, resulting in a central-difference scheme for those second-order derivatives. Take q as an example. From equations (44) and (45),

$$q_i = -k_T RT_i (J_b)_i - k \frac{T_{i+1} - T_i}{r_{i+1} - r_i}, \quad (96)$$

where

$$(J_b)_i = n_i (D_m)_i \left\{ (\alpha_D)_i \frac{X_{i+1} - X_i}{r_{i+1} - r_i} + \frac{1}{RT_i} \frac{1}{m_i} \left[\left(\frac{m_2 X_2 - m_1 X_1}{n} \right)_i \frac{p_{i+1} - p_i}{r_{i+1} - r_i} + (X_1 X_2)_i (m_1 h_2 - m_2 h_1)_i \frac{T_{i+1} - T_i}{r_{i+1} - r_i} \frac{1}{T_i} \right] \right\}. \quad (97)$$

The second order derivative in the viscous stress $\frac{\partial^2 u}{\partial r^2}$ is discretized by

$$\frac{2}{(r_{i+1} - r_i)} \left[\left(\frac{u_{i+1} - u_i}{r_{i+1} - r_i} \right) - \left(\frac{u_i - u_{i-1}}{r_i - r_{i-1}} \right) \right].$$

The first order of u in the dissipation of energy

$$\text{equation is discretized as } \frac{1}{2} \left[\left(\frac{u_{i+1} - u_i}{r_{i+1} - r_i} \right) + \left(\frac{u_i - u_{i-1}}{r_i - r_{i-1}} \right) \right].$$

They are standard central

difference when the grid is uniform, $u_{i+1} - u_i = u_i - u_{i-1}$.

Referring to (91), the time step size is chosen as

$$\Delta t = 0.5 \frac{(\Delta r)_{\min}}{|u|_{\max} + a_{\max}}. \quad (98)$$

Because this is not a strict derivation, the speed of sound is only roughly estimated as

$$\text{if it is in the air } a_{\max} = \sqrt{1.4 p_{\max} / \rho_{\min}}.$$

A complete explicit method is used here. In spite of all its drawbacks, it seems necessary with need to model all the various coefficients. The time-proceeding computational procedure is outlined here.

- 1) Give initial condition in pressure p , temperature T , mole fraction X_I , velocity u and geometry.
- 2) Use the thermal equation of state (63) to get another major variable during solution, molar concentration n . Since Peng-Robinson is not V explicit, a numerical method to solve V from p and other variables is important. See Appendix 2.
- 3) Calculate time step size.
- 4) Solve fundamental equations (37) through (40) using two-step prediction-correction to get n , u , X_I and T at new time step. Solve (39) to get X_I and $\frac{\partial X_I}{\partial t}$ at first in each iteration, as it will be used in (37).
- 5) Calculate p from equation (65) for use of next time step.
- 6) Output result at specified time step.
- 7) Repeat from step 3).

3.3.3 Formulation of Pressure

Since pressure p is one of the major driving forces in the whole procedure, and the finite difference form of its derivative is important to the result. When calculating mass and heat fluxes, a forward difference is used. For the spatial difference in the energy equation, it takes a central-difference form:

$$\left(\frac{\partial p}{\partial r}\right)_i = \frac{1}{2} \left[\left(\frac{p_{i+1} - p_i}{r_{i+1} - r_i}\right) + \left(\frac{p_i - p_{i-1}}{r_i - r_{i-1}}\right) \right]. \quad (99)$$

Pressure p depends on other major unknowns n , u , X_I , and T through the equations of state in a complicated way. It is very difficult to evaluate p from EOS (65) accurately. Especially for the liquid state (in fact “incompressible”) or the state of high temperature (above critical point) but low n , the deviation of p calculated from n could be significant to the result. To improve the computation, $\Delta p = p - p_0$, where p_0 is the initial value of the pressure, is updated instead of p in each time step.

3.3.4 Artificial Viscosity

The discontinuity at an interface needs to be dealt with, at least at the initial instant. Artificial viscosity is applied to catch the discontinuity better.

$$(\Delta X)_{i,modified} = (\Delta X)_i + c(X_{i+1} - 2X_i + X_{i-1}). \quad (100)$$

The same forms are used in all four fundamental equations. The coefficient c is chosen around 0.005, but the coefficient used in the momentum equation must be 100 times larger than the other 3 equations to obtain a stable result. A possible reason is that since the velocity u in this problem is actually around zero, oscillation even in a limited range would overrun the physical change of velocity.

3.3.5 Numerical Model of the Surface

There are at least two ways to treat the interface numerically. The first is to solve the two separated regions inside and outside the interface, whenever it exists, and use the boundary condition at the surface to patch them together. The obvious problem with this approach is when the interface does not exist, e.g., when the droplet surface is heated over the critical point, or when the existence of the interface is

unknown, the solution will subsequently fail. The second and preferable choice is to consider the interface as part of the solution and the whole region is treated as one solution domain. The problems to be addressed in such an approach include: determining whether the interface or discontinuity of density exists; identifying the moving of the interface or the radius regression if the interface does exist; using the latent heat relation instead of the energy equation in the system when phase transition occurs.

When the surface is between node i and $i + 1$, the conditions (52) through (55) will be cast in the following form:

$$q_{i+1} - q_i = L_b F_{ems} \quad (101)$$

$$\frac{dR_d}{dt} = u_i - \frac{1}{\rho_i} F_{ems} \quad (102)$$

$$u_{i+1} = u_i - \left(\frac{1}{\rho_{i+1}} - \frac{1}{\rho_i} \right) F_{ems} \quad (103)$$

$$J_i = J_{i+1}. \quad (104)$$

As one of the most interesting variables to be studied, the radius of the droplet will change (regress) continuously during the process of evaporation. Thus the surface of the droplet cannot be kept on a known grid node for a fixed grid network. To calculate F_{ems} , an interpolation of variables is made on the two nodes around the interface by using the distances as weighting factors. In practice, if the surface is very close to a node, say i , we always suppose it is between i and $i+1$. In other words, we suppose node i is inside the droplet, or on the surface, to avoid possible ambiguity in the formulation. As for the variables like mass and heat fluxes at the node near the surface, it is more reasonable to evaluate these terms from neighbor nodes on the

same side with itself. At next time step, the interface condition will move to a new interval of nodes when the solution indicates it should do so.

Besides the detection and moving of interface, it is nontrivial to compute F_{ems} . It is an extra unknown, and not determined by the equilibrium physical properties, although we are using thermodynamic properties based on an equilibrium approximation.

4. Results of Numerical Experiments

4.1 EOS and Properties

4.1.1 Equations of State

Basically, the EOS in this model is a modified Peng-Robinson EOS. The Peng-Robinson EOS is a widely used cubic EOS. Figure 6 is a graphical representation of this equation for the case of concentration $X_1=0$ (pure oxygen). The eleven curves, respectively, correspond to the temperatures $T = 59.75, 78.67, 97.59, 116.51, 135.43, 154.35, 173.27, 192.19, 211.11, 230.03,$ and 248.95 °K. The 6th curve displays the result at the critical temperature 154.35 °K. Actually the pattern of these curves is very close to that of Van der Waals EOS. While it may describe both the liquid and gas phases, the region of phase change has to be inserted artificially, as shown in figure 7. Then figures 8 and 9 show the result for pure hydrogen, at the temperature of $19.05, 21.89, 24.73, 27.57, 30.41, 33.25, 36.09, 38.93, 41.77, 44.61,$ and 47.45 °K. Figures 10 and 11 present the results for a mixture of equal molar concentrations of O_2 and H_2 ($X_1=0.5$), at the temperature of $39.40, 50.28, 61.16, 72.04, 82.92, 93.80, 104.68, 115.56, 126.44, 137.32,$ and 148.20 K. Figure 12 shows the result when the EOS is in explicit form of volume (getting v from p), using the same EOS as figure 6. It seems trivial since the curves are the same as figure 7, but it is important and non-trivial to solve for the volume from the EOS. See appendix 2 for the numerical method to solve the equation.

In the present implementation, pressure can be computed as a function of temperature, molar volume and species concentration X_1 , through different types of

EOS's which have been incorporated in the model and can be chosen by a flag variable in the code. EOSs include the Van der Waals, Peng-Robinson, and Peng-Robinson with phase-changing region inserted. Also there is a choice as to whether to include the volume modification.

Figures 13 and 14 show the effect of species concentration X_1 on the molar concentration n and density ρ of the mixture, in which temperature is given at $T=200$ °K and pressure $P = 1$ atm. The density's dependence on X_1 is approximately linear in the present case, but that is not necessarily always true.

Figure 15 is an enthalpy graph. In other words, it displays the caloric EOS's based on equations (88) and (89). The graph is made only for 1 atm pressure. The five curves correspond to $X_1 = 0., 0.25, 0.5, 0.75,$ and 1, respectively.

4.1.2 Heat Capacity and Viscosity

Figures 16 to 21 exhibit the specific heat C_p . Figures 16 and 17 are for pure hydrogen, 18 and 19 for pure oxygen, and 20 and 21 for a typical mixture ($X_1 = 0.5$). Two figures are made for each case since the value range at sub-critical and supercritical conditions are different in the order of magnitudes. Note that for the sub-critical case, C_p is infinite (or not defined) in the phase-transition region.

Figure 22 shows the viscosity at temperatures from 100°K to 300°K, but the pressure is fixed at one atm pressure. The five curves correspond to different hydrogen concentrations of mixture from 0 (pure O_2) to 1 (pure H_2). The curve on the top is for the case of $X_1 = 0$.

4.1.3 Other Coefficients

Figure 23 shows diffusivity at 1 atm pressure. The diffusivity evaluation has to be improved after considering the fact that gas has a much larger diffusivity than liquid, typically 10^4 times.

Figure 24 shows the thermal expansion rate, α_v , at 1 atm initial pressure. Figure 25 is for conductivity. It is not formulated as a function of pressure. Figure 26 is for the coefficient α_D plotted at 1 atm pressure, which describes the deviation from the ideal mixture.

4.2 Vaporization and Diffusion Processes

4.2.1 Typical physical and geometric condition

In the experiment of reference [P-8], the diameter of the n-Pentane droplet in nitrogen surrounding is 1800μ (1.8 mm), where the temperature is $850 \text{ }^\circ\text{R}$ (1335.65 $^\circ\text{K}$), and the pressure varies from 200 to 1400 psi (about 1.4 to 9.7 MPa). In reference [P-9], the operating conditions of three different rocket motors are listed as in the following table.

Motor Type	Condition	Fuel Injector	Oxidizer Injector	Combustor
H-1 (Saturn 1-B S-1B Stage)	Temperature (K)	297.0	90.2	3329.5
	Pressure (MPa)	5.36	5.43	4.5
F-1 (Saturn V S1-C Stage)	Temperature (K)	294.3	89.5	3546.0
	Pressure (MPa)	12.8	11.0	7.8
Space Shuttle main Engine	Temperature (K)	879.0	126.0	3700.0
	Pressure (MPa)	24.8	33.0	22.58

Critical properties of three typically involved substances are in the following table ^[P-9].

Substance	Critical Pressure (MPa)	Critical Temperature (K)
Hydrogen	1.3	33.3
Oxygen	5.04	154.4
RP-1	2.344	685.95

In a typical example, the fuel (droplet) and oxidizer (surrounding) are chosen to be H_2 and O_2 . Referring to the foregoing actual condition and considering that the present computation is focused on supercritical phenomena, the following initial parameters are typical. The radius of droplet is $r = 0.001\text{m}$. The initial pressure is $p_0 = 10\text{ atm} = 1.01325 \times 10^6\text{ N/m}^2$. The temperature is $T = 300\text{ K}$. For demonstrating the model, various parameters and configurations are tested in the next section.

4.2.2 Simulation Results

(1) Above Critical Point

The first numerical study presented here is the case beginning at an initial temperature of 200°K throughout the solution domain. Pressure is 1 atm . While pressure is low, the temperature is above the critical condition. At the initial instant, the spherical "droplet" region is occupied by pure oxygen. The outside surrounding is pure hydrogen. The oxygen sphere is actually in the gas phase, but there is a discontinuity of density and concentration at the interface. Inside the interface, the density of oxygen is 1.957kg/m^3 . Outside the interface it is 0.1219 kg/m^3 for hydrogen. Since the density difference is relatively small compared with a real liquid

droplet, and the equation of state is not used over the two-phase and transition region, the numerical solution is easier than for the case with a two-phase initial condition.

The choice of putting oxygen inside is based on the intent to extend to a higher nearly uniform initial temperature when O_2 is in liquid state and H_2 is in gas phase.

Figures 27-1 through 27-6 show the time-dependent process in which the initial distribution of temperature (27-1) changes to a valley and peak pair around the original interface between two species. Figures 27-1 to 27-6 present the distributions respectively at six computational time steps of 0, 100, 200, 500, 1000 and 2000. The corresponding physical time is respectively 0, 0.5×10^{-5} , 0.9×10^{-5} , 2.3×10^{-5} , 4.6×10^{-5} , and 9.2×10^{-5} seconds,

From analysis of the actual computation procedure cases by the model, it is revealed that the major contribution of the temperature change comes from the term for the mass flux gradient in the energy equation (4). Though initially there are no gradients of temperature and pressure, the discontinuity of species concentration combined with the difference of unit mass enthalpy results in the change of the temperature, in spite of the fact that the molar enthalpies of the two sides are actually very close to each other.

As time proceeds, the range of this valley-peak is stretched out. However, because there is still a larger gradient of concentration and unit mass enthalpy, the amplitude keeps growing at least until 0.1 millisecond.

Figures 28-1 to 28-6 show the velocity distribution at the same time sequence as in Fig. 27. The pattern of the valley-peak of velocity is more complicated than that

of temperature, but it is quite obvious that these distortions are being smeared. Basically the results show that the mixture inside the interface moves globally toward the center, while outside the interface, the global velocity is outward. The result is not surprising after considering the fact that hydrogen, which has a lower density than oxygen, diffuses inwards.

Figures 29-1 to 29-6 present the changing pressure. Although at the beginning, the pressure jump results from the temperature discontinuity and the large gradient of concentration, the pressure tends to become uniform as the time proceeds.

Figures 30-1 to 30-6 are the time sequence of the concentration distribution. It is clear from these figures that the two species are undergoing mixing. Figures 31-1 to 31-6 show the density changes, which are calculated from the results of molar concentration of mixture and mean molecular weight.

To show the results more vividly, Figs. 32 and 33 present the sequences of concentration and temperature distribution, respectively, in a photo type of image. In Fig. 32 the white color represents hydrogen and black oxygen. The grayscale shows concentration. In Fig. 33, the median gray stands for initial temperature and the lighter color shows higher temperature.

(2) Higher Pressure

Figures 34 to 38 are the results for the case at a pressure of 10 atm, which is much higher than the previous case, at the time step 2000. Figure 34 shows pressure keeps constant because either perturbation or error in this case is smaller comparing the absolute value pressure. Figure 35 displays an almost identical temperature distribution as at 1 atm. This shows that pressure has no significant direct influence

on the temperature change near the interface. The velocity change in Fig. 36 is larger than at 1 atm. The distribution of the species concentration and the density in Figs. 37 and 38 are almost the same as at 1 atm, except that density is proportionally larger.

The next numerical test is for the case of 50 atm pressure, which is above the critical pressures of both species. Pressure (Fig. 39) has a larger change near the original interface than the low-pressure case. Other parameters do not change much. Figure 40 shows a temperature “valley” that is smaller. Figure 41 shows a proportionally larger density distribution.

(3) Liquid Droplet

When the droplet is in the liquid phase, the density difference across the interface is much larger than in the gas phase. The equations of state will be used over the two-phase transition range. Since the model becomes less stable numerically, computational cases at the lower temperature in which only gas phase is involved are tested first. Figures 42, 43, and 44 show the results of density, temperature and concentration for the case of initial temperature 100°K at 500 computational time steps, while pressure is still taken at 1 atm. The procedure is then to gradually lower the initial temperature, which makes the numerical solution tend to be less stable. Figures 45, 46, and 47 show the modeling results with an initial temperature 91°K. This temperature is slightly above the boiling point of oxygen. The results from these two cases are rather similar qualitatively. Also, the only difference between these results (at initial temperature 100°K and 91°K) and the higher initial temperature case presented earlier, is that the temperature changes in a larger scale and the distribution curves are more complicated around the interface. The results shown in Figs. 48, 49

and 50 have an initial temperature 91°K for inside the droplet while outside the droplet, the temperature is 100°K . That is, there is a difference in the initial temperature of the two species. There is no significant difference in the results of these three cases. It should be mentioned that small numerical oscillations of concentration appear on the hydrogen side of the interface in all three test cases.

As the initial temperature is lowered under oxygen's boiling point, the results become quite different. The temperature changes more drastically during the mass transportation process. The artificial viscosity has to be adjusted in the numerical scheme to get a stable solution. Figures 51, 52, and 53 are the distributions of density, temperature and concentration at the time step 200 starting from an initial temperature of 90°K uniformly. Numerical oscillation of the concentration is very obvious on the oxygen side. After applying a physical constraint for concentration, which ranges from 0 to 1, the corresponding results are shown in Figs. 54, 55, and 56.

What is most remarkable in the solutions is the qualitative difference between results for initial temperatures of 91°K and 90°K . The latter, i.e., at the initial temperature of 90°K , is under the boiling point of oxygen, 90.15°K . The change of temperature around the interface is in opposite direction of all the gas cases. That change comes from the inward diffusion of hydrogen gas, whose enthalpy is much higher than that of liquid oxygen. In reality, the diffusivity in the liquid phase is much lower than that of gas, as mentioned before. The continuous model of diffusivity over the two phase range is too rough. The latent heat absorbed when liquid changes into gas also counteracts that trend of temperature change. The results imply that

modeling diffusivity accurately and integrating latent heat in the caloric EOS are very important to make the present model complete.

The density near the origin of the droplet is influenced strongly by the numerical oscillation, which is closely related to the numerical boundary condition there.

The interface treatment was not implemented in the above result for simplicity. So the whole process is dominated by diffusion. On the other hand, the difference between liquid and gas diffusivities is not modeled accurately enough. There is a difference of the order-of-magnitude in the diffusivities between the liquid and gas phase. Both problems are coupled to make the result of liquid droplet tentative. Nevertheless, the temperature distribution in the above results strongly suggests that the droplet could be heated up over the critical condition before it is completely vaporized.

One of the fundamental difficulties in incorporating a separated interface condition into the model is how to establish a physically accurate model of the interface condition; especially how to calculate and use the mass emission rate F_{ems} . The possible implementation of the interface boundary condition is discussed further in the next section. As long as the interface is already blurred for the supercritical conditions, the above stated problem does not influence the model.

An interesting phenomenon in the two-phase case is the pressure peak that appeared around the interface. Figure 57 shows the result: the conditions are the same as in Figs. 54 to 56. It is not clear which factor in the model contributes to this phenomenon the most.

(4) Effects of Numerical Schemes

As mentioned above, artificial viscosity is important in obtaining meaningful results. In the gas cases, a 100 times larger artificial viscosity is used in momentum equation than in other equations to obtain the stable solution. In modeling two-phase cases, an artificial viscosity 100 time larger in energy equation is also needed. Without adequate artificial viscosity, the temperature change rate due to discontinuity is actually of infinite, so numerically it brings other parameters outside the physical range. As a result, the numerical solution fails.

The boundary conditions at the origin affects the results as well, as we can see in the above two-phase case at an initial temperature of 90°K. Another example is presented here to show the difference. Figures 58, 59, and 60 display the results at a lower initial temperature of 80°K. They are similar to the case of 90°K. The origin conditions used are

$$T(1) = T(2);$$

$$p(1)=p(2);$$

$$X_1(1)=X_1(2),$$

and molar concentration of mixture n at origin is calculated from them. These conditions are basically interpreted as no gradient of solution variables at the origin. If a difference condition for n , i.e., $n(1) = n(2)$, is imposed, the results are shown in figures 61 to 63. The density distribution is more reasonable than before since the density is directly related to n .

Other factors that could affect the numerical solutions include computational grid, time-step length, different methods to discretize pressure derivative, far-field

solution conditions, and far-field boundary location. Most of these were tested and chosen to have the present values as introduced in the previous section. All the results presented here were obtained on a uniform grid of 310 points. Ten nodes of the grid are in the inner part (“droplet” region) and 300 nodes are in the outer region (surrounding). A finer grid and a corresponding smaller time step, a grid which is gradually stretched away from the droplet, and a smaller time step on the same grid have all been tested and they hardly make a noticeable changes in the results. Since the pressure is computed from the basic variables which are solved for system of equations at each time step, a smoothing treatment has been used, which is in effect, to add a term of artificial viscosity.

Figures

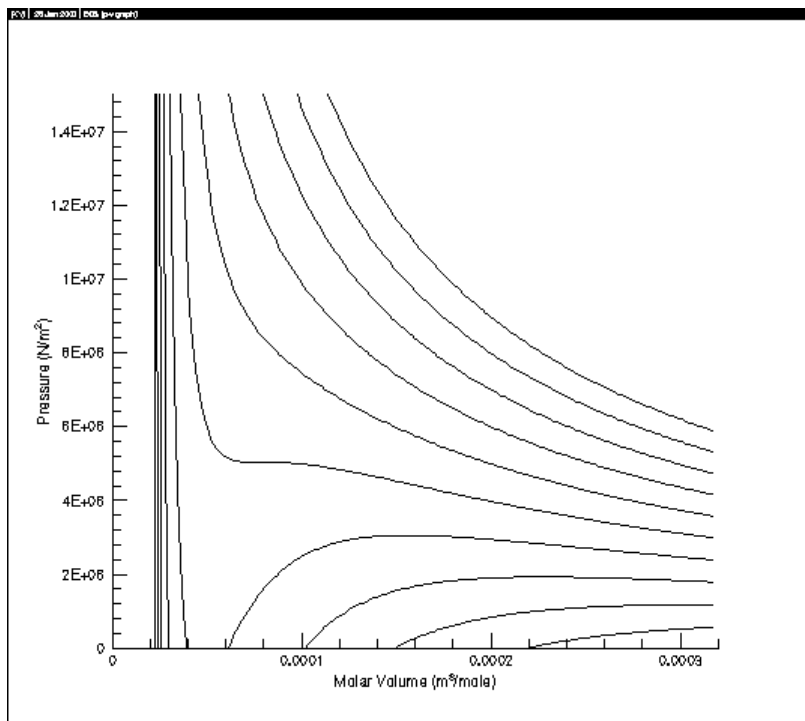


Figure 6 Peng-Robinson EOS for Oxygen

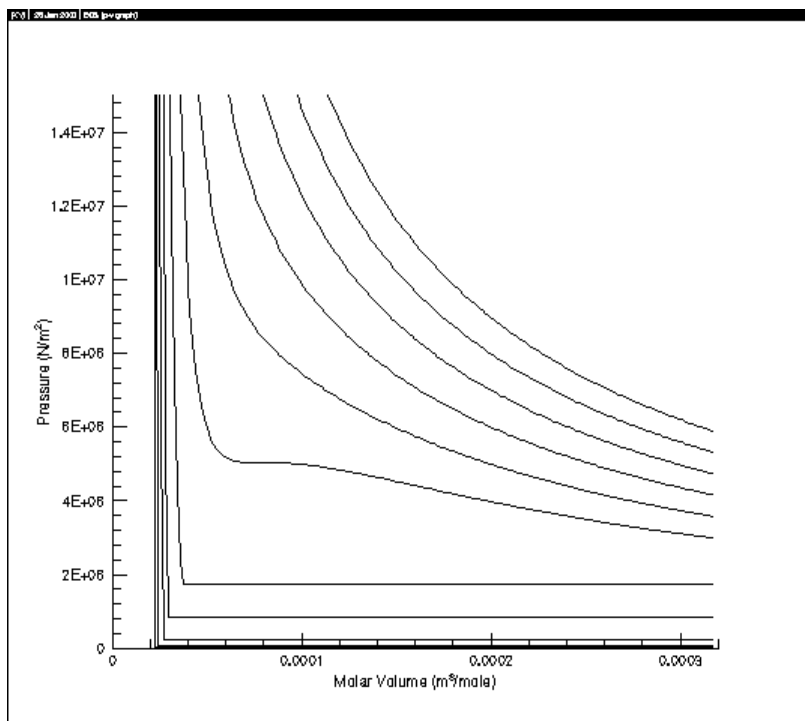


Figure 7 Peng-Robinson EOS for Oxygen, transition included

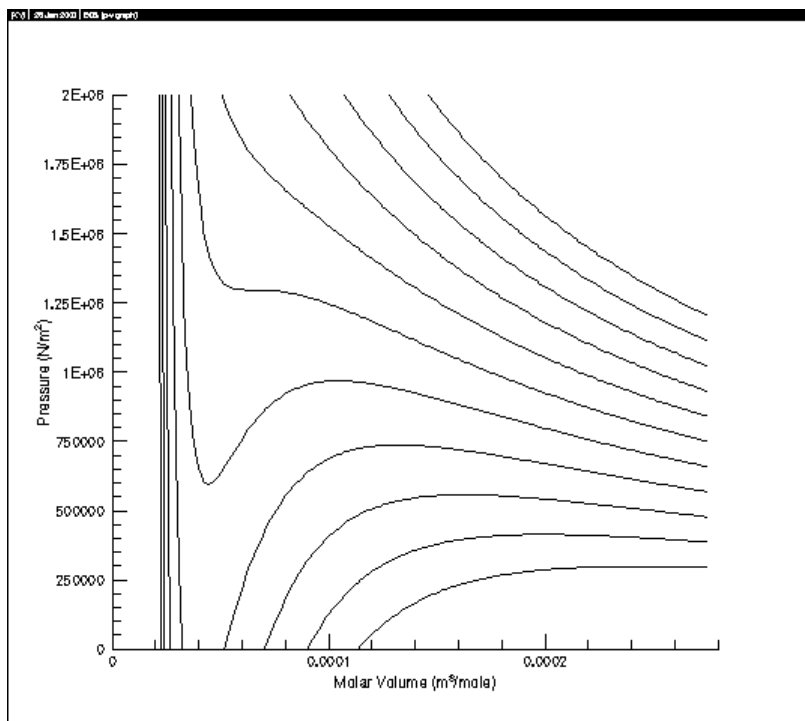


Figure 8 Peng-Robinson EOS for Hydrogen

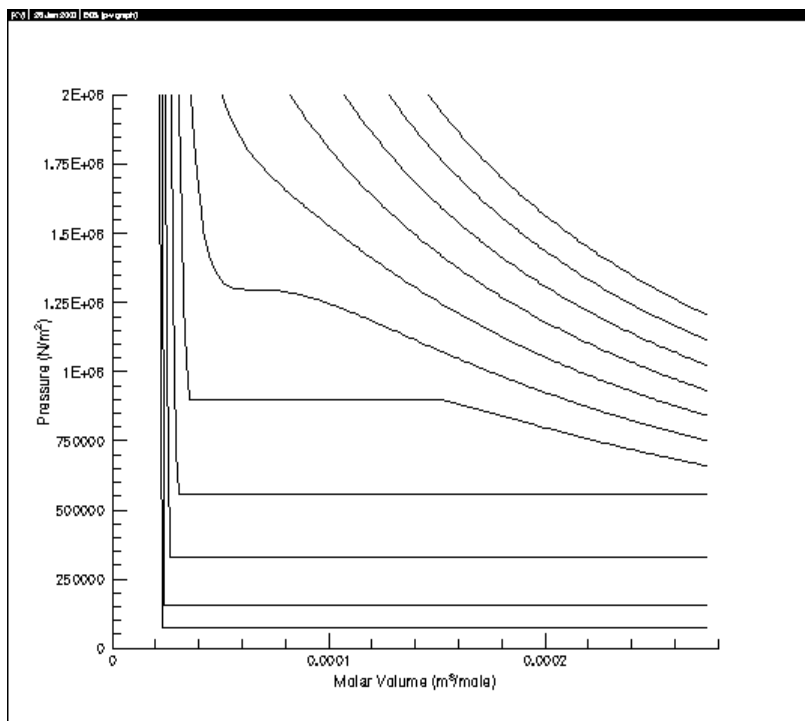


Figure 9 Peng-Robinson EOS for Hydrogen, transition included

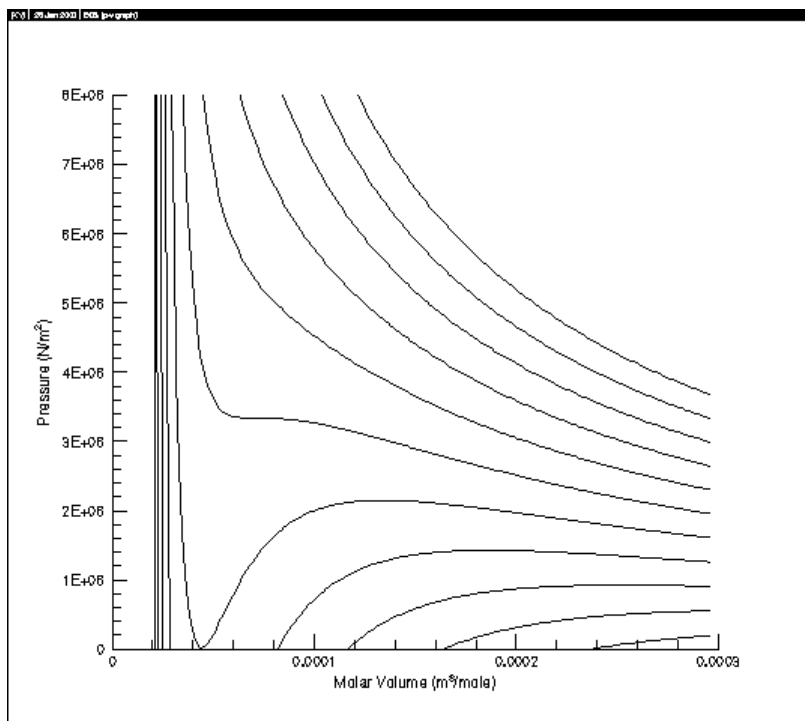


Figure 10 Peng-Robinson EOS for mixture

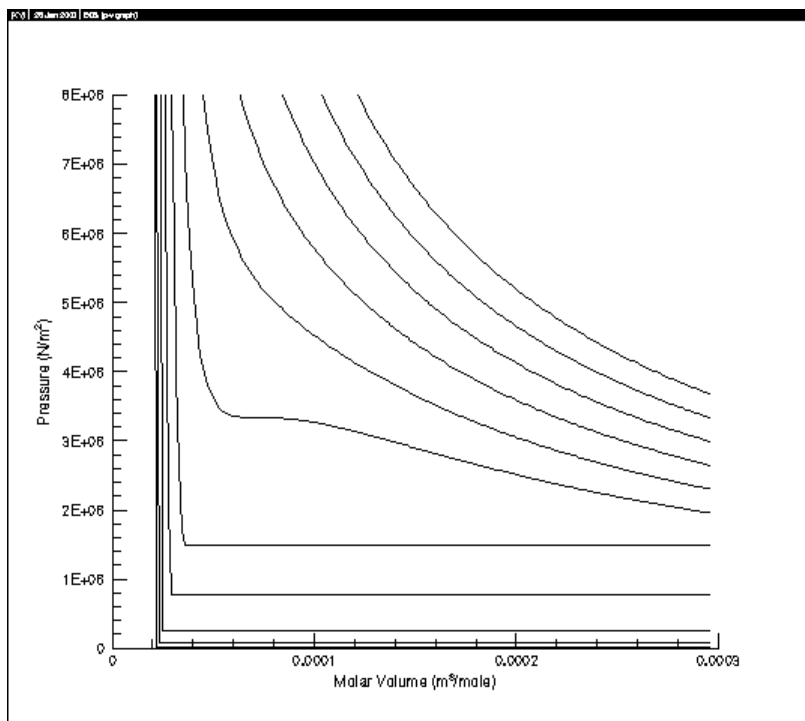


Figure 11 Peng-Robinson EOS for mixture, transition included

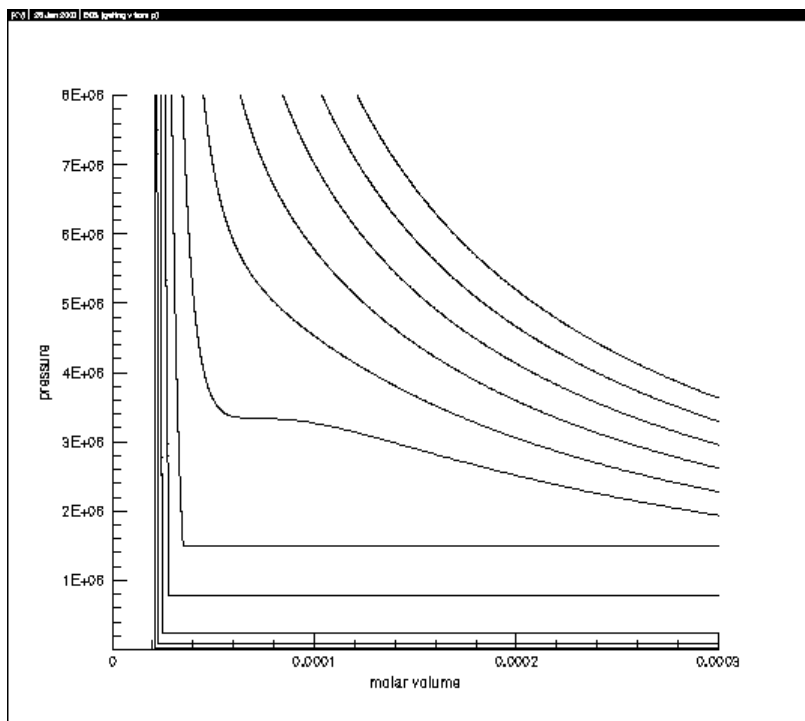


Figure 12 Peng-Robinson EOS, volume explicit

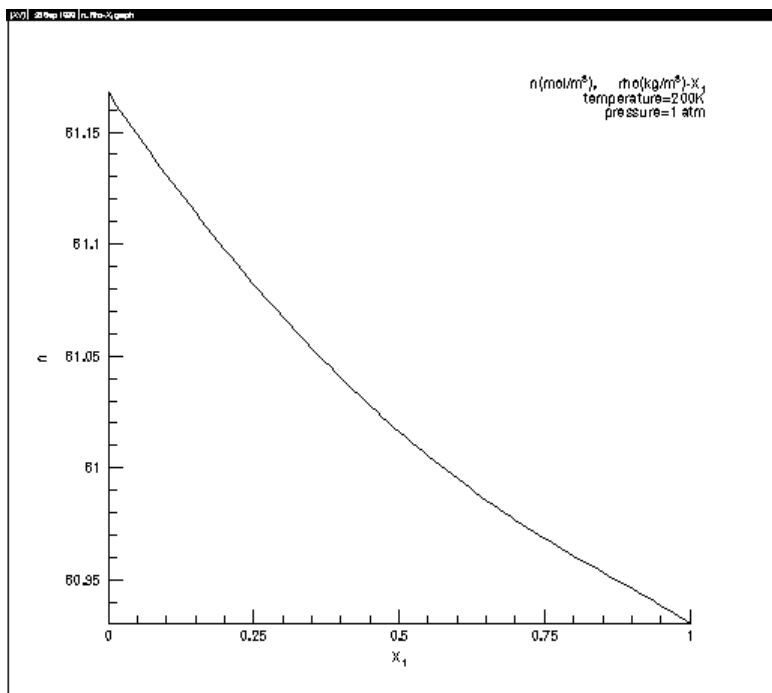


Figure 13 Molar concentration of mixture to species concentration

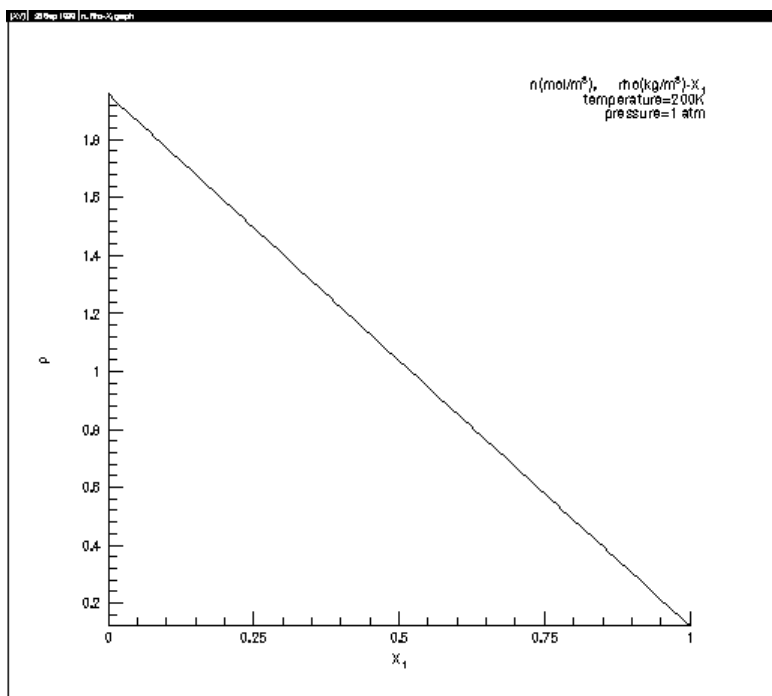


Figure 14 Mixture density to species concentration

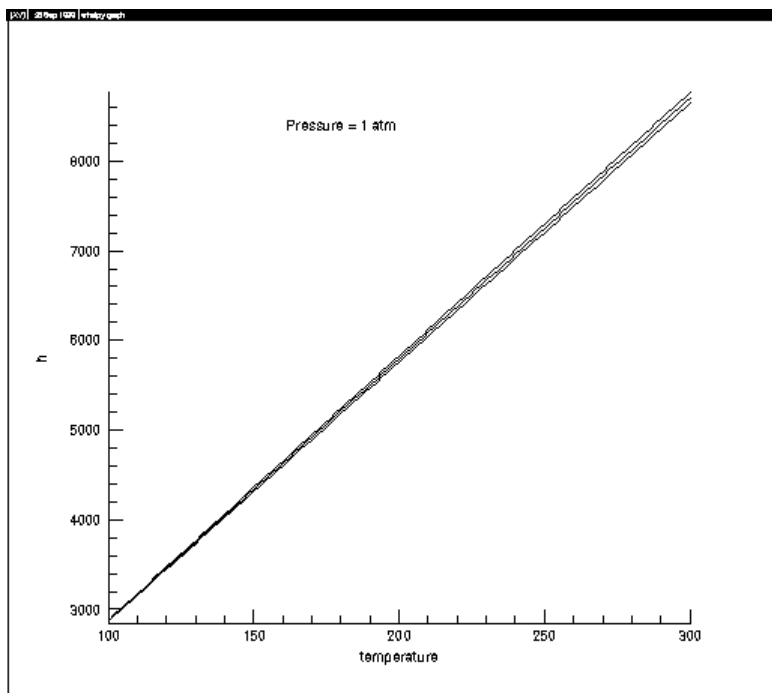


Figure 15 Enthalpy to temperature

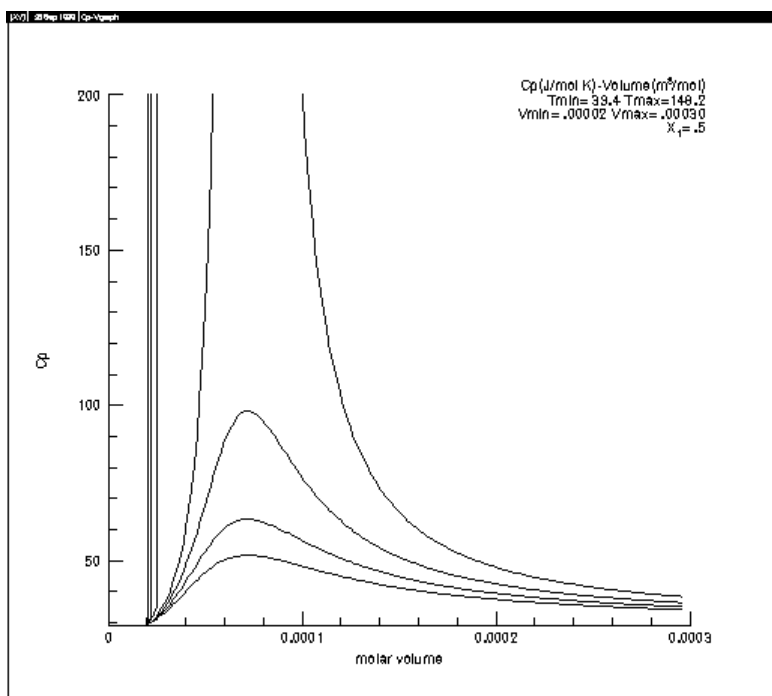


Figure 16 Cp of hydrogen, low temperature

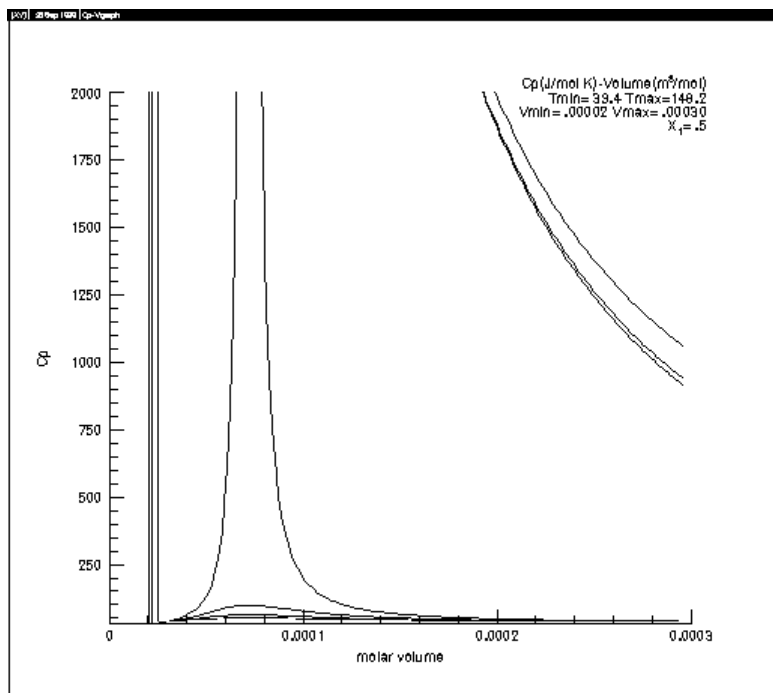


Figure 17 C_p of hydrogen, high temperature

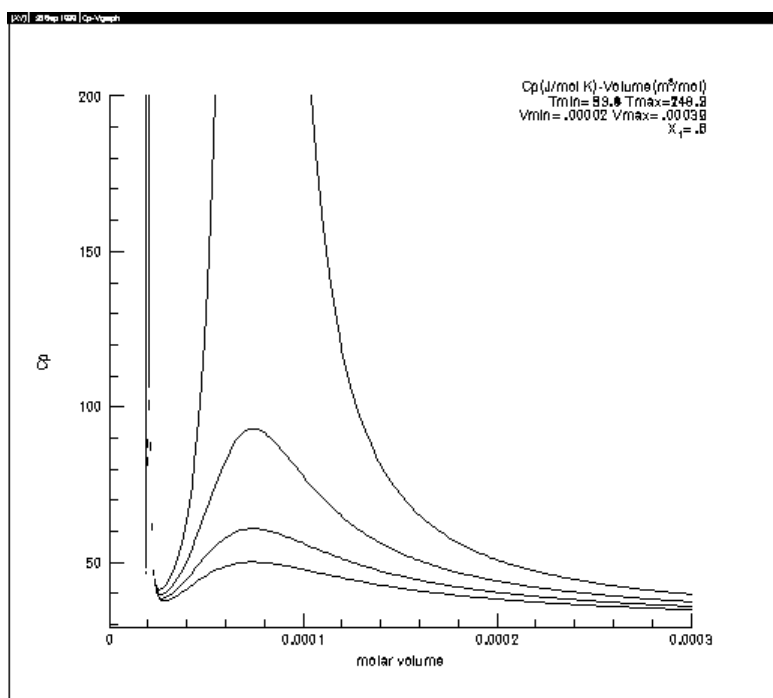


Figure 18 C_p of oxygen, low temperature

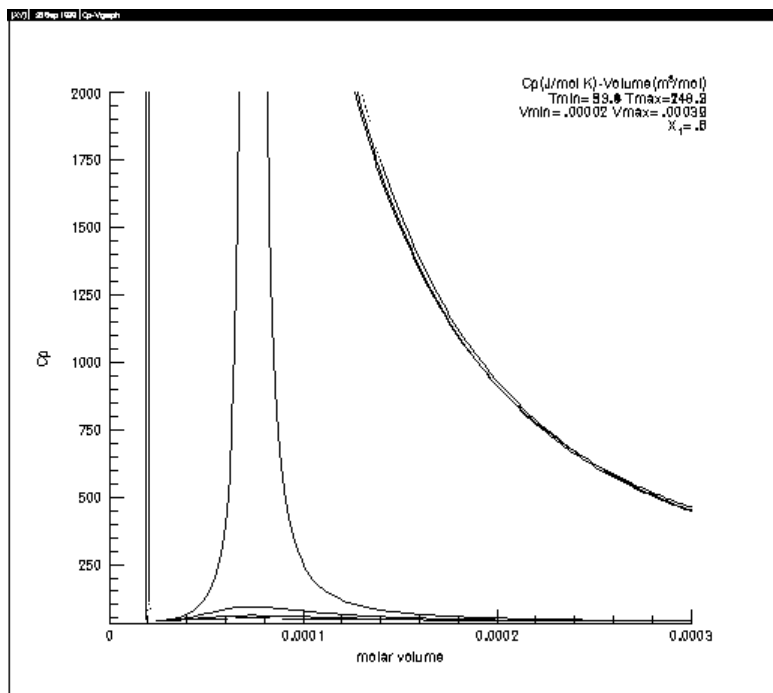


Figure 19 C_p of oxygen, high temperature

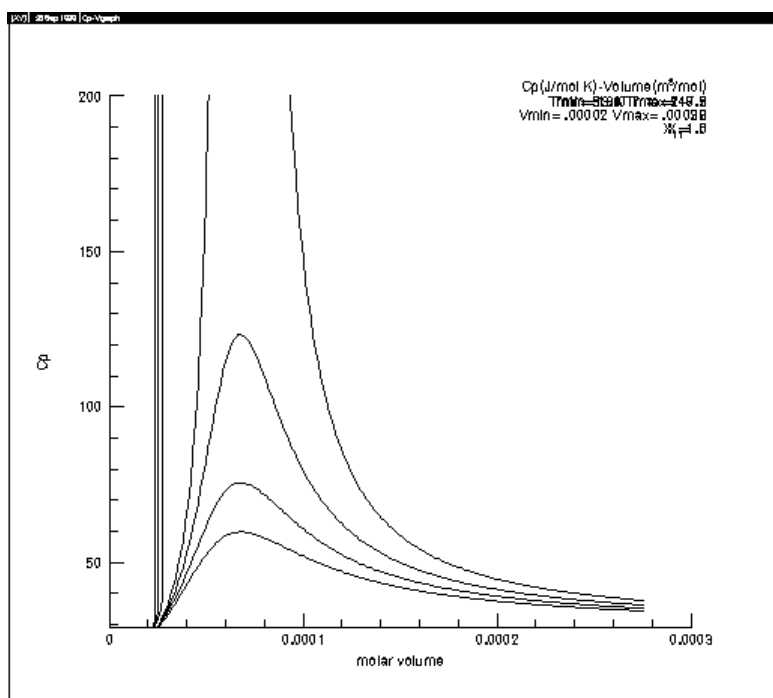


Figure 20 C_p of mixture, low temperature

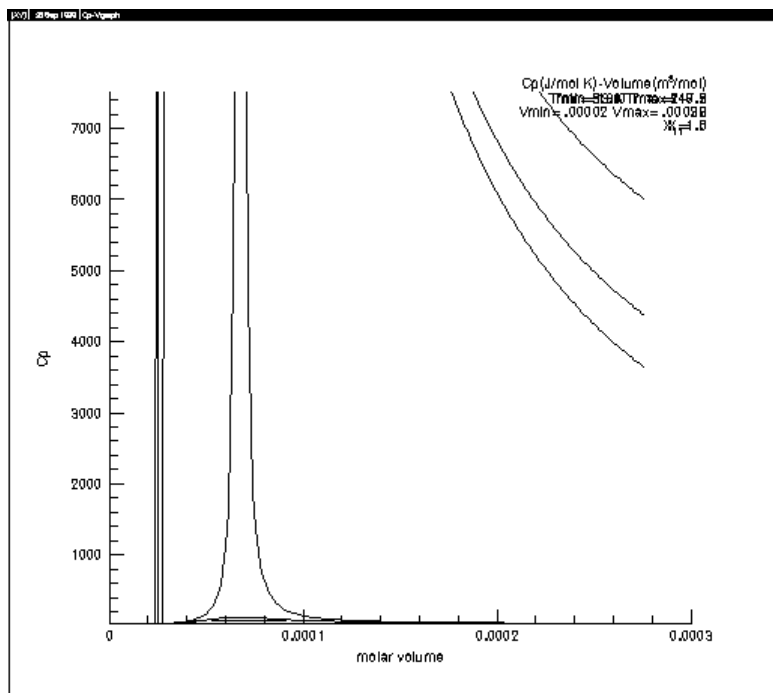


Figure 21 Cp of mixture, high temperature

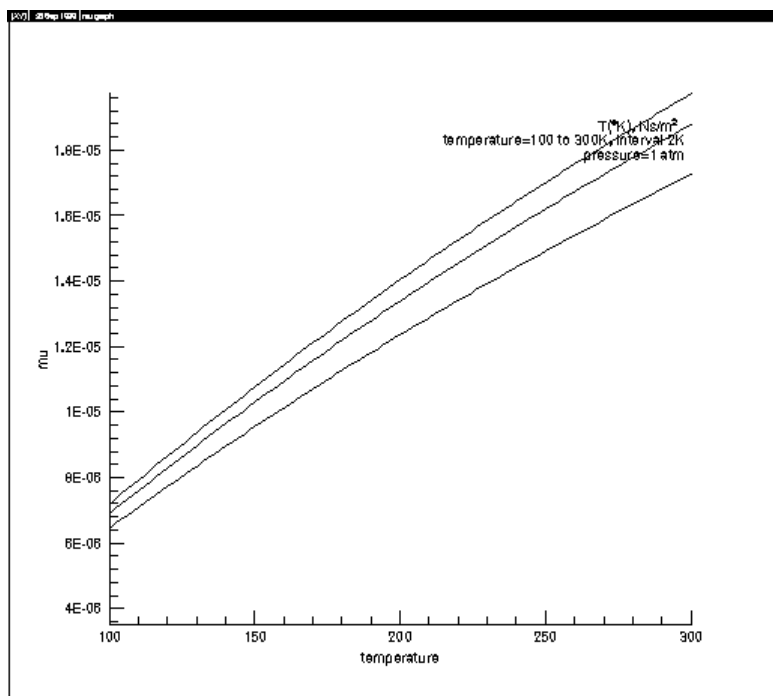


Figure 22 Viscosity to temperature

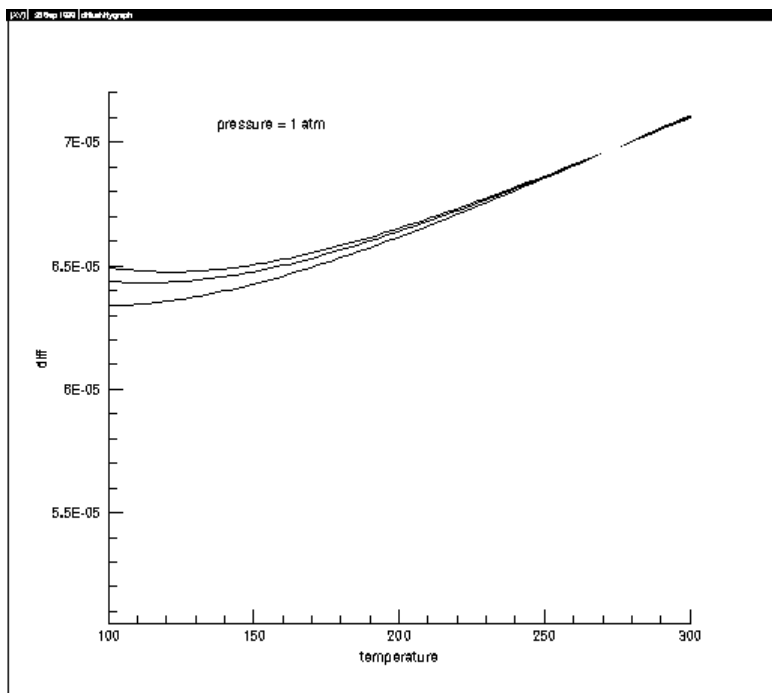


Figure 23 Diffusivity

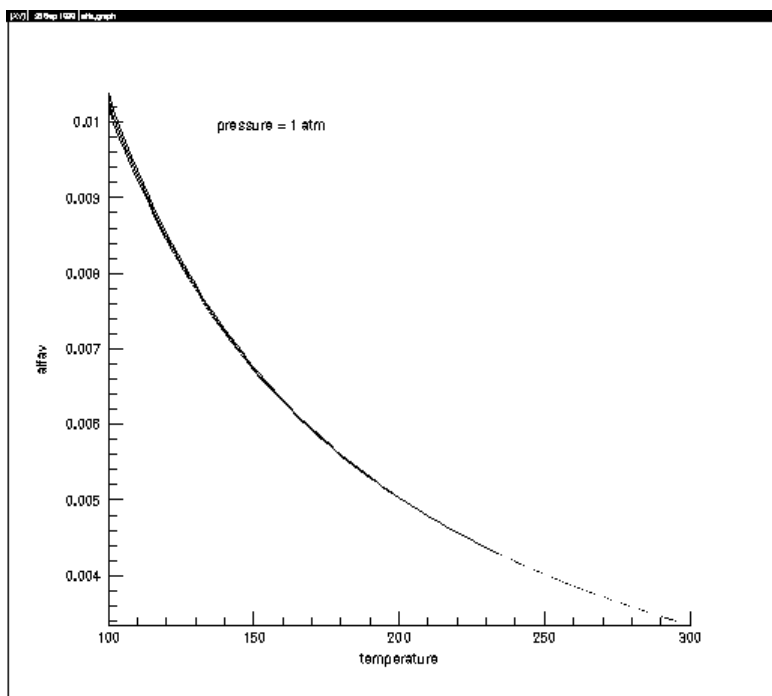


Figure 24 Thermal expansion rate

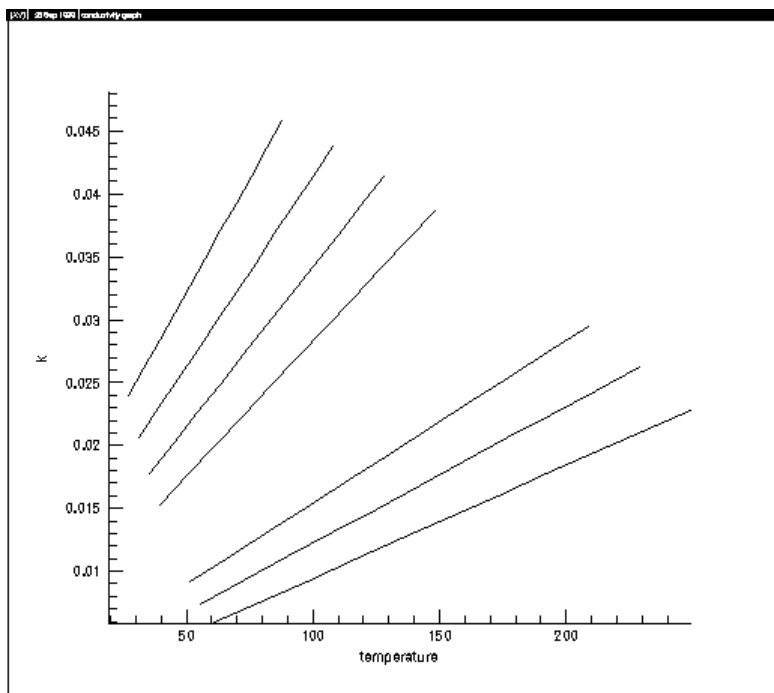


Figure 25 Conductivity

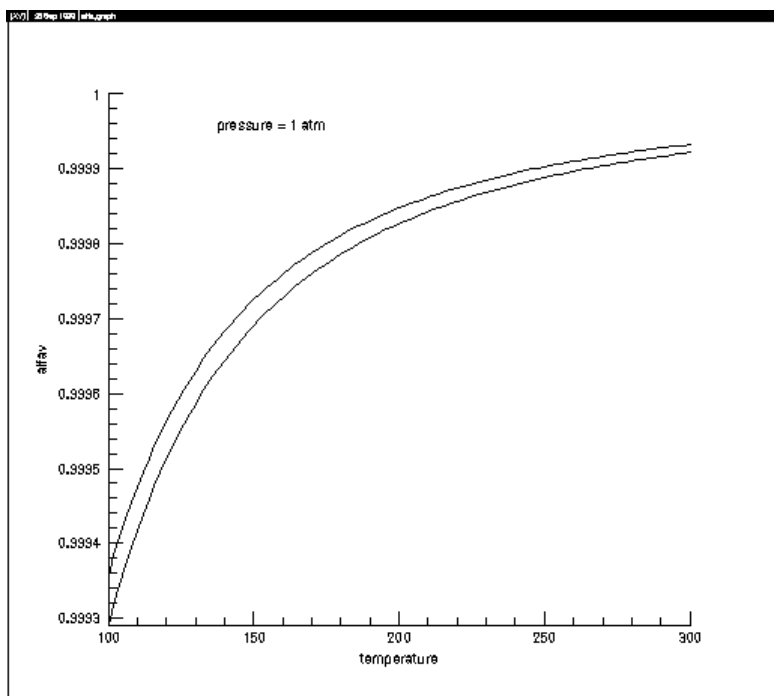


Figure 26 Coefficient α_D

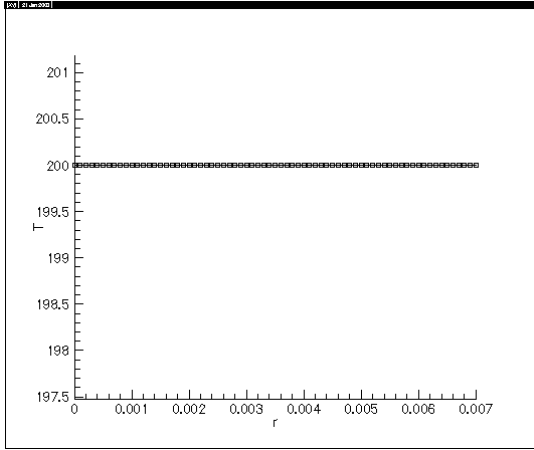


Figure 27-1 Temperature, 200°K, step 0

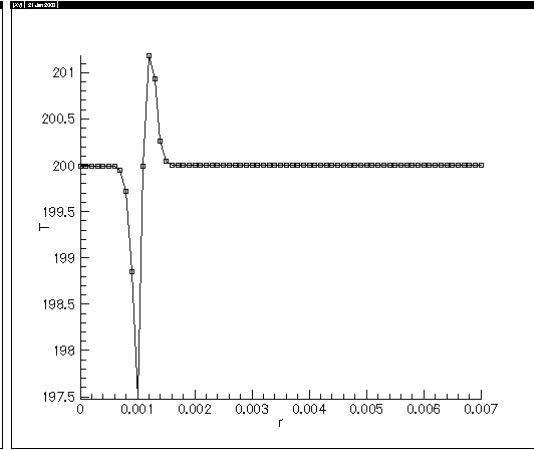


Figure 27-2 Step 100

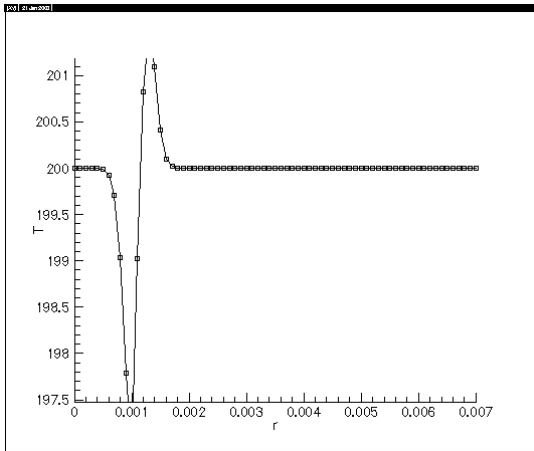


Figure 27-3 Step 200

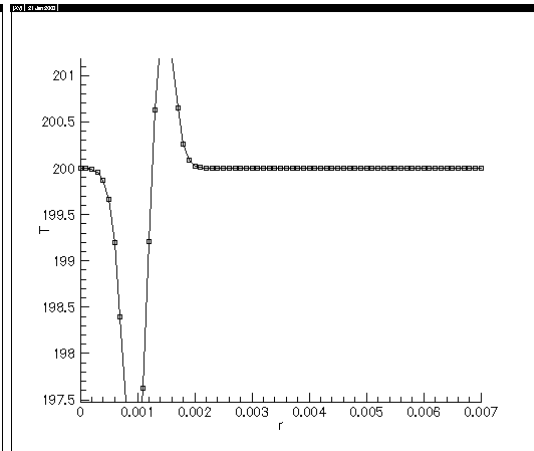


Figure 27-4 Step 500

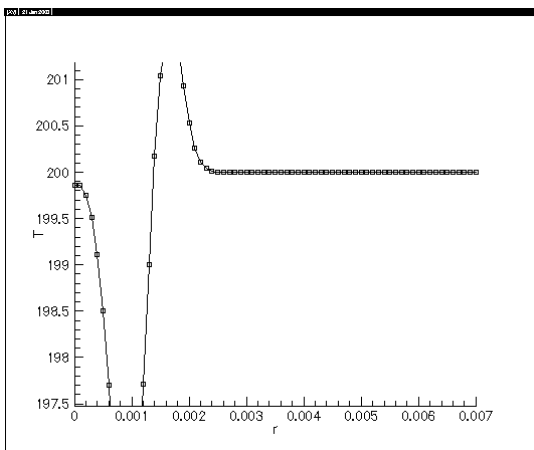


Figure 27-5 Step 1000

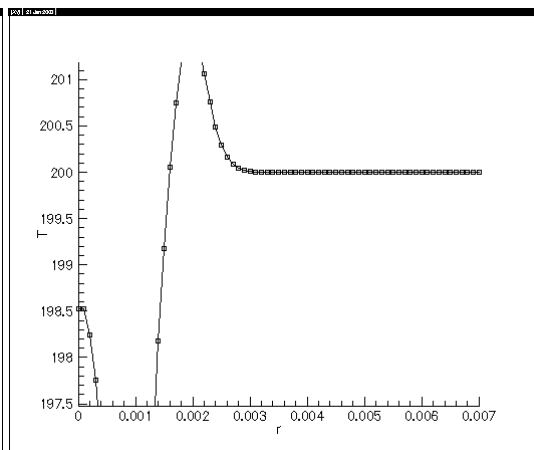


Figure 27-6 Step 2000

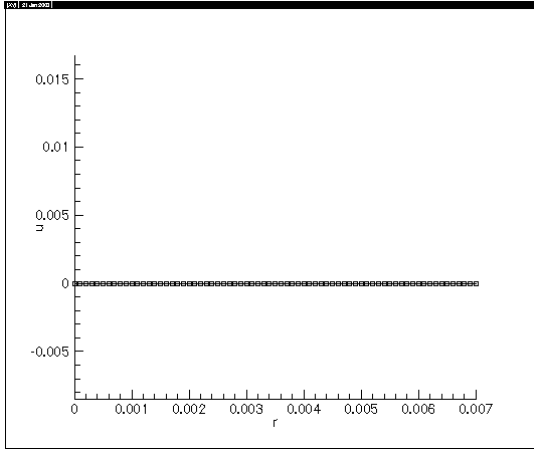


Figure 28-1 Velocity, step 0

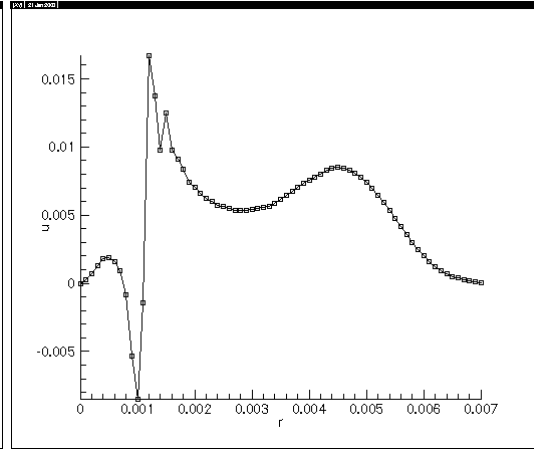


Figure 28-2 Step 100

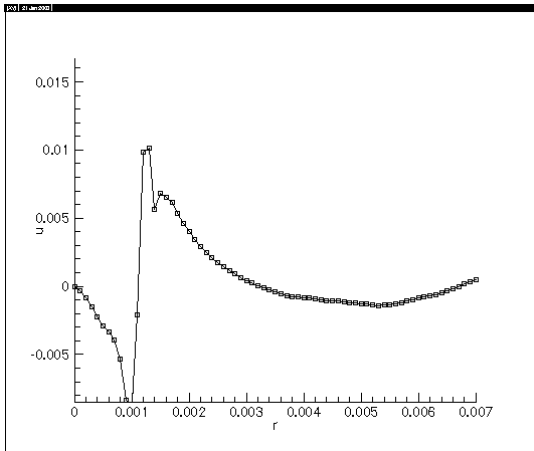


Figure 28-3 Step 200

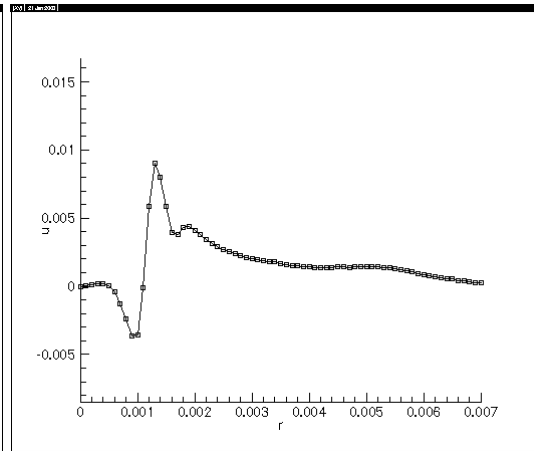


Figure 28-4 Step 500

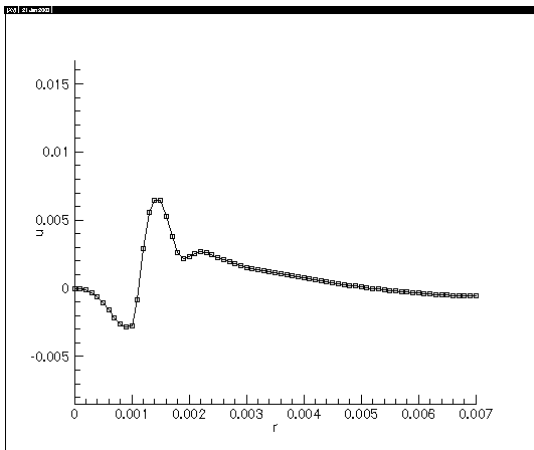


Figure 28-5 Step 1000

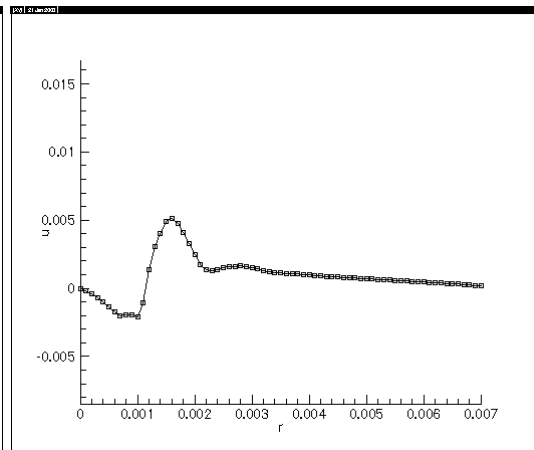


Figure 28-6 Step 2000

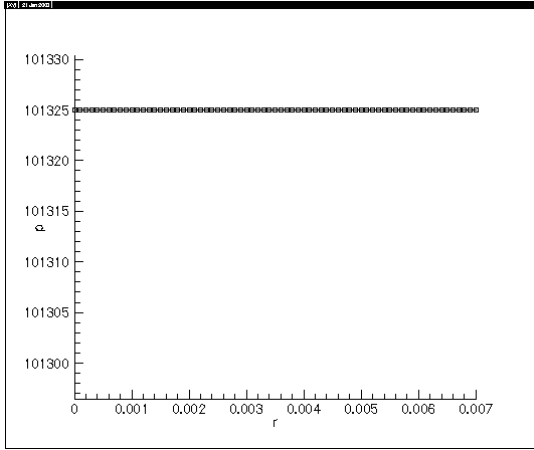


Figure 29-1 Pressure, step 0

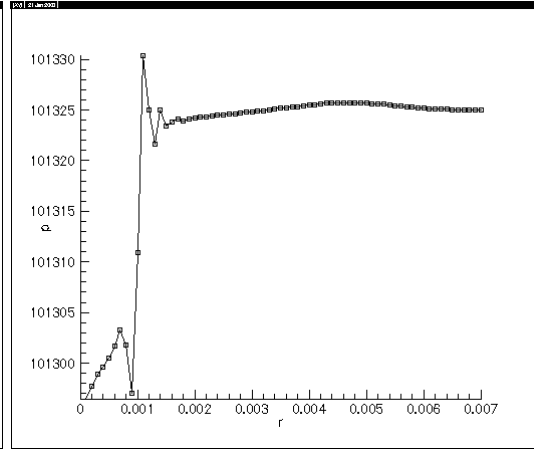


Figure 29-2 Step 100

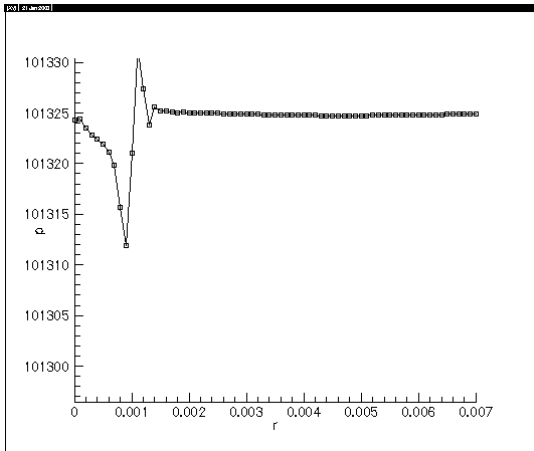


Figure 29-3 Step 200

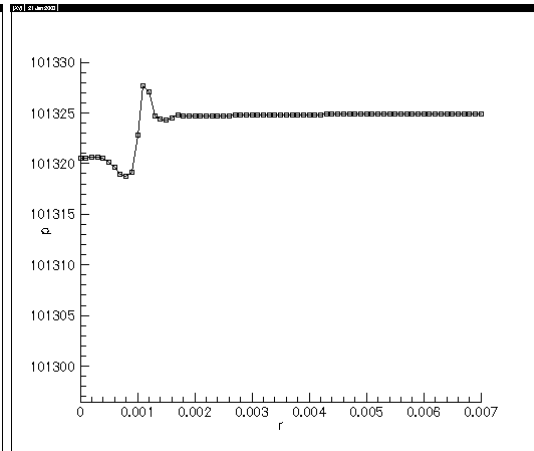


Figure 29-4 Step 500

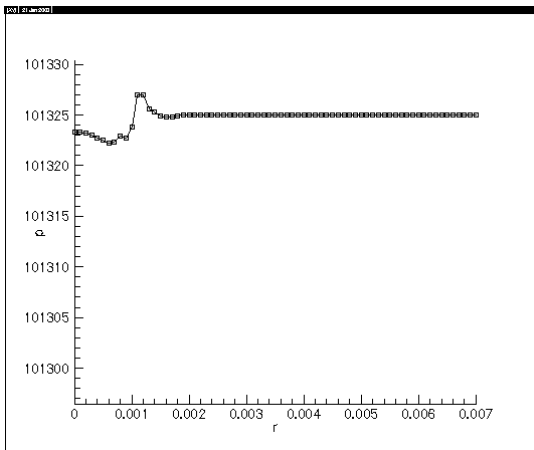


Figure 29-5 Step 1000

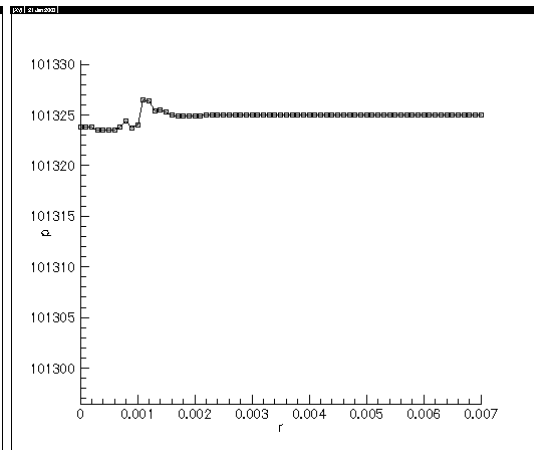


Figure 29-6 Step 2000

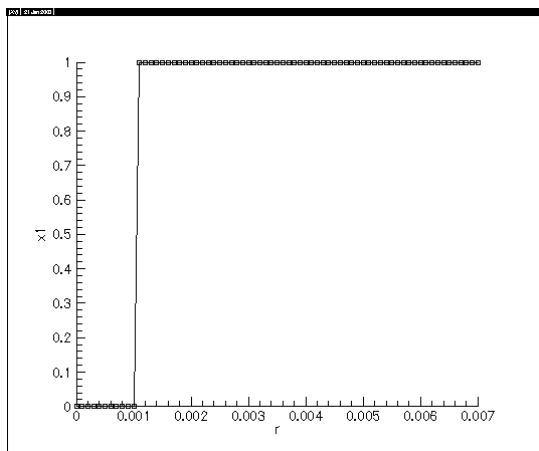


Figure 30-1 Species concentration, step 0

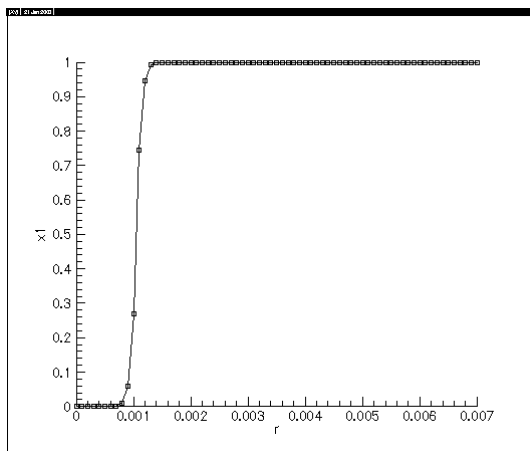


Figure 30-2 Step 100

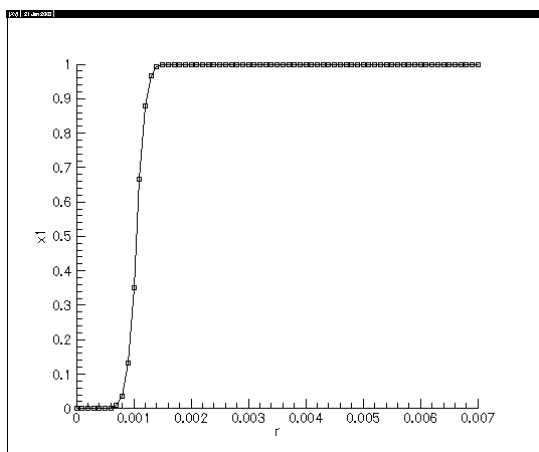


Figure 30-3 Step 200

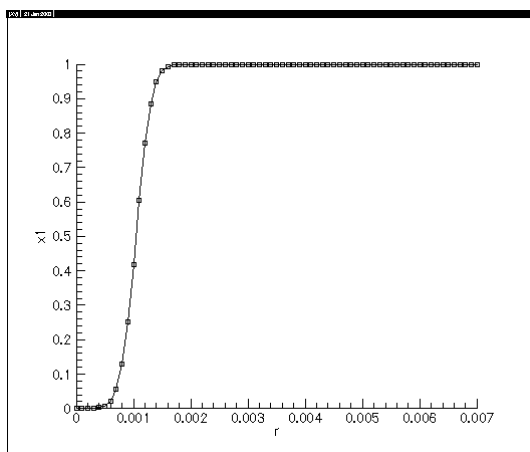


Figure 30-4 Step 500

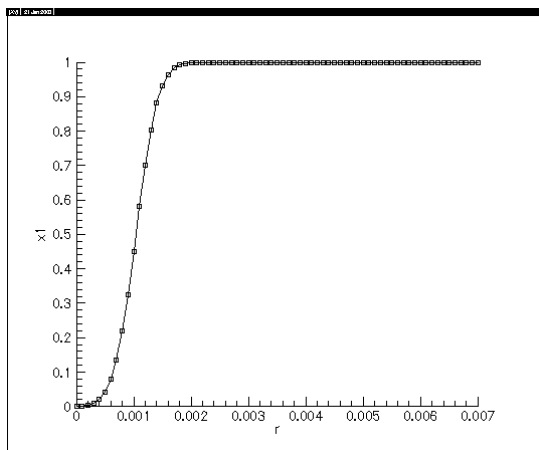


Figure 30-5 Step 1000

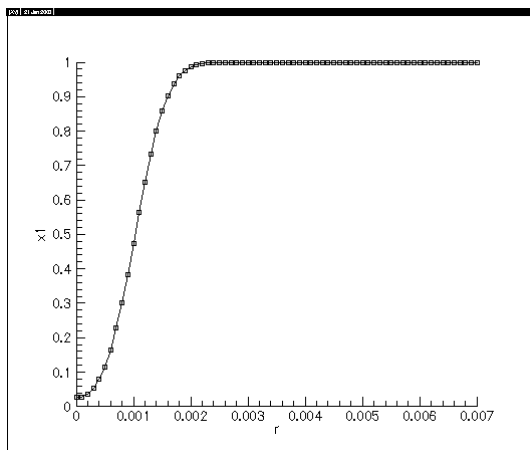


Figure 30-6 Step 2000

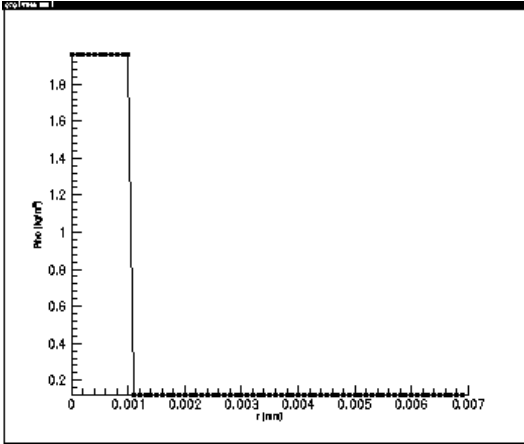


Figure 31-1 Density, step 0

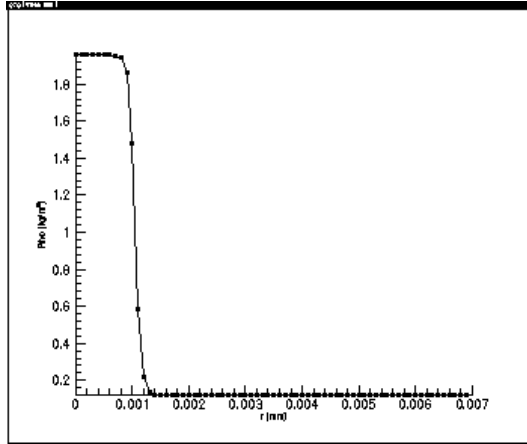


Figure 31-2 Step 100

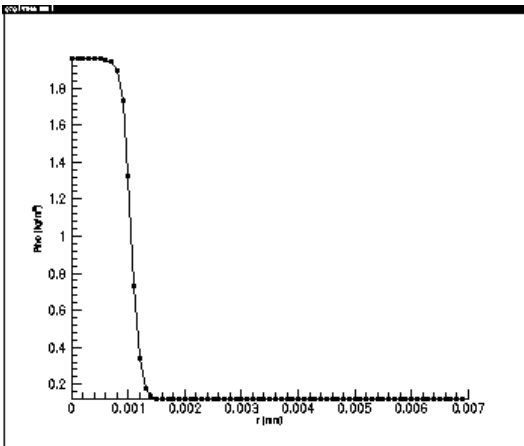


Figure 31-3 Step 200

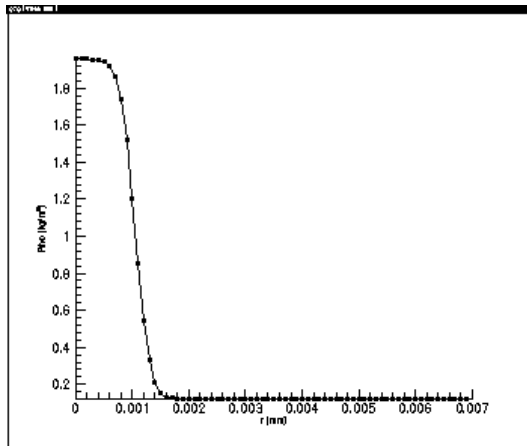


Figure 31-4 Step 500

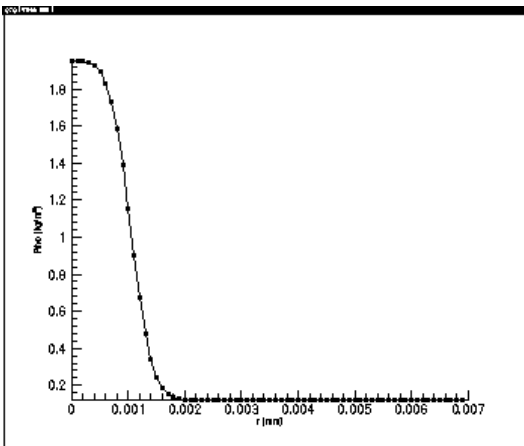


Figure 31-5 Step 1000

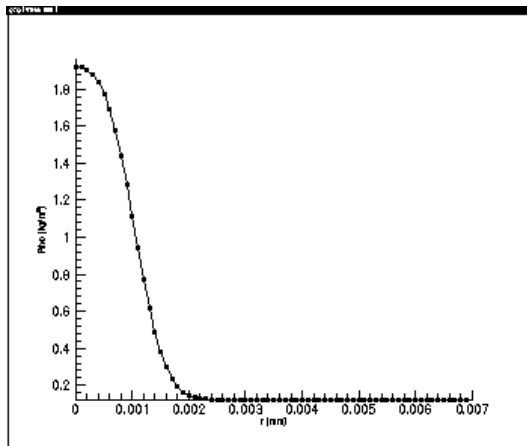


Figure 31-6 Step 2000



Figure 32 Species Concentration

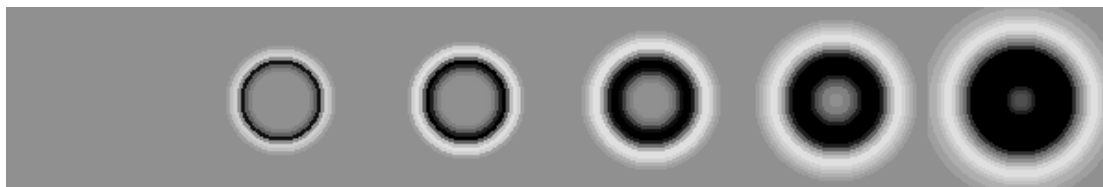


Figure 33 Temperature

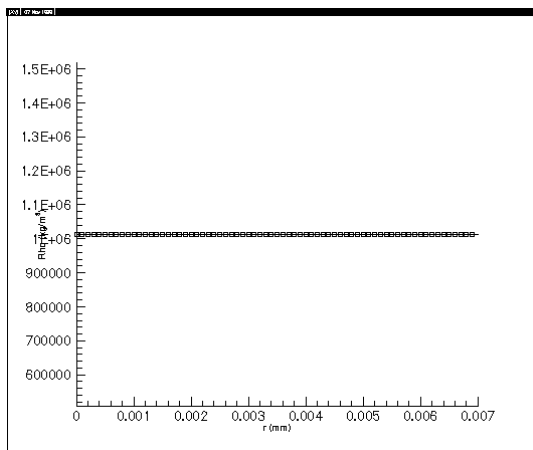


Figure 34 Pressure, 10atm, step 2000

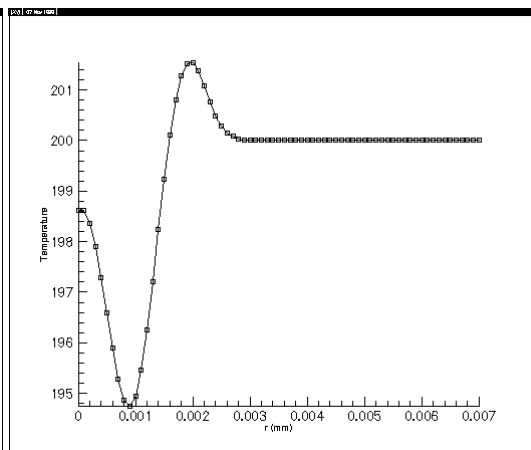


Figure 35 Temperature, 10atm, step 2000

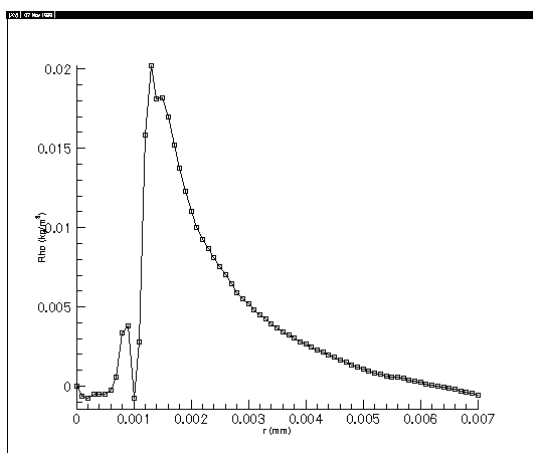


Figure 36 Velocity, 10atm, step 2000

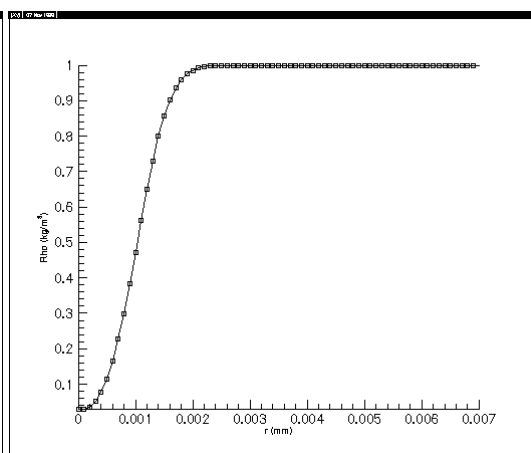


Figure 37 Concentration, 10atm, step 2000

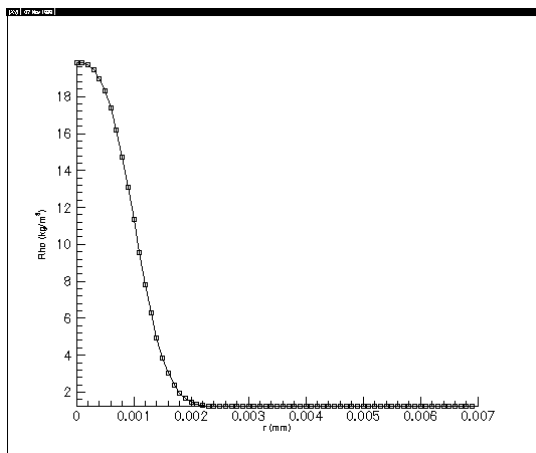


Figure 38 Density, 10atm, step 2000

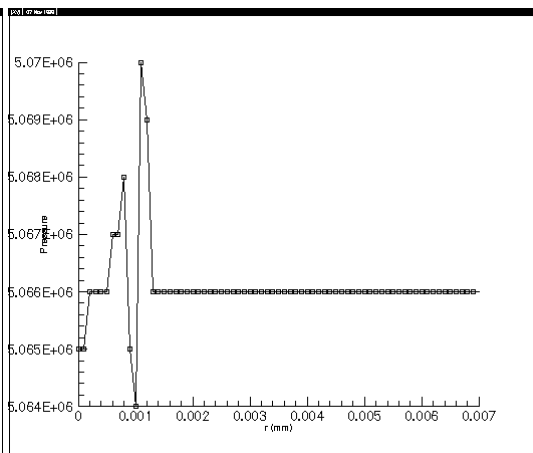


Figure 39 Pressure, 50atm, step 2000

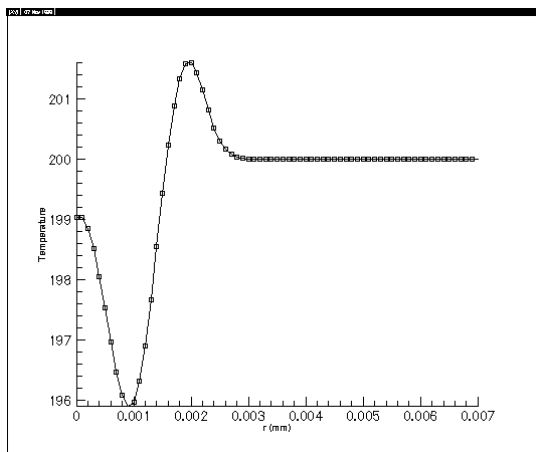


Figure 40 Temperature, 50atm, step 2000

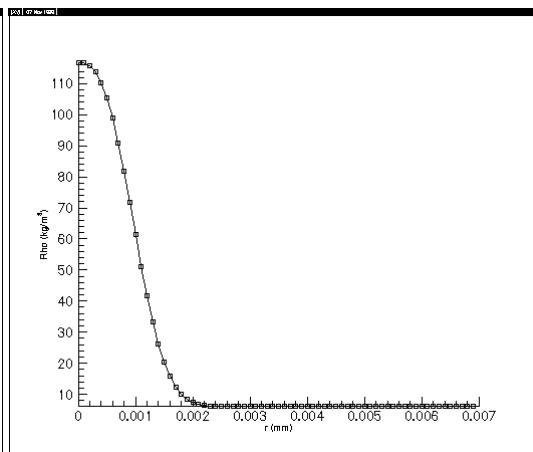


Figure 41 Density, 50atm, step 2000

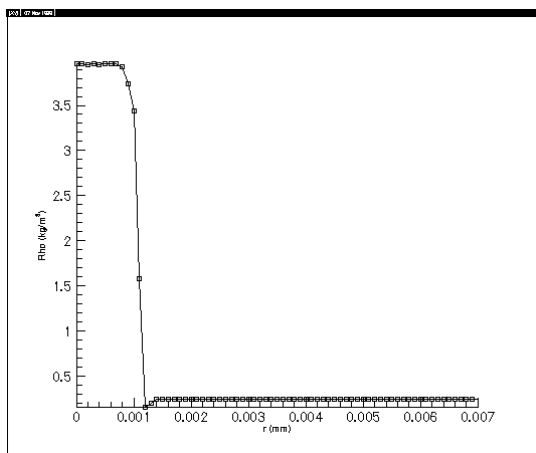


Figure 42 Density, 100K, step 500

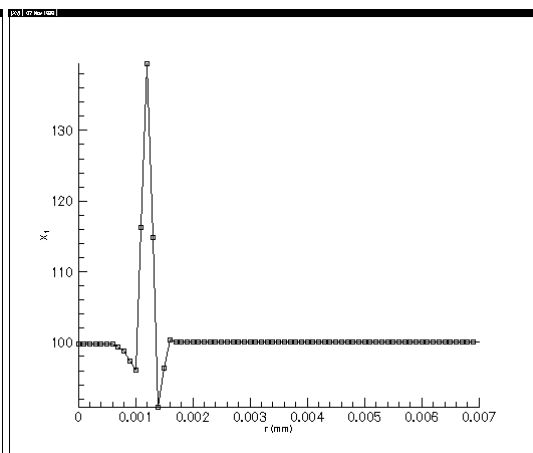


Figure 43 Temperature, 100K, step 500

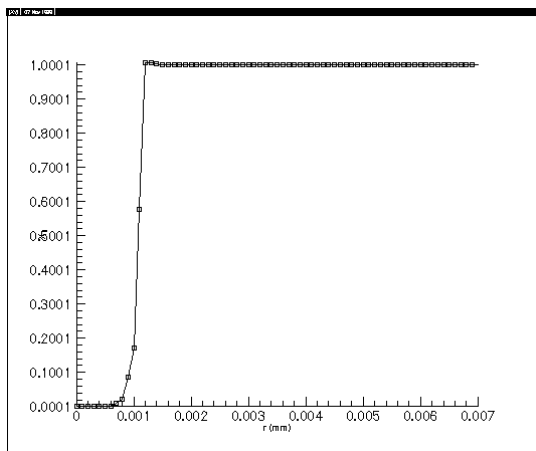


Figure 44 Concentration, 100K, step 500

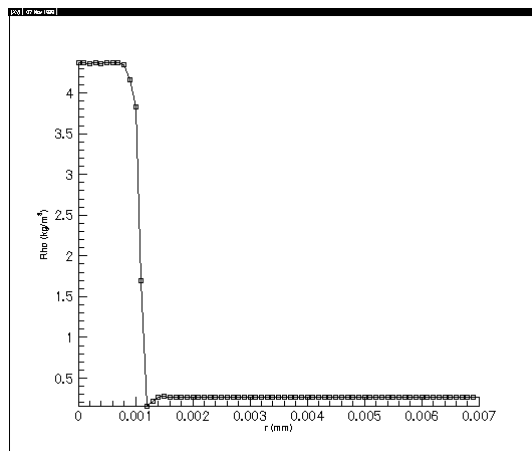


Figure 45 Density, 91K, step 500

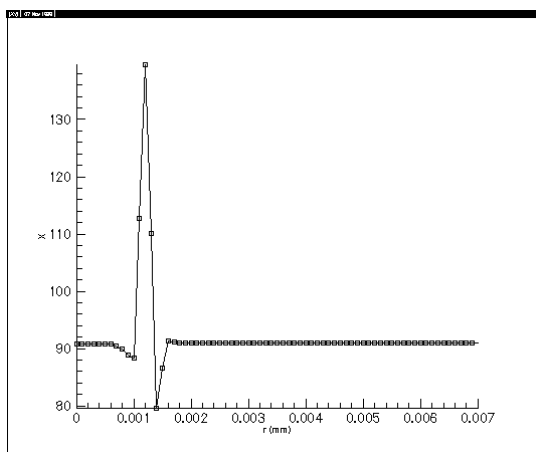


Figure 46 Temperature, 91K, step 500

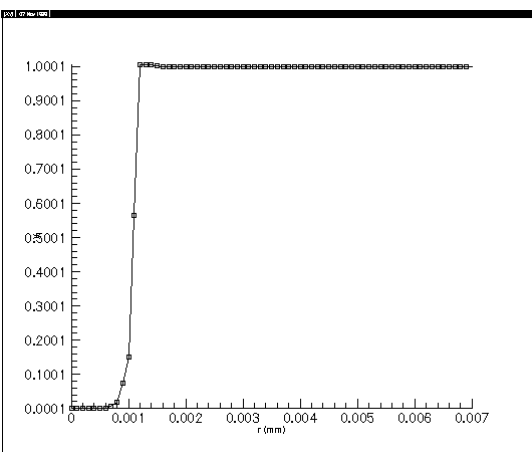


Figure 47 Concentration, 91K, step 500

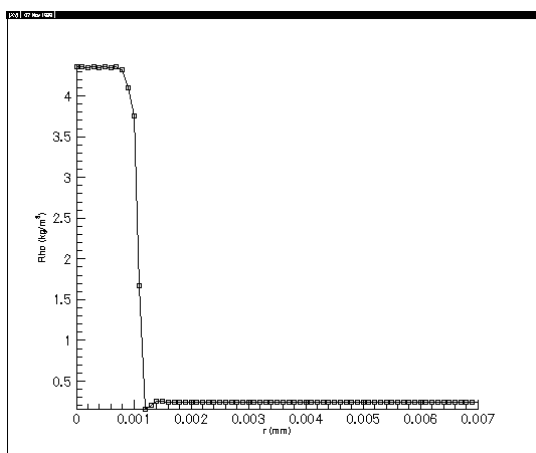


Figure 48 Density, 91K-100K, step 500

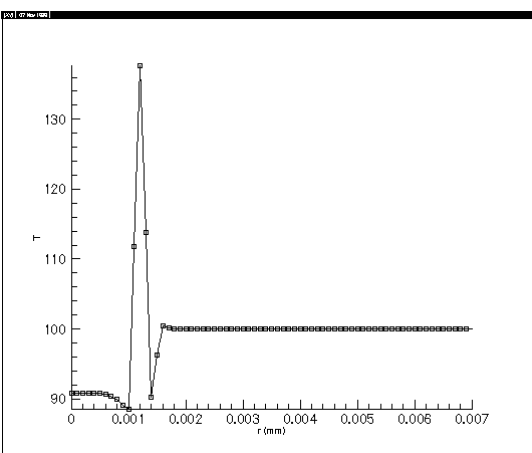


Figure 49 Temperature, 91K-100K, step 500

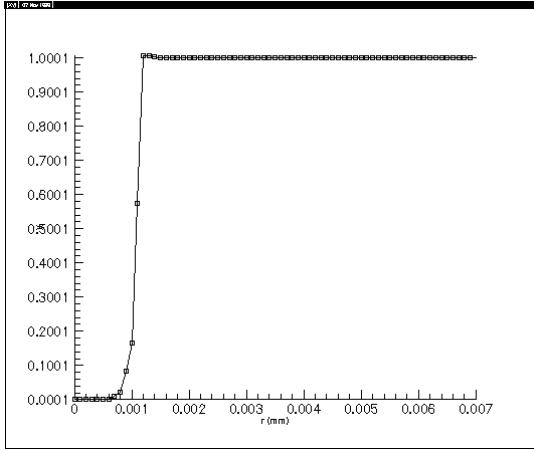


Figure 50 Concentration, 91K-100K, step 500

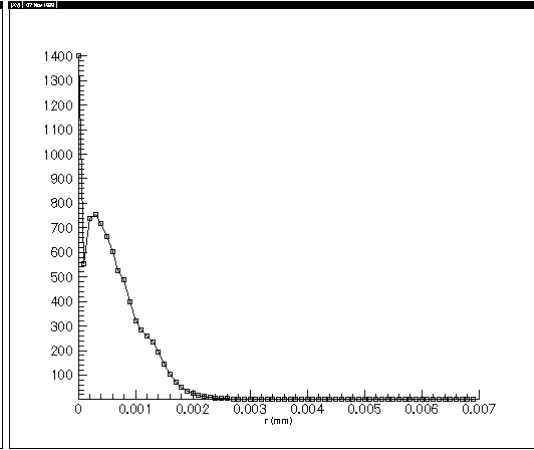


Figure 51 Density, 90K, step 200

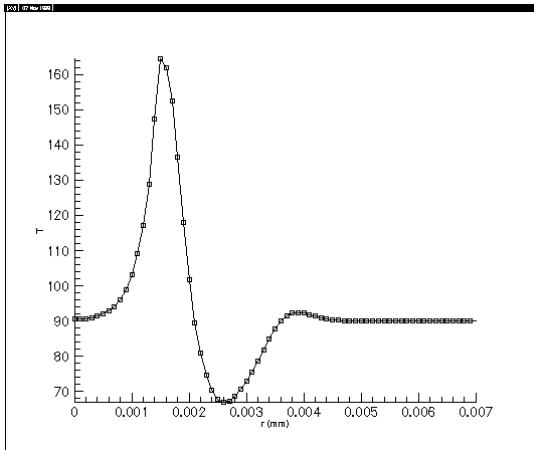


Figure 52 Temperature, 90K, step 200

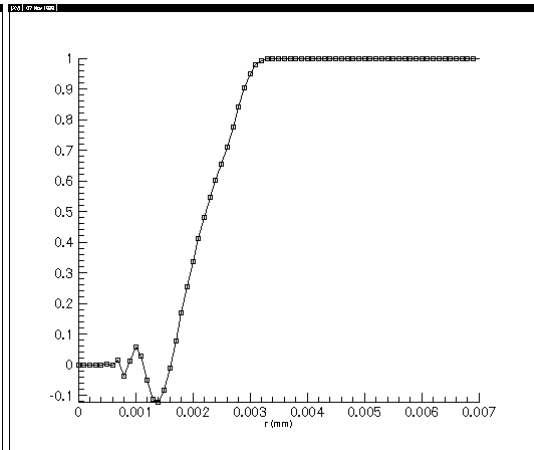


Figure 53 Concentration, 90K, step 200

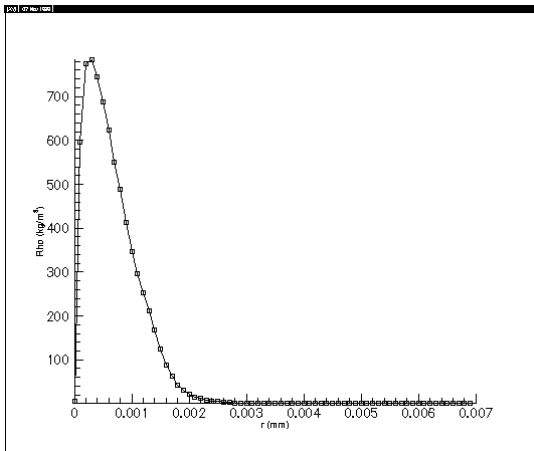


Figure 54 Density, 90K, X_1 constrained, step 200

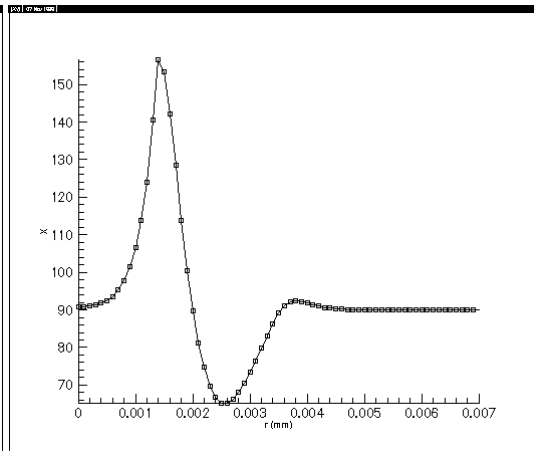


Figure 55 Temperature, 90K, X_1 constrained, step 200

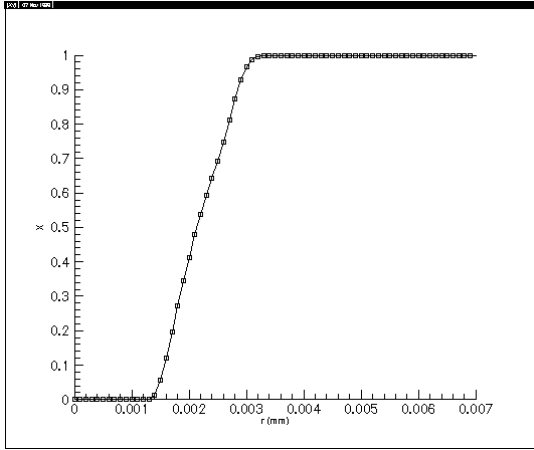


Figure 56 Concentration, 90K, constrained step 200

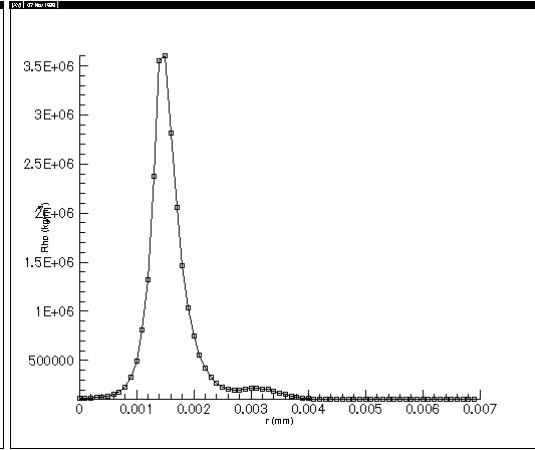


Figure 57 Pressure, step 200

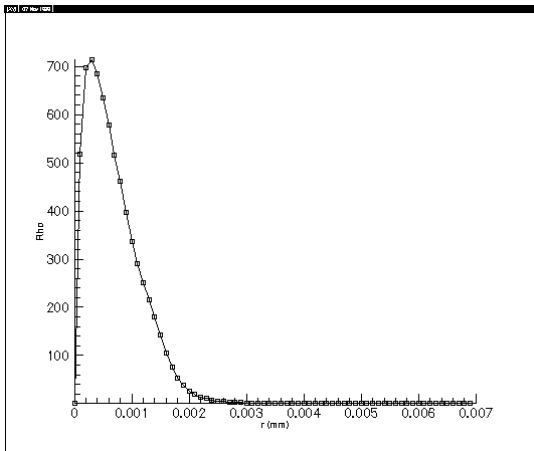


Figure 58 Density, 80K, step 200

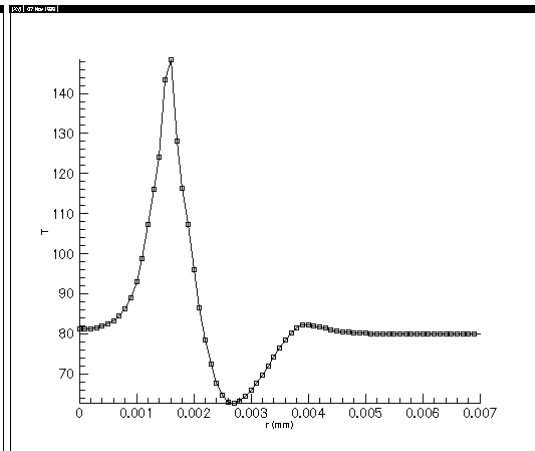


Figure 59 Concentration, 80K, step 200

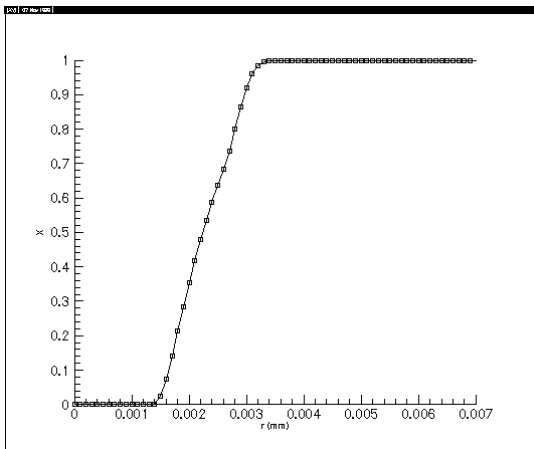


Figure 60 Concentration, 80K, step 200

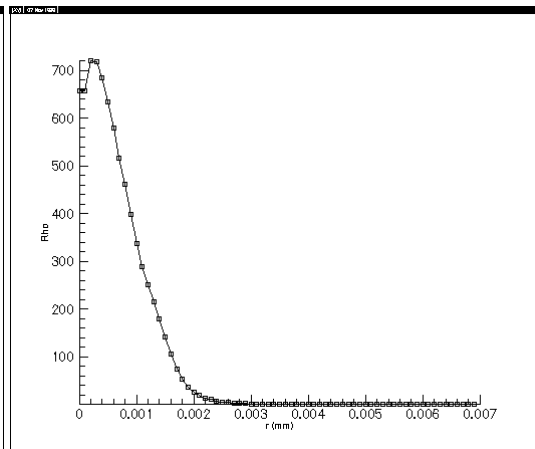


Figure 61 Density, new origin condition, step 200

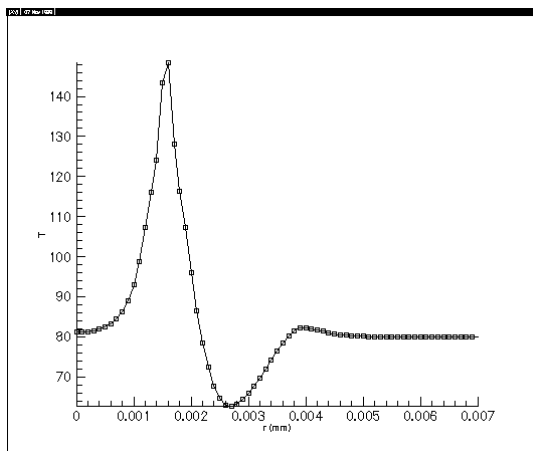


Figure 62 Temperature, new origin condition, step 200

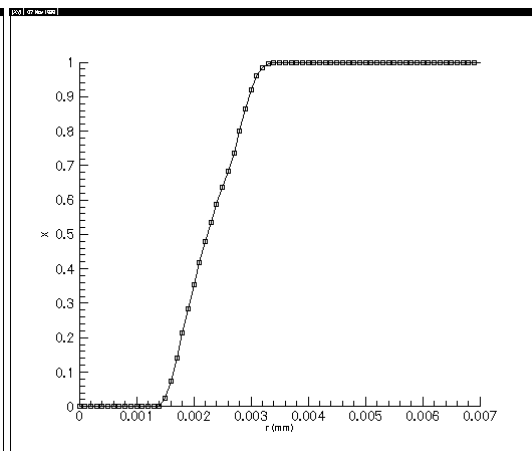


Figure 63 Concentration, new origin condition, step 200

5. Discussion

5.1 Existence of Droplet Surface

Although one of the most amazing characteristics of the droplet under supercritical condition is the “blurred” surface, it is still necessary to deal with the surface and the condition on it in case it would exist, or in other words, the droplet has a clear surface instead of the blurred one. Basically, the liquid in the droplet is always at sub-critical condition before it evaporates. We can never isolate a problem in which only a supercritical condition applies. For clarity, we can discuss this from two different points of view.

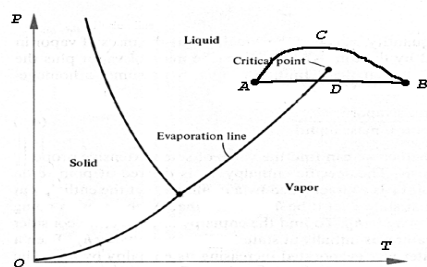


Figure 64 State Near Critical Point

The first is the distribution of pressure and temperature at a certain instant. In this case, it is in principle easier to determine whether a droplet has a blurred or clear surface. Figure 64 is a typical p - T diagram. If we suppose the same substance is inside and

outside the droplet, we can use it to explain the blurred surface. Near the critical point, there are two possible continuous distributions of pressure and temperature from state A to B , on curve ACB or ADB . The curve ADB crosses the evaporation line and the intersection point is where two different phases border each other. If the distribution is along ACB , the droplet is blurred.

Another point of view is when we consider the time dependent process of state change at a certain position or of a certain particle. (Lagrange or Euler point of

view has nothing to do with what we are discussing here.) In this case, let us consider Fig. 64 as a p - T diagram in the usual sense. The problem is actually no longer whether the surface is blurred or not, but whether phase transition occurs. If the change is along curve ACB mentioned above, it will be continuous without phase change. We need not consider density discontinuity and latent heat. Otherwise, phase change and the condition on the interface have to be considered on a curve across evaporation line, like ADB . The problem in practice is that the equation of state in use, no matter be it in the analytic or numerical in form, has to tell us whether the fluid is in the liquid or gas phase. The reason is that, although the cubic equations we use, like the Peng-Robinson EOS, includes both phases in its solution, they have multiple solutions in the portion of evaporation procedure instead of to describe it physically. The solution could change continuously along curve ACB to an unphysical one if the equation can not determine the actual phase only by pressure and temperature.

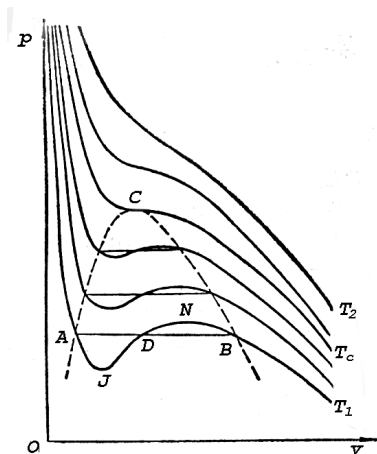


Figure 65 Isotherms Near Critical Point

Isotherms based on the cubic equation are shown in Fig. 65. When the temperature is below the critical temperature, the p - T curve has a portion with multiple solutions. A straight-line section AB corresponding to the phase change procedure should be used instead of the portion of multiple solution. We have two choices to determine the saturation pressure, or the p coordinate of the line AB . One is using the tabulated value to equation-fit or

interpolate for specific substance, like oxygen or hydrogen in the present work. This method is definitely feasible. Another method is more generic but needs further discussion on the detailed implementation. That is numerically solving the Maxwell equal area law, which states that the area of AJD equals area of DNB . Superheated liquid or super-cooled vapor is called a secondary stable equilibrium, which is ignored in the present model.

Usually the substance in phase change can be described in bulk by the proportion of vapor phase x , from which a specific volume is determined as $v = xv_B + (1-x)v_A$, where subscripts A and B denote liquid and vapor phase respectively. But in the present droplet model, we can use this method to assign a film molar volume V for the node at the interface, while only one phase could be confirmed for any other specific position.

5.2 Evaporation Rate

Whenever the interface does exist, the continuous fundamental equations do not apply because the derivatives are not defined. The solutions in the two separated regions bordered by the interface have to be connected by the interface conditions (52) to (55). With these equations, we are able to determine four extra variables which cannot be determined from the fundamental equations. They are the discontinuities of heat flux $q_b^G - q_b^L$, species flux $J_{1b}^G - J_{1b}^L$, velocity $u_b^G - u_b^L$, and the regression rate of the droplet radius $\frac{dR_d}{dt}$, supposing we know the latent heat L_b (of the mixture) and the mass emission flux F_{ems} . Equation (55) is de-coupled from the other three. The key point to solve the first three equations is to determine the mass

emission flux F_{ems} , or the evaporation rate, which is not determinable in this case from the equilibrium thermodynamic properties.

The discussions of evaporation rate in classical texts are almost all about the equilibrium state. But in the present problem, we have to determine the evaporation rate for a non-equilibrium procedure. Its value is important to describe the surface of the droplet, and cannot be determined from other variables, which are actually equilibrium thermodynamic properties, in principle. J. Harstad ^[P2] proposed the relation (49) based on the molecular theory.

But it is not easy to get the exact values of these variables. A simpler formulation to approximate them based on equation (49) is proposed and tested in this research. The accommodation coefficient is assumed to be 1, which means that all the vapor molecules colliding with the surface of the liquid is condensed, and all the liquid molecules reaching at the vapor surface is evaporated. It is not necessarily true in practice. It is chosen for simplicity after considering that accurate estimation of accommodation coefficient is not available.

The concentration in equilibrium n_{equil} is obtained using $n = 0.01603P_{sat}/T$ ^[B9], where P_{sat} is saturation pressure in mmHg and T is in °K. The values of n_{equil} for hydrogen and oxygen at $0.7T_r$ are 222.5 mole/m³ and 104.0 mole/m³ respectively. As for saturation pressure, two choices were mentioned in the previous section. Or, a reference value at certain temperature can be used, say $0.7T_r$, plus equation $p = p_0 \exp(-L/RT)$.

As mentioned in section 2.4, the mean normal velocity of a molecule u_{Tj} can be calculated for an ideal gas by

$$u_{Tj} = \left(\frac{RT}{2\pi m_j} \right)^{\frac{1}{2}} \quad (105)$$

or for a pure liquid by

$$u_{Tj} = \frac{RT}{N_A h_p} \left(\frac{V}{N_A} \right)^{\frac{1}{3}} \exp(-\beta \Delta G_0), \quad (106)$$

where $\Delta G_0 = 0.408(\Delta h_{vap} - RT)_{T=T_{nb}}$. Exploring further for a more generic case will not be conducted as part of the present study. Further discussion can be based on calculating the values at a typical condition. At 160°K, which is the film temperature in the previous numerical model, the value for hydrogen from equation (105) is 323.7m/s, that from equation (106) is 4413m/s. For oxygen, the two values are respectively 81.34m/s and 658.3m/s. In both cases, results for the liquid are several times larger than for gas. More research is needed to determine if this conclusion is true. A simple average of the values from equations (105) and (106) was proposed to be used in equation (49) to implement the model of the interface. Considering that latent heat and saturation pressure are still functions of temperature, further simplification is necessary for development of the model.

5.3 Surface Tension

Another difference between “blurred” surface and “clear” surface that has to be taken into account is the surface tension in the case of a “clear” surface. In fact, surface tension plays an important role in phase change.

Let us consider some basic facts of surface tension for the droplet in equilibrium. First, pressure in the droplet at the surface, p_d , has to be larger than that of outside vapor pressure, p_v , to maintain the mechanical equilibrium.

$$p_d = p_v + \frac{2\sigma}{R_d}, \quad (107)$$

where σ is the surface tension and R_d is the radius of the droplet. Referring to that relation for an equilibrium case, we can presume pressure discontinuity $\frac{2\sigma}{R_d}$ instead of continuous pressure on the droplet surface in the present dynamic problem.

Second, the vapor pressure above is different from the vapor pressure (saturation pressure) on a plain surface. The difference can be described as

$$(p_v - p_{v0} + \frac{2\sigma}{R_d})v = RT \ln \frac{p_v}{p_{v0}}, \quad (108)$$

where p_{v0} is the vapor pressure at a plain surface, v is the molar specific volume of the droplet at the surface. In most practical problems, $p_{v0} - p_v \ll \frac{2\sigma}{R_d}$ is valid, producing

$$\ln \frac{p_v}{p_{v0}} = \frac{2\sigma v}{RTR_d}. \quad (109)$$

Rearranging equation (105), we get the definition of critical radius

$$r_c = \frac{2\sigma v}{RT \ln \frac{p_v}{p_{v0}}}. \quad (110)$$

Under certain vapor pressure p_v conditions, if $R_d > r_c$, the droplet will grow by condensation; if $R_d < r_c$, the droplet will evaporate until vanished ^[B23]. That means that only the droplet with, at smallest, the critical radius can exist in equilibrium if the vapor pressure does not change. But the actual evaporation process usually begins with an outside stimulation other than the fluctuation.

Surface tension could be an important factor and is ignored in the previous models, but it is critical to have correct data for surface tension of certain substances to make an improvement in modeling. If a mixture of different components is considered, it is a significant problem to develop a reasonable mixing rule. The first stage for the future study is to develop a procedure for evaluation of surface tension σ for the species of the droplet or the mixture at near critical condition, as those discussed in R. H. Perry's handbook ^[B16].

5.4 Future Improvement of the Model

To make the model applicable for more general cases, forced and/or free convection in the droplet surrounding, multicomponent fuel, existence of combustion, and effect of spray are some of the foreseeable factors which must be integrated in the model. Besides the complexity of the mathematical formulations, these additions will make the numerical solution even more difficult. Another important aspect to be improved, which will impact the framework much, is the refinement of the model of various parameters and coefficients. For example, the viscosity η and the heat conductivity k of the mixture, the mutual diffusion D_m , and the ratio of thermal to mutual diffusion k_T , can be modeled more accurately. It is also important to generate comprehensive experimental data to validate all the models. A correct mixing rule of critical properties T_c, P_c is also a significant factor in this model. When more than two components are considered, the mixing rule becomes more challenging.

To deal with the boundary condition at the interface, more information such as accommodation coefficient α_{c_j} of each species is required, with which tremendous difficulties are associated. If the droplet contains multiple components, the problem

becomes more complicated. Even the determination of a simple parameter like boiling point T_{nb} used in the model is difficult. The latent heat of vaporization Δh_{vap} of each species or diffusion coefficient D , etc., which are functions of other variables, require great effort to model.

Besides the mathematical formulation, the numerical scheme to simulate these equations constitutes a major challenge. For example, artificial viscosity for certain difference schemes, like the one used in the present modeling, is crucial to control the strong numerical oscillation at the discontinuity of the droplet surface. The choice of artificial viscosity seems arbitrary, but the physics behind it plays an important role. An appropriate difference scheme is important for successful implementation of the model. It changes the model from being impractical to practical if a workable scheme exists, or vice versa. An implicit scheme is a good choice to improve the model in the next step of research. It will enhance the numerical stability and enable a larger grid size. An improved grid, such as adaptive grid, will also make difference in the modeling results. Since the gradients of variables are different in order of magnitude, the adaptive-grid technique should be helpful for capturing these unknown variations.

6. Conclusion

6.1 Major Improvements in this model

1) Equations of states applicable to the supercritical condition are used. Actual EOS of H_2 and O_2 are formulated and integrated into the model. Not only is this method applicable in the range of supercritical condition, but the specific phase is to be determined by the model itself too.

2) Thermodynamic properties are systematically modeled as function of pressure, temperature, and composition of H_2 - O_2 mixture. These models generally cover liquid, gas, and supercritical states in a universal form. The defect of previous model with constant or pre-determined properties is also amended.

3) Transport coefficients are modeled as functions of pressure, temperature and composition. Although the present result is to some extent only a conceptual one, it opens the possibility of generalization.

4) General form of transport phenomena is considered including Sorot and Dufour effects. Not all the components are equally significant in specific examples, but this methodology makes the model much more general. Even if implementations are made for individual cases, a universal transport model proved feasible by this study is helpful.

5) Complete unsteady model is evaluated. All the deviations caused by the pseudo-steady assumption are thus eliminated.

6.2 Drawbacks of this model

1) No convection is considered. Due to the restriction of spherical symmetry, convection has been ignored in the models. The numerical solution for the problem with convection will be much more difficult.

2) Only two specific species, O_2 and H_2 , are considered due to the potential application for the national and international interests. Equations of state have to be developed for every involved species and for the mixture in the model.

6.3 Important topics for future research

Even in such a universal model, some interesting issues in applications are not yet addressed. They could be either included in the future improvement, or considered to guide the development of the model. Among them are:

- 1) Effect of convection;
- 2) Effect of combustion and the modeling of combustion around the droplet, which often exists in practical application;
- 3) Effect of spray;
- 4) Multiple components, either of droplet itself or of the surrounding.

Although there are still a lot of issues to be resolved to refine the model, the ideas presented in this research form a new integrated framework to simulate and study droplet phenomenon, which goes from subcritical, critical to supercritical states.

Reference

BOOKS

1. Bellman, R., *Perturbation Techniques in Mathematics, Engineering & Physics*, Dover Publications, Inc., 1972 (QA 871 B44 1972)
2. Bender, E., translated by S. Agnus and E. E. Adalin, *The Calculation of Phase Equilibria from a Thermal Equation of State Applied to the Pure Fluids Argon, Nitrogen, Oxygen and their mixtures*, Verlag C. F. Muller Karlsruhe, 1973 (QD 503 B4613)
3. Bird, R. B., W. E. Stewart, E. N. Lightfoot, *Transport Phenomena*, John Wiley & Son, New York, 1960 (QA 929 B5)
4. Burghardt, M. D., *Engineering Thermodynamics with Application*, Happer & Row, New York, 1982 (TJ 265 B87)
5. Crockett, W. E., *Chemical Engineering - A Review for the P. E. Exam*, John Wiley & Sons, 1986 (TP 155 C74 1986)
6. Cussler, E. L., *Diffusion: Mass Transfer in Fluid System*, Cambridge University Press, 1992 (TP 156 D47 C878 1984)
7. Emanuel, G., *Advanced Classical Thermodynamics*, AIAA Education Series, 1987 (TJ 265 E555)
8. Goldenfield, N., *Lectures on Phase Transition and the Renormalization Group*, Addison-Wesley Publishing Company, 1992 (QC 175.16 P5 G65)
9. Grassmann, P., *Physical Principles of Chemical Engineering*, Pergamon Press, 1971 (TP/155/G6213/1971)
10. Hanley, H. J., *Transport Phenomena in Fluids*, Marcel Dekker, 1969 (QC/175.2/T7)
11. Hala, H., J. Pick, V. Fried and O. Vilim, translated by G. Standart, *Vapor-Liquid Equilibrium*, Pergamon Press, 1967 (TP 156 E65 H313)
12. Hinch, E. J., *Perturbation Methods*, Cambridge University Press, 1991 (QA 871 H56 1991)
13. Law, C. K., *Recent Advances in Droplet Vaporization and Combustion*, Prog. Energy Combust. Sci., Vol. 8., pp. 171-201, 1982
14. McGlashan, M. L., *Chemical Thermodynamics*, Academic Press, 1979 (QD 504 M32)
15. Mouritsen, O. G. , *Computer Studies of Phase Transitions and Critical Phenomena*, Springer-Verlag, 1984 (QC 175.16 P5 M68)
16. Perry, R. H., C. H. Chilton, *Chemical Engineers' Handbook*, 5th edition, 1973 (TP 151 C52 1973)
17. Prausnitz, J. M., P. L. Chueh, *Computer Calculations for High-Pressure Vapor-Liquid Equilibria*, Prentice-Hall, Inc., 1968 (TP 156 E65 P69)
18. Reid, R. C., J. M. Prausnitz, B. E. Poling, *The Properties of Gas and Liquid*, 4th edition, McGraw-Hill
19. Reid, R. C., T. K. Sherwood, *The Properties of Gas and Liquid*, McGraw-Hill, 1958 (TP 242 R4)

20. Romano, A., Thermomechanics of Phase Transitions in Classic Field Theory, 1993
21. Smith, J. M., Chemical Engineering Kinetics, McGraw-Hill, 1970 (TP 149 S58 1970)
22. Smith, J. M., H. C. Van Ness, Introduction to Chemical Engineering Thermodynamics, McGraw-Hill, 1975 (TP 149 S582 1975)
23. Wang, Z., Thermodynamics and Statistical Physics, Advanced Education Press, China, 1984

PAPERS

1. Aggarwal, S. K., A Review of Droplet Dynamics and Vaporization Modeling for Engineering Calculations, J. Engineering for Gas Turbines & Power, Vol. 117, pp. 453-461, July 1995
2. Harstad, J., and J. Bellan, A Model of Critical and Supercritical Evaporation of Drops in Clusters, NASA Marshall Space Flight Center, 1993
3. Kono, M., Japan's Research on Droplet and Droplet Array Combustion, CASI 96N15564, Aug., 1995
4. Law, C. K., Recent Advances in Droplet Vaporization and Combustion, Prog. Energy Combust. Sci., Vol. 8., pp. 171-201, 1982
5. Mo, J., Literature Study of Supercritical Droplet Gasification, The University of Memphis, 1996
6. Samuel. P., A Numerical Study of the Unsteady Effects of Droplet Evaporation and Ignition in Homogeneous Environments of Fuels and Air, J. Energy Resources Tech., Vol. 116., pp. 194-200, Sept. 1994
7. Savery, W., et al, Experiments on Droplet Vaporization at Supercritical Pressures, AIAA Paper 70-6
8. Torda, T. P., et al, Liquid Droplet Evaporation in Stagnant High Pressure and High Temperature environment, NASA CR-72373, May 1968
9. Yang, V., Multicomponent Droplet Vaporization at Near Critical Conditions, JANNAF Workshop on Liquid Behavior at Critical and Supercritical Conditions, September 6, 1989

WEB SITES

1. Fluctuations and Critical Phenomena, http://www.ipst.umd.edu/critical_phenomena
2. Equation of state, <http://www.srtca.shell.nl/software/sope/equa.html>
3. NIST WebBook, <http://webbook.nist.gov/>
4. Fundamentals of Thermodynamics, <http://www.engrng.pitt.edu/~chewww/CHE2101/syllabus/syllabus.html>
5. Introduction to Applied Thermodynamics, <http://www.egr.msu.edu/~lira/preface.htm>
6. About Mixcalc, <http://pages.recom.com/~fmejia/info.htm>
7. Simulation Of Phase Equilibrium, <http://www.srtca.shell.nl/software/sope/sope.html>

8. Prediction of Phase Equilibrium in Binary Mixture Using an improved Equilibrium of State and a Theoretically Consistent Mixing Rule, <http://www.finearts.com.au/abstract/cec/108-0027.htm>
9. Chemical Engineering, Univ. of Delaware, <http://www.che.udel.edu/faculty/full/sandler/pub.html>
10. Series Method for Analysis of Soave-Redlich-Kwong and Similar Equation, <http://www.finearts.com.au/abstract/cec/108-0029.htm>
11. Phase Equilibrium of Binary Lennard-Jones Mixtures with Cubic Equation of State, <http://www.srtca.shell.nl/publications/1994/VI-1.html>
12. CHE 666 Lecture Index (Multicomponent Mass Transfer), http://opus.utah.edu:80/~smith/Classes/666/lectures/lecture_index.html
13. Introduction (about tracer diffusion and mutual diffusion), <http://turbo.che.ncsu.edu/sunders/nodel.html>
14. FAQs: Internet Resources for Chemical Engineers, <http://www.retallick.com/resources/netresrc.html>
15. University of Alabama in Huntsville, Department of Chemical and Materials Engineering, <http://chemeng.uah.edu/>
16. University of Victoria, Canada, Mechanical Engineering, <http://www.me.uvic.ca/>
17. University of California, San Diego, Department of Mechanical and Aerospace Engineering, <http://www-mae.ucsd.edu/>
18. RWTH Aachen, Germany, <http://www.rwth-aachen.de/>
19. Princeton University, Mechanical and Aerospace Engineering, <http://www.princeton.edu/~mae/MAE.html>
20. Pennsylvania State University, Chemical Engineering, <http://gibbs.che.psu.edu/index.html>

NEWSGROUPS

1. sci.engr.mech
2. sci.engr.chem
3. sci.physics.computational-fluid-dynamics

Appendices

Appendix 1 Properties of H_2 and O_2

Parameters	H_2	O_2
Critical temperature ($^{\circ}K/^{\circ}C$)	33.2/-239.9	154.4/-118.8
Critical pressure (kPa/atm)	1300/12.8	5040/49.7
Critical density (10^3 kg/m^3)	0.0310	0.430
Critical volume ($10^{-6} \text{ m}^3/\text{mole}$)	65	74
Critical compressibility	0.3297	0.2745
Molar weight (10^{-3} kg/mole)	2.02	32.00
Normal boiling point ($^{\circ}K/^{\circ}C$)	20.45/-252.7	90.15/-183
Melting point ($^{\circ}K$)	14.01	54.8
Heat of vaporization (cal/mole)	216	1629
u_T as ideal gas at 160K	323.7	81.34
u_T as pure liquid at 160K	4413.	658.3
Temperature when $p_{\text{sat}}=2\text{atm}(^{\circ}C)$	-250.2	-176.0
Temperature when $p_{\text{sat}}=5\text{atm}(^{\circ}C)$	-246.0	-164.5
p_{sat} at $T_r=0.7$ (atm)	2.2321	4.8422
T_r ($^{\circ}K/^{\circ}C$)	23.275/-249.875	108.045/-165.105
N_{equil} at $T_r=0.7$ (mole/m^3)	222.5	104.0

Appendix 2 Algorithms of Equation Solution

Peng-Robinson equation of state is pressure explicit. When we want to get V (then n) from p , a cubic equation of V has to be solved. By the method of Newtonian iteration, we can get solution of $f(x) = 0$ if $x_{i+1} = x_i - f(x_i)/f'(x_i)$, $i = 1, 2, \dots$, can converge. However, this method is too sensitive to the 'correct' initial value of x . In this program, if we use simpler equation of state for ideal gas to estimate the initial value of V , it turns out not to converge to the real V . If using more complicated equation of state, as van der Waals equation, it itself is as difficult to solve as Peng-Robinson equation.

A combination of Newtonian iteration and bisection methods is used in this program. Central point of the supposed region where solution exists is chosen as the initial value. When using Newtonian iteration, if the new value is out of region, or the change is too small, using bisection method to get next x_{i+1} . The subroutine RTSAFE is adapted from *Handbook of FORTRAN77 Algorithm* (by He, Guangyu, Science Press, China, in Chinese).

Appendix 3 Computerized Diagram of Viscosity

The computer program called VIS.FOR is developed based on figure 3-44 in *Chemical Engineers' Handbook* by R. H. Perry, which is used to look up viscosity of gas for different temperature under 1 atm pressure. VISLQD.FOR based on figure 3-45 is the counterpart of liquid.

To find out a value of viscosity, we should have a point on the left side vertical axis representing the temperature, and a point in the mesh for each specific substance since every substance that can be looked up in this figure is assigned a pair of coordinates. When we connect these two points and stretch the line to cross the right side vertical axis, which represent viscosity, to get the value we want. We can present the geometric relation on the figure as

$$\mu = \mu_0 + \Delta\mu(y_r), \quad y_r = y_r(y_l, x, y), \quad y_l = y_l(T).$$

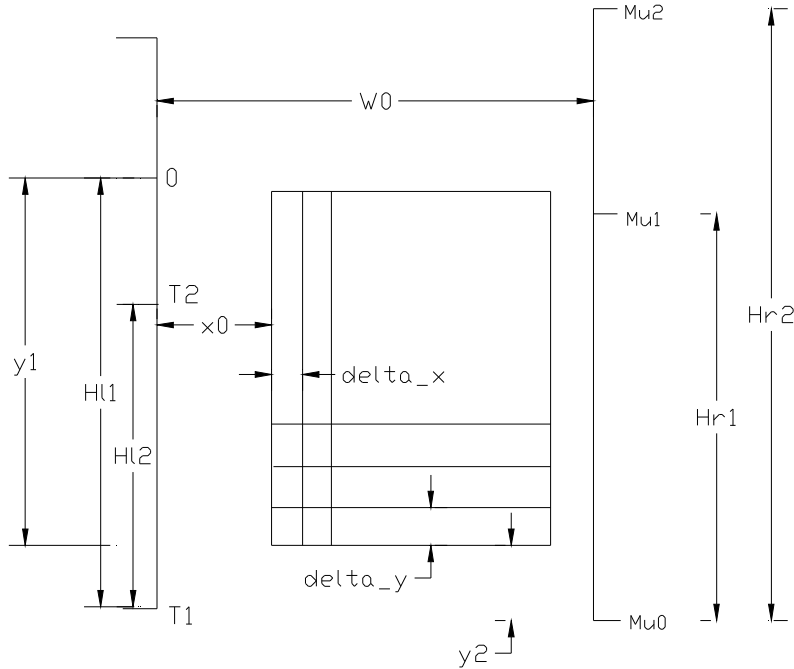
Let us discuss the case of gas first. $y_r = y_r(y_l, x, y)$ is a pure geometric relation and both μ and T are logarithm function of vertical coordinates y_r and y_l respectively. If we suppose the form

$$\Delta\mu = b_1(e^{b_2 y_r} - 1) \quad (\text{A-1})$$

and

$$y_l = c_1 \ln(1 + c_2 T). \quad (\text{A-2})$$

we can measure the figure to determine the relation $y_r = y_r(y_l, x, y)$ and all the parameters in relation (A-1) and (A-2). On the following stretch of figure 3-44, we can measure the lengths shown below.



Length h	w_0	x_0	y_1	y_2	Δx	Δy	H_{l1}	H_{l2}	H_{r1}	H_{r2}
(cm)	10.25	3.15	11.7	1.45	0.356	0.355	12.7	6.15	7.57	16.3

$T_1 = 1000$ °C. $T_2 = 300$ °C. $\mu_0 = 0.005$ Centipoises. $\mu_1 = 0.02$ Centipoises. $\mu_2 = 0.1$ Centipoises. From these parameters, we have

$$y_r = y_1 + y_2 + y_l + \frac{w_0}{x_0 + x} (y - y_1 - y_l), \quad (\text{A-3})$$

where y_r 's zero is at the lowest point μ_1 , y_l 's zero is at zero of temperature, both having upward positive direction. x and y are the mesh-coordinates of a specific substance.

From equation (A-2), we have $\begin{cases} -H_{l1} = c_1 \ln(1 + c_2 T_1) \\ -H_{l2} = c_1 \ln(1 + c_2 T_2) \end{cases}$. Solving it with

Newtonian iteration method (NEWTON.FOR), we get $c_1 = -8.2$ cm, $c_2 = 0.0037$ /°C.

From equation (A-1) and $\mu_0 = 0.005$, we have $\begin{cases} \mu_1 - \mu_0 = b_1 (e^{b_2 H_{r1}} - 1) \\ \mu_2 - \mu_0 = b_1 (e^{b_2 H_{r2}} - 1) \end{cases}$.

Solving it with Newtonian iteration, we get $b_1 = 0.00496$ Centipoises = 0.00496×10^{-3} kg m⁻¹sec⁻¹, $b_2 = 0.184$ /cm.

The following table shows good identity between experimental results ^[1-3] and this program.

GAS	x	Y	T(°C)	Experiment	Calculation
O ₂	11.0	21.3	20	0.0203	0.0203
H ₂ O	8.0	16.0	100	0.0127	0.0126
CO ₂	9.5	18.7	20	0.0146	0.0145
Hg	5.3	22.9	380	0.0654	0.0635
N ₂	10.6	20.0	20	0.0175	0.0176
CH ₄	9.9	15.5	20	0.0109	0.0108

Similar method can be used for liquid. The only obvious difference is that the temperature axis is in opposite direction. The measured values are as following.

Length h	w ₀	x ₀	y ₁	y ₂	Δx	Δy	H _{l1}	H _{l2}	H _{r1}	H _{r2}
(cm)	10.53	3.27	2.15	0.85	0.349	0.35	13.9	7.93	5.6	16.85

$T_1 = 200$ °C. $T_2 = 100$ °C. $\mu_0 = 0.1$ Centiposes. $\mu_1 = 1$ Centiposes. $\mu_2 = 100$ Centiposes.

The computational results are: $c_1 = 24.3$ cm, $c_2 = 0.00386/^\circ\text{C}$, $b_1 = 0.1$ Centiposes = 0.1×10^{-3} kg m⁻¹sec⁻¹, $b_2 = 0.409/\text{cm}$.

The verification for liquid is in the following table. The result for liquid is not as good as for gas, but it is still satisfying for most substances verified here.

LIQUID	X	y	T(°C)	Experiment ^[B3]	Calculation
C ₆ H ₆	12.5	10.9	20	0.647	0.659
Br ₂	14.2	13.2	26	0.946	0.952
C ₂ H ₅ OH	10.5	13.8	20	1.194	1.228
H ₂ SO ₄	8.0	25.1	25	19.15	19.36
Glycerol	2.0	30.0	20	1069.	867.0
Na	16.4	13.9	103.7	0.686	0.7068
			250	0.381	3.976
			700	0.182	0.1356
Hg	18.4	16.4	-20	1.85	1.802
			20	1.55	1.577
			100	1.21	1.27
			200	1.01	1.028

Appendix 4 Linear Fitting of Conductivity

In the FORTRAN program MEDFIT.FOR and SORT.FOR adopted from *Handbook of FORTRAN77 Algorithm* (by He, Guangyu, Science Press, China, in Chinese), the general-purposed subroutine MEDFIT, which will call SORT (heap sorting), is used to fit the thermal conductivity as a linear function of temperature ensuring minimum absolute deviation. The format of parameters to call MEDFIT is (X, Y, NDATA, A, B, ABDEV), where X and Y are the input arrays of argument and

function respectively, NDATA is the number of elements used to fit, A and B are output coefficients of fit, and ABDEV is the absolute deviation.

NDATA is 5 in this program. The comparison between the fitting result of thermal conductivity of H₂ and O₂ and actual experimental data is shown below.

Temperature (°K)	H ₂ (Fit)	H ₂ (Experiment)	H ₂ (Fit)	O ₂ (Experiment)
100	7.6	6.7	0.93	0.93
150	10.3	10.1	1.37	1.38
200	13.0	13.1	1.82	1.83
250	15.6	15.7	2.26	2.26
300	18.3	18.3	2.70	2.66
350	21.0	20.4	3.15	2.98
400	23.6	22.5	3.59	3.30

Appendix 5 Table of Notations

A	Helmholtz energy
A_d	surface area of droplet
a_i	activity of species i
a	a factor in equation (41), $(\frac{V}{N_A})^{\frac{1}{3}}$ according to Harstad
a	a coefficient in P-R EOS
b	a coefficient in P-R EOS
C_p	heat capacity at constant pressure, per unit mass
D	diffusion coefficient
D_m	mutual diffusion coefficient
\vec{e}_r	unit vector on radial direction
F_{ems}	mass emission flux
f_i	fugacity of species i
ΔG_{mix}	change of Gibbs free energy (free enthalpy) in mixing pure constituents
ΔG^E	excess Gibbs free energy (excess free enthalpy)
ΔG_0	barrier height (activation energy)
H	enthalpy
h	partial mass enthalpy of mixture
h_i	partial molar enthalpy of species i
h_p	Planck's constant, 6.62×10^{-34} joule·sec
Δh_{vap}	latent heat of vaporization
$\vec{J}_i, J_{i\beta}$	molar flux relative to mass-average velocity of species i
\vec{J}_b	part of the flux expression, equation (23)
k	heat conductivity of mixture
k_T	ratio of thermal to mutual diffusion
L_{ij}	transport matrix for Fick diffusion
L_{iq}	transport coefficients for thermal diffusion (Soret effect)

L_{qj}	transport coefficients for Dufour effect
L_{qq}	transport coefficients for Fourier diffusion
L_d	latent heat at droplet interface with surrounding
L	any of the thermodynamic properties
m	number-mean molecular weight
m_i	molecular weight of species i
m_d	mass of droplet
N_A	Avogadro's number, 6.02×10^{23} /mole
n	molar concentration (number of moles per unit volume)
n_i	molar concentration of species i
P, p	pressure
\bar{q}, q_β	heat flux
R	gas constant, $8.314 \text{ joule}^\circ\text{K}\cdot\text{mole}$
R_d	radius of droplet
r	radial coordinates in spherical coordinate
S	entropy
s	partial molar entropy
T	temperature
t	time
u_α	velocity component in Cartesian coordinate
u	radial velocity
u_{Tj}	mean normal velocity of a molecule of species j due to thermal fluctuation
V	partial molar volume
v_r	radial velocity
W_l	part of expression in equation (38)
X	mole fraction
x_α	Cartesian coordinates
Z	compressibility factor
α	index for Cartesian coordinates
α_D, α_{Di}	the coefficient $1 + X_i \left. \frac{\partial \ln \gamma_i}{\partial X_i} \right _{T,p}$
α_{cj}	accommodation of species j
β	index for Cartesian coordinates
β	$1/RT$
γ_i	activity coefficient of species i
Δ	the change (of Gibbs free energy)
η	mixture viscosity
θ	component of spherical coordinate
μ_i	chemical potential of species i
ρ	density
$\tau_{\alpha\beta}$	viscous stress tensor
ϕ_v	viscous dissipation term in energy equation
ϕ_l	fugacity coefficient of species 1
ϕ	component of spherical coordinate

ω argument of function used in P-R EOS

Superscript

0 reference value

0 infinite dilution (about activity coefficient γ_i or excess Gibbs free energy ΔG^E)

* pure substance

* for ideal solution (about the Gibbs free energy change ΔG_{mix})

G gas (surrounding)

L liquid (droplet)

p perfect gas

Subscript

0 infinite dilution

1, 2 1st or 2nd species

b interface boundary

b part of the flux expression, in equation (23) \bar{J}_b

c critical property

c correction of partial molar volume (for proper Z_c of pure limits)

D correction of partial molar volume (for effect of reference state)

d droplet

equil at equilibrium

I, j species index

α, β species index

nb normal boiling point

r radial direction in spherical coordinate

r reduced value (of temperature)

Mathematical Operations

D/Dt substantial derivative

$exp(x)$ exponential function of x

$f(\omega)$ the function used in P-R EOS

$ln(x)$ logarithm of x to the base e

∇ nabla operator

To the Graduate Council:

I am submitting herewith a dissertation written by Zhou Ji entitled "A Universal Model of Droplet Vaporization Applicable to Supercritical Conditions." I have examined the final copy of this dissertation for form and content and recommend that it be accepted in partial fulfillment of the requirements for the degree of Doctor of Philosophy with a major in Mechanical Engineering.

Jiada Mo, Ph.D.
Major Professor

We have read this dissertation and
recommend its acceptance:

Srikant Gir, Ph.D.

John I. Hochstein, Ph.D.

Edward H. Perry, Ph.D.

Sam B. Thomason, Ph.D.

Accepted for the Council:

Linda L. Brinkley, Ph.D.
Vice Provost for Research
& Dean of the Graduate School